

DIGITAL ACCESS TO SCHOLARSHIP AT HARVARD
DASH.HARVARD.EDU

HARVARD LIBRARY


Idiosyncratic Olfactory Behavior and its Neural Basis

Citation

Smith, Matthew Anthony-y. 2020. Idiosyncratic Olfactory Behavior and its Neural Basis. Doctoral dissertation, Harvard University Graduate School of Arts and Sciences.

Link

https://nrs.harvard.edu/URN-3:HUL.INSTREPOS:37368916

Terms of use

This article was downloaded from Harvard University's DASH repository, and is made available under the terms and conditions applicable to Other Posted Material (LAA), as set forth at

https://harvardwiki.atlassian.net/wiki/external/NGY5NDE4ZjgzNTc5NDQzMGIzZWZhMGFlOWI2M2EwYTg

Accessibility

https://accessibility.huit.harvard.edu/digital-accessibility-policy

Share Your Story

The Harvard community has made this article openly available.
Please share how this access benefits you. Submit a story

HARVARD UNIVERSITY
Graduate School of Arts and Sciences



DISSERTATION ACCEPTANCE CERTIFICATE

The undersigned, appointed by the

Department of Molecular and Cellular Biology

have examined a dissertation entitled

Idiosyncratic Olfactory Behavior and its Neural Basis

presented by Matthew Smith

candidate for the degree of Doctor of Philosophy and hereby certify that it is worthy of acceptance.

Signature Florian Engert (Jun 1, 2020 12:38 EDT)

Typed name: Prof. Florian Engert

Signature Samuel Kunes

Typed name: Prof. Samuel Kunes

Signature Venkatesh Murthy
Venkatesh Murthy (Jun 1, 2020 12:46 EDT)

Typed name: Prof. Venkatesh Murthy

Signature _____

Typed name: Prof.

Signature _____

Typed name: Prof.

Date: 5/27/20

Idiosyncratic Olfactory Behavior and its Neural Basis

A Dissertation presented

by

Matthew Smith

in partial fulfillment of the requirements

for the degree of

Doctor of Philosophy

in the subject of Biology

Harvard University

Cambridge, Massachusetts

May, 2020

© 2020 Matthew Smith

All rights reserved.

Dissertation Advisor: Benjamin de Bivort Matthew Smith

Idiosyncratic Olfactory Behavior and its Neural Basis

Abstract

Individuality is a fundamental feature of animal behavior. Such behavioral idiosyncrasy exists across animals responding to an identical stimulus, and even within a single animal from moment-to-moment. Behavioral idiosyncrasy is essential to a number of evolutionary strategies to overcome ecological challenges. Despite this importance, the neural mechanisms by which idiosyncratic behavior arises is still unclear.

We have found that isogenic *Drosophila melanogaster* raised in identical environments exhibit idiosyncratic olfactory preferences that are stable across multiple days, representing something akin to a fly personality. The amount of individuality across animals can be tuned through activity of local neurons within the antennal lobe and selective neuromodulators. The observed individuality is, in part, the result of differences in odor coding within the peripheral nervous system. We paired behavior and two-photon imaging to show that idiosyncratic calcium dynamics in both olfactory receptor neurons and projection neurons predict individual preferences for an aversive odorant, suggesting that variation at the periphery of the olfactory system determines individual preference for an odor's presence. Lastly, we also show that isogenic animals exhibit individuality in learning responses that generalizes across stimulus modalities, both unconditioned and conditioned. These findings add to our perspective on individuality of behavior, and identify sources of variation in neural circuits that could function as substrates for natural selection or ecological strategies.

This page is intentionally left blank

Table of contents: **Pg#**

1) Introduction 1
2) Chapter I: Idiosyncratic neural coding and neuromodulation of olfactory individuality in *Drosophila* 14
3) Chapter II - Loci of individuality in the *Drosophila* olfactory circuit 44
4) Chapter III: Individuality in generalized learning responses 65
5) Conclusion 80
6) Appendix I: Chapter I Supplemental Material 94
7) Appendix II: Chapter II Supplemental Material 130
8) Appendix III: Chapter III Supplemental Material 154

Introduction

Individuality is a fundamental feature of behavior throughout the animal kingdom. We can draw relatable examples from human behavior- including differences in speech patterns, gait, learning styles, and odor preferences(1–4). Not only does the behavior of an individual vary from moment to moment, but identical stimuli may consistently evoke very different behavioral responses in different individuals. It is this behavioral variability that represents an essential piece of evolutionary strategies to ecological challenges (5–7). Despite the importance of understanding the mechanisms of producing behavioral diversity, little work has focused on understanding behavioral idiosyncrasy from a neural circuit perspective.

We know that individual differences are influenced through the intersection of genetic encoded and environmental differences. However, individuality in behavior is still observed even when both genetics and environment are held constant, suggesting that there are other factors that influence individuality (6). For example, within mice that were inbred for 30 years, observed behavioral variability was only reduced by 20-30% (8). Even human identical twins that have identical genetic backgrounds and are raised in the same environment show distinct behavioral differences(9). There has been increasing evidence to suggest that differences not explained by genotype or environment may arise from elements of randomness, or stochasticity (5, 7, 10–12). These elements would be unpredicted and nonheritable contributors to behavioral variability. This hypothesis is supported by deterministic physical laws that describe the unpredictability of events on the molecular scale, which makes developmental biology near impossible to replicate identically across organisms (6). The brain, given its plasticity and role in producing behavior, is a tissue that we can expect to observe more evidence of randomness. This is, in part, because variability in animal behavior can be a readout of variability in neural tissue. And we are

hypothesizing that within the brain, there may exist neural populations that are more susceptible to randomness and variability than others (13). We are terming the neurons that harbor significant inter-individual differences in anatomy and physiology, that influence observed individuality in behavior, "loci of individuality". We believe that inter-individual differences in these loci of individuality may be able to tune the amount of behavioral variability within a group of isogenic animals.

The goal of this collection of work was to understand the neurobiological mechanisms of individuality in ecologically relevant behaviors, including odor preferences, behavioral habituation, and learned odor associations. We aim to answer the following fundamental questions about idiosyncrasy in behavior and neural coding:

1) How behavioral responses to identical stimuli vary across individuals.

2) Determine how the neural coding of identical stimuli in a model sensory system varies across individuals and obtain mechanistic understanding of how these differences arise.

3) Examine the extent to which neural differences translate into idiosyncratic differences.

To answer these questions we have utilized the molecular genetics and neuroscience toolkit in the fruit fly, *Drosophila melanogaster*. Diverse idiosyncratic behaviors have been described in many species, including *Drosophila* (5, 7, 11, 14). We have found that even in isogenized stocks of fruit flies, individuals display idiosyncratic behaviors in a number of paradigms, this includes phototaxis, thermal preference, and locomotor biases (5, 7, 10, 11, 15–17). Locomotor bias has been one of the most extensively studied behaviors within the lab (5, 10, 16). In locomotor bias, while not showing a species-level bias, individual flies prefer to choose either left or right turns in branching mazes. These idiosyncrasies are not heritable, but last the lifetime of the flies, and therefore constitute a form of personality. Understanding the neural basis of the many dimensions

of behavioral variability will be important to understanding the processes that shape evolution and behavior.

Closely related *Drosophila* species have specialized behavioral responses to certain odorants and *D. melanogaster* strains derived from the same wild population display dramatic and consistent differences in odor preference. Thus, olfactory behavior in *Drosophila* represents an ecologically relevant behavior. It is unknown where such ecological pressures may impart biases in neuronal circuitry. Throughout my PhD I have utilized this olfactory circuit in *Drosophila* to better understand our questions about individuality.

To understand the neural basis of behavioral individuality, we chose to focus on the sensory end of the well-studied neural circuit, the *Drosophila* olfactory system. Individual-specific differences in behavior could arise at any layer of the circuit between sensory input and motor output. We chose to focus on the first two layers of the olfactory circuit to determine to what extent differences in sensory processing diversify behavior, and whether sensory signals become more or less individual-specific as information moves from sensory periphery to the brain. Another reason we believe that the olfactory system is well suited for studying individuality in behavior is that we can draw clear examples in human behavior of individuality in odor preferences- there are many smells that yield a variety of preferences (e.g. gasoline)(18). However, in human odor preference, it is clear that such individuality is influenced significantly by genetics and environment (19). In addition to this relatable mammalian precedent of high individual variation in olfactory behavior, the early layers of the *Drosophila* olfactory system are especially well-suited to this question. Flies have a relatively small number (~50) of distinct classes of odorant receptor neurons. These input neurons make stereotyped connections to second order (projection) neurons that relay olfactory information deeper into the brain. The clusters of synapses connecting these populations

(glomeruli) are stereotypically arranged and compactly situated within the brain, allowing us to monitor, and compare between individuals, the complete representation of an odorant at this processing stage. Additionally, there is a potential substrate for individuality amidst the stereotyped connections between input neurons and projection neurons. These synapses are interconnected by local interneurons, which are highly variable across individuals, with diverse connections and morphology that are clearly not deterministic. Thus, this system offers an excellent opportunity to evaluate the contribution of individual differences in sensory processing at the level of neural activity to the olfactory behavior of the animal. And many parallels can be drawn from the invertebrate olfactory system in respect to the mammalian system in terms of anatomy and physiology. The antennal lobe is analogous to the mammalian olfactory bulb, and the projection neurons are analogous to the mitral/tufted cells, which project to the mushroom body and analogous mammalian olfactory cortex. (20).

In the *Drosophila* olfactory system there are regions of the early sensory circuit that have been described to exhibit high fly-to-fly variability, and may be substrates in which behavioral variability can generated (21–25). Individual-to-individual fluctuations in this early sensory systems will propagate onward and influence stimulus coding brain-wide. This has been shown in the parallel circuitry of the mammalian brain, in which sensory noise can drive differential behavior on a trial-by-trial basis. Thus, it is plausible that early olfactory processing in the invertebrate system is the site of individual differences that are responsible for behavioral variability.

The olfactory receptor neurons (ORNs) represent the most peripheral region of the odor processing circuit. The number of olfactory receptor classes remains stereotyped (~50) and number of ORNs (~1500), but the number of receptors expressed in each neuron could vary

significantly(4, 26). The ORNs project to the antennal lobe (AL), which is the first region of odor coding within the fly brain. The ORNs project into micro-compartments called glomeruli within the antennal lobe. The glomeruli consist of a single ORN class projecting into a single glomerulus and synapsing with dendrites from projection neurons (PNs), there are around 50 distinct glomeruli. Within the antennal lobe there are various circuit elements that are present to tune the incoming olfactory information. This includes a set of interneurons, called local neurons (LNs). These LNs are variable in terms of physiologic response and morphology, and are responsible for refining, or tuning, the incoming odor information (21, 22, 27). These LN's neural processes interconnect glomeruli within the AL, with some linking a substantial fraction of the total glomeruli. The LNs are predominantly inhibitory and release GABA as their neurotransmitter. The composition of these diverse LN types differs significantly across flies, and is a plausible loci of olfactory individuality into, the otherwise, quite anatomically stereotyped AL, and may represent a plausible loci of individuality(21–25). In fact, it is the remarkable stereotypy of the dendrites of the PNs that make the AL an idea location for studying inter-fly differences. Each glomerulus within the AL is uniquely identifiable by anatomical position, morphology and ORN input, allowing the identification and comparison of glomerular responses across animals. In terms of physiology, PNs show less trial to trial individuality and have a higher signal-to-noise ratio, as multiple ORNs converge onto a PN. The ORNs have a noisy baseline activity, but are more effective at coding to odor dynamics than PNs, including duration and concentration. It is plausible that fly-to-fly variability in expression of receptors within ORNs could propogate individual differences in odor coding downstream.

Within other *Drosophila* behaviors, neurotransmitters have proven to play an important role in modulating intragenotypic behavior (5, 10, 11, 14, 16). In the olfactory circuit, there is a

single pair of serotonergic neurons that innervates into the AL, called contralaterally-projecting serotonin-immunoreactive deuterocerebral interneurons (CSD)(28–31). Serotonin's role across many organisms is to modulate motivation or regulate mood(32), in *Drosophila* the CSD neuron activation may regulates olfactory and pheromone processing within the AL(28), and also shown to be important in regulating olfactory behavior in *Drosophila* larvae(33). This may represent an opportunity for direct serotonergic control of incoming olfactory signal and modulation of behavioral variability.

The PNs project from the antennal lobe and convey information to the calyx of the mushroom body (MB), the center of learning and memory within the *Drosophila* brain, as well as the Lateral Horn (LH), the region believed responsible for innate behavioral responses. The MB, as the learning and memory center, could represent a region in which intragenotypic variability arises(34, 35). Despite most learning based plasticity occurring in the MB, within honeybees there is evidence that individual variation in plasticity of the AL could produce individual differences(36).This could be plausible in flies, since a key plasticity coincidence detector, *rutabaga*, is expressed throughout the AL(37). The PNs synapse onto the dendrites of the Kenyon cells (KCs) that make up the calyx of the MB. The process of learning in the MB occurs through coincidence detection, the occurrence of two molecular events, increased calcium from acetylcholine released from active PNs onto KCs and cAMP levels increased through dopamine released via dopaminergic neurons (DANs) (38). The combination of these two events activates the calcium dependent adenylate cyclase which will trigger a signaling cascade resulting in neuronal changes. It is the DANs that are the most prevalent modulatory neuron in the MB responsible for conveying negative and positive valence information and release dopamine locally to modify the KC-MBON synapse (34, 39, 40). It is plausible that *rutabaga* may impart intragenotypic

variability through individual-to-individual expression across animals. The MB also may impart individuality through the variation in expression of genes that regulate plasticity of learning, facilitate fasciculation, vesicle production, and triggering signaling cascades. In *Drosophila*, these include *rutabaga, dop1r1, amnesiac*, and *dunce*. This variability in expression may become apparent in learning events, where more significant expression leads to more or less changes in neuronal function. Measuring individual differences in learning will help determine if this individual variation in plasticity expression can affect output behavior(41–43).

Within humans there are a number of examples of individuality in behavior, this includes differences in learning dimensions, or even termed learning skills(44). There are a number of psychology tools used to describe such individual differences in generalized learning dimensions (3) and cognitive styles to vocational practices. Reversal learning may be another method to measure individuality in behavior plasticity in a rapid and high throughput manner. The reversal learning paradigm is one that has been used in vertebrates to measure something akin to impulsivity and susceptibility to addictive behaviors(45). This has been studied in *D. melanogaster* as well, as a metric of cognitive flexibility(46–49). This represents a more molecularly challenging task than normal classical conditioning, in the sense that a fly will need to unlearn a specific process, meaning the previously encoded DAN and odor information will need to be modified(50–52). It remains an open question if there exists individuality in learning in respect to such behavioral plasticity. If there is individuality in learning and behavioral plasticity, it suggests that there could be a generality to learning performance across different modalities(53). Before such a study, we must rule out variability in sensory processing as a source of variability in learning. One can think of controlling this by choosing a very controllable US or CS and meticulously monitoring the delivery system(54). Another solution is found in more modern implementations of a classical

conditioning assay in *Drosophila*, using opto-genetics(39). I'm interested in the olfactory conditioning paradigm, so sensory input would occur at olfactory receptor neurons for the encoded odor presented. It is feasible that any observed differences in learning could occur at this sensory periphery level. There would be a number of ways to evaluate this, one being to measure the amount of expression for a particular receptor, another being multiple unconditioned stimulus modalities within a single fly. Using differing US modalities would be the easiest and most efficient method to test the basis of individuality, assuming the modalities do not share the same circuitry. We believe this could be an interesting study showing that in highly controlled conditions there many exist an invertebrate general intelligence, which varies among individuals. This is the idea that individual learning ability transcends different domains of learning(55, 56).

1. F. Horst, S. Lapuschkin, W. Samek, K.-R. Müller, W. I. Schöllhorn, Explaining the unique nature of individual gait patterns with deep learning. *Sci. Rep.* **9**, 2391 (2019).

2. K. Pisanski, J. Raine, D. Reby, Individual differences in human voice pitch are preserved from speech to screams, roars and pain cries. *R Soc Open Sci* **7**, 191642 (2020).

3. R. E. Boyatzis, D. A. Kolb, Assessing Individuality in Learning: the learning skills profile. *Educ. Psychol. Rev.* **11**, 279–295 (1991).

4. J. D. Mainland, *et al.*, The missense of smell: functional variability in the human odorant receptor repertoire. *Nat. Neurosci.* **17**, 114–120 (2014).

5. J. S. Kain, *et al.*, Variability in thermal and phototactic preferences in Drosophila may reflect an adaptive bet-hedging strategy : BET-HEDGING EXPLAINS THERMOTACTIC VARIABILITY. *Evolution* **69**, 3171–3185 (2015).

6. K. Honegger, B. de Bivort, Stochasticity, individuality and behavior. *Curr. Biol.* **28**, R8–R12 (2018).

7. J. Akhund-Zade, S. Ho, C. O'Leary, B. de Bivort, The effect of environmental enrichment on behavioral variability depends on genotype, behavior, and type of enrichment https:/doi.org/10.1101/557181.

8. K. Gärtner, A third component causing random variability beside environment and genotype. A reason for the limited success of a 30 year long effort to standardize laboratory animals? *Laboratory Animals* **24**, 71–77 (1990).

9. N. L. Segal, *et al.*, Genetic and experiential influences on behavior: Twins reunited at seventy-eight years. *Pers. Individ. Dif.* **73**, 110–117 (2015).

10. K. Skutt-Kakaria, P. Reimers, T. A. Currier, Z. Werkhoven, B. L. de Bivort, A neural circuit basis for context-modulation of individual locomotor behavior https:/doi.org/10.1101/797126.

11. J. F. Ayroles, *et al.*, Behavioral idiosyncrasy reveals genetic control of phenotypic variability. *Proc. Natl. Acad. Sci. U. S. A.* **112**, 6706–6711 (2015).

12. K. S. Kakaria, B. L. de Bivort, Ring Attractor Dynamics Emerge from a Spiking Model of the Entire Protocerebral Bridge. *Front. Behav. Neurosci.* **11**, 8 (2017).

13. A. Sugie, G. Marchetti, G. Tavosanis, Structural aspects of plasticity in the nervous system of Drosophila. *Neural Dev.* **13**, 14 (2018).

14. C. Pantoja, *et al.*, Neuromodulatory Regulation of Behavioral Individuality in Zebrafish. *Neuron* **91**, 587–601 (2016).

15. S. M. Buchanan, J. S. Kain, B. L. de Bivort, Neuronal control of locomotor handedness in Drosophila. *Proc. Natl. Acad. Sci. U. S. A.* **112**, 6700–6705 (2015).

16. J. S. Kain, C. Stokes, B. L. de Bivort, Phototactic personality in fruit flies and its suppression by serotonin and white. *Proc. Natl. Acad. Sci. U. S. A.* **109**, 19834–19839 (2012).

17. K. S. Honegger, M. A.-Y. Smith, M. A. Churgin, G. C. Turner, B. L. de Bivort, Idiosyncratic neural coding and neuromodulation of olfactory individuality in Drosophila. *Proc. Natl. Acad. Sci. U. S. A.* (2019) https:/doi.org/10.1073/pnas.1901623116.

18. A. R. Hirsch, Nostalgia: A neuropsychiatric understanding. *ACR North American Advances* (1992).

19. X. Zhang, S. Firestein, Nose thyself: individuality in the human olfactory genome. *Genome Biol.* **8**, 230 (2007).

20. A. S. Bates, P. Schlegel, R. J. V. Roberts, N. Drummond, Complete connectomic reconstruction of olfactory projection neurons in the fly brain. *BioRxiv* (2020).

21. Y.-H. Chou, *et al.*, Diversity and wiring variability of olfactory local interneurons in the Drosophila antennal lobe. *Nat. Neurosci.* **13**, 439–449 (2010).

22. N.-F. Liou, *et al.*, Diverse populations of local interneurons integrate into the Drosophila adult olfactory circuit. *Nat. Commun.* **9**, 2232 (2018).

23. M. Fişek, R. I. Wilson, Stereotyped connectivity and computations in higher-order olfactory neurons. *Nat. Neurosci.* **17**, 280–288 (2014).

24. V. Bhandawat, S. R. Olsen, N. W. Gouwens, M. L. Schlief, R. I. Wilson, Sensory processing in the Drosophila antennal lobe increases reliability and separability of ensemble odor representations. *Nat. Neurosci.* **10**, 1474–1482 (2007).

25. S. R. Olsen, V. Bhandawat, R. I. Wilson, Divisive normalization in olfactory population codes. *Neuron* **66**, 287–299 (2010).

26. P. K. Richgels, S. M. Rollmann, Genetic variation in odorant receptors contributes to variation in olfactory behavior in a natural population of Drosophila melanogaster. *Chem. Senses* **37**, 229–240 (2012).

27. Y. Seki, J. Rybak, D. Wicher, S. Sachse, B. S. Hansson, Physiological and morphological characterization of local interneurons in the Drosophila antennal lobe. *J. Neurophysiol.* **104**, 1007–1019 (2010).

28. X. Zhang, Q. Gaudry, Functional integration of a serotonergic neuron in the Drosophila antennal lobe. *Elife* **5** (2016).

29. A. M. Dacks, D. S. Green, C. M. Root, A. J. Nighorn, J. W. Wang, Serotonin modulates olfactory processing in the antennal lobe of Drosophila. *J. Neurogenet.* **23**, 366–377 (2009).

30. T. R. Sizemore, A. M. Dacks, Serotonergic Modulation Differentially Targets Distinct Network Elements within the Antennal Lobe of Drosophila melanogaster. *Sci. Rep.* **6**, 37119 (2016).

31. B. Roy, *et al.*, Metamorphosis of an identified serotonergic neuron in the Drosophila olfactory system. *Neural Dev.* **2**, 20 (2007).

32. H. G. Ruhé, N. S. Mason, A. H. Schene, Mood is indirectly related to serotonin, norepinephrine and dopamine levels in humans: a meta-analysis of monoamine depletion studies. *Mol. Psychiatry* **12**, 331–359 (2007).

33. K. Vogt, *et al.*, Internal state configures olfactory behavior and early sensory processing in Drosophila larva. *bioRxiv*, 2020.03.02.973941 (2020).

34. T. Hige, Y. Aso, M. N. Modi, G. M. Rubin, G. C. Turner, Heterosynaptic Plasticity Underlies Aversive Olfactory Learning in Drosophila. *Neuron* **88**, 985–998 (2015).

35. K. S. Honegger, R. A. A. Campbell, G. C. Turner, Cellular-resolution population imaging reveals robust sparse coding in the Drosophila mushroom body. *J. Neurosci.* **31**, 11772–11785 (2011).

36. L. Rath, C. Giovanni Galizia, P. Szyszka, Multiple memory traces after associative learning in the honey bee antennal lobe. *Eur. J. Neurosci.* **34**, 352–360 (2011).

37. T. Zars, R. Wolf, R. Davis, M. Heisenberg, Tissue-specific expression of a type I adenylyl cyclase rescues the rutabaga mutant memory defect: in search of the engram. *Learn. Mem.* **7**, 18–31 (2000).

38. G. U. Busto, I. Cervantes-Sandoval, R. L. Davis, Olfactory learning in Drosophila. *Physiology* **25**, 338–346 (2010).

39. A. Claridge-Chang, *et al.*, Writing memories with light-addressable reinforcement circuitry. *Cell* **139**, 405–415 (2009).

40. Y.-C. Kim, H.-G. Lee, K.-A. Han, D1 dopamine receptor dDA1 is required in the mushroom body neurons for aversive and appetitive learning in Drosophila. *J. Neurosci.* **27**, 7640–7647 (2007).

41. C. Arican, J. Bulk, N. Deisig, M. P. Nawrot, Cockroaches show individuality in learning and memory during classical and operant conditioning. *bioRxiv*, 825265 (2019).

42. L. Li, *et al.*, A possible structural correlate of learning performance on a colour discrimination task in the brain of the bumblebee. *Proc. Biol. Sci.* **284** (2017).

43. J. Haenicke, N. Yamagata, H. Zwaka, M. Nawrot, R. Menzel, Neural Correlates of Odor Learning in the Presynaptic Microglomerular Circuitry in the Honeybee Mushroom Body Calyx. *eNeuro* **5** (2018).

44. D. R. Stronck, The educational implications of human individuality. *Am. Biol. Teach.* **42**, 146–151 (1980).

45. A. Izquierdo, J. D. Jentsch, Reversal learning as a measure of impulsive and compulsive behavior in addictions. *Psychopharmacology* **219**, 607–620 (2012).

46. Q. Ren, H. Li, Y. Wu, J. Ren, A. Guo, A GABAergic inhibitory neural circuit regulates visual reversal learning in Drosophila. *J. Neurosci.* **32**, 11524–11538 (2012).

47. Y. Wu, Q. Ren, H. Li, A. Guo, The GABAergic anterior paired lateral neurons facilitate olfactory reversal learning in Drosophila. *Learn. Mem.* **19**, 478–486 (2012).

48. B. R. Foley, P. Marjoram, S. V. Nuzhdin, Basic reversal-learning capacity in flies suggests rudiments of complex cognition. *PLoS One* **12**, e0181749 (2017).

49. N. Mancini, *et al.*, Reversal learning in Drosophila larvae. *Learn. Mem.* **26**, 424–435 (2019).

50. K. P. Siju, V. Stih, S. Aimon, J. Gjorgjieva, R. Portugues, Valence and state-dependent population coding in dopaminergic neurons in the fly mushroom body. *bioRxiv* (2019).

51. R. L. Davis, Mushroom bodies and Drosophila learning. *Neuron* **11**, 1–14 (1993).

52. H. Qin, *et al.*, Gamma neurons mediate dopaminergic input during aversive olfactory memory formation in Drosophila. *Curr. Biol.* **22**, 608–614 (2012).

53. C. Brandes, R. Menzel, Common mechanisms in proboscis extension conditioning and visual learning revealed by genetic selection in honeybees (Apis mellifera capensis).

Journal of Comparative Physiology A **166**, 545–552 (1990).

54. C. D. O. Beck, B. Schroeder, R. L. Davis, Learning Performance of Normal and MutantDrosophila after Repeated Conditioning Trials with Discrete Stimuli. *J. Neurosci.* **20**, 2944–2953 (2000).

55. J. Duncan, *et al.*, A neural basis for general intelligence. *Science* **289**, 457–460 (2000).

56. K. Banerjee, *et al.*, General intelligence in another primate: individual differences across cognitive task performance in a New World monkey (Saguinus oedipus). *PLoS One* **4**, e5883 (2009).

Page was left intentionally blank

Chapter I: Idiosyncratic neural coding and neuromodulation of olfactory individuality in *Drosophila*

Abstract

Innate behavioral biases and preferences can vary significantly among individuals of the same genotype. Though individuality is a fundamental property of behavior, it is not currently understood how individual differences in brain structure and physiology produce idiosyncratic behaviors. Here we present evidence for idiosyncrasy in olfactory behavior and neural responses in *Drosophila*. We show that individual female *Drosophila* from a highly inbred lab strain exhibit idiosyncratic odor preferences that persist for days. We used *in vivo* calcium imaging of neural responses to directly compare projection neuron (second-order neurons that convey odor information from the sensory periphery to the central brain) responses to the same odors across animals. We found that, while odor responses appear grossly stereotyped, upon closer inspection, many individual differences are apparent across antennal lobe (AL) glomeruli (compact microcircuits corresponding to different odor channels). Moreover, we show that neuromodulation, environmental stress in the form of altered nutrition, and activity of certain AL local interneurons affect the magnitude of inter-fly behavioral variability. Taken together, this work demonstrates that individual *Drosophila* exhibit idiosyncratic olfactory preferences and idiosyncratic neural responses to odors, and that behavioral idiosyncrasies are subject to neuromodulation and regulation by neurons in the AL.

Introduction

Individuality is a fundamental feature of behavior. For instance, the same smell or song may evoke very different responses in two individuals. What is the biological basis for these differences? While behavioral differences must originate with differences in neural activity, little is known

about how idiosyncratic behavioral differences are reflected in neural activity. We used statistical behavioral analysis and live brain imaging to assess idiosyncratic odor responses in fruit flies, and found that the same odors produce different behavioral responses across flies and that these odors evoke subtly different patterns of brain activity across flies. Moreover, neuromodulators and sets of neurons in the olfactory region of the fly's brain directly modulate the degree of fly-to-fly variability in a flexible way.

Olfaction is a deeply personal sense. We know from common experience that smells elicit strong reactions linked to both past experiences and the perceptual qualities of the odors themselves. Behavioral reactions to an odor (e.g., durian or gasoline) can vary greatly among individuals, evoking responses that can range from attraction to utter aversion, but the mechanisms by which volatile molecules are mapped into perceptual space [1-3] and drive behavior are not well understood. In humans, both socio-cultural experience [4-6] and genetic polymorphisms in odorant receptors [7,8] have been shown to explain some individual variation in odor perception. For example, people with hypomorphic receptor mutations experience anosmias for specific odors [9]. Presumably, such alterations in sensory detection affect downstream neural responses, and thus odor perception, but currently little is known about how this idiosyncrasy manifests in the activity of deeper neural circuits.

A major obstacle to studying idiosyncrasy in neural circuit stimulus responses is the need to identify corresponding circuit elements across individuals. This is difficult in large organisms with complex, redundant neural circuits, where individual neurons are not identifiable, i.e., directly comparable across individuals. Moreover, testing hypotheses about the involvement of specific circuit components in shaping the distribution of behavioral responses across individuals requires

large sample sizes (often hundreds of individuals, because precisely measuring a distribution requires measuring rare individuals in its tails). This requirement alone largely precludes the use of mammals, or other large vertebrates, to study these effects.

We addressed these challenges by leveraging the identifiable and grossly stereotyped neuroanatomy of the antennal lobe (AL) of the fruit fly, *Drosophila melanogaster*. The *Drosophila* AL has around 50 identifiable odor-coding channels, which are arranged into spatially distinct glomeruli [10-12]. The glomeruli are stereotyped with respect to their sensory neuron inputs, shape and size, and efferent innervation by extrinsic projection neurons (PNs) that convey odor information deeper into the brain [13-15]. Overlaid on this coarse stereotypy, however, is a complex network of AL local neurons (LNs) providing dense inter-glomerular connections [16,17]. The roles of LNs in tuning AL odor responses are diverse [16-19] and may offer several mechanisms for diversifying individual odor responses in the AL. In one study of the morphology of singly-labeled LNs, there were far more anatomical classes of LNs across individuals than there are LNs per hemisphere in an individual fly [16], implying that the complement of LNs in each fly is unique to that individual.

Individuality in *Drosophila* behavior has been observed in phototaxis [20], spontaneous locomotor biases [21], thermal preference [22], spontaneous microbehaviors [23,24], and object-fixated locomotion [25]. These differences persist over days and represent something like fly personality. Individual behavioral outcomes likely have a partial origin in stochastic events during development [26], and genetic factors determine the magnitude of behavioral variability in isogenic populations [27]. Additionally, post-developmental activity of specific neural circuits also

tunes individuality, meaning it is potentially under the real-time control of the nervous system [20,21]. It is likely that these factors are at work in regulating individual odor preferences, but the extent of individuality of odor coding — whether individual nervous systems represent the same stimulus in the same way — has not been examined in this context. Using an automated odor-preference assay, we measured significant individuality in odor preference that was stable across days. Using volumetric two-photon microscopy, we observed individuality in the representation of odors in the AL. Pharmacological and thermogenetic experiments established that multiple LN subsets and neuromodulatory axes affect odor preference individuality, forming a circuit with the potential to dynamically tune odor preference variability in response to environmental cues.

Results

To determine whether individual flies exhibit idiosyncratic odor behaviors, we built an instrument to simultaneously measure the odor preference of 15 isolated flies (Fig 1A). In this rig, where each fly moves freely through a linear corridor in which two odor stimuli are pumped [28]. The airflow bearing these odor cues is laminar, forming a sharp boundary between the two odor compartments at the middle of the corridor that vent to the room (Fig 1B and S1A). Each experiment consisted of a three minute "pre-odor period" in which filtered, dehumidifiedclean air was pumped into both compartments followed by a three minute "odor-choice period" when alternative odor stimuli filled each half of each arena, lastly followed by a 30 second "post-odor period" of filtered, dehumidifiedclean air (Fig 1C).

In this setup, flies expressed olfactory preference by walking into, and staying in their preferred odor compartment (Fig 1C). Flies were tracked with computer vision and preference was quantified as the fraction of time each fly spent in a compartment. For example, in experiments where flies chose between odorants 3-octanol (OCT) and 4-methylcyclohexanol (MCH), preference was quantified as the proportion of time in OCT (with 0/1 indicating a complete preference for MCH/OCT respectively). In a clear sign that flies express odor preference in this assay, we observed that they frequently turned around at the compartment boundary (Fig S1B) when odors were present, while far fewer reversals occurred in the absence of odor (Fig 1C). The frequency of these reversals decreased over the three minute odor-choice period, presumably as flies adapt/habituate to the stimuli. Thus, the odor-choice period and our quantification of preference were limited to three minutes. We observed a broad distribution of odor preference scores in OCT-MCH choice experiments among highly inbred wild type (iso^{KH11} strain; see Methods) females, reared in the same environment. Indeed, the observed distribution was broader than expected under a null model in which all animals sample their odor-choice behavior from the same distribution (Fig 1D; $p<0.001$). Even in such "all flies are identical" scenarios, one would still observe apparent variation in the measured preference scores because we are only able to assess odor choices over a three minute window. That the observed distribution is broader than this null distribution (dashed lines in Fig 1D, F) indicates that flies are behaving idiosyncratically. Additionally, the observed distribution of preference scores was broader than the distribution of "sham" scores calculated from the pre-odor period (gray lines in Fig 1D), whose dispersion reflects individual variability in locomotion and sampling error (Fig S1C, D) but not responses to odors. We quantified this difference in variance between the observed and null behavioral distributions as an "Individuality score" (IS), which, at 0.0174 for the OCT-MCH choice, was significantly

greater than 0 (p<0.001; See Methods). Beyond the pair of aversive odorants OCT and MCH, we also observed idiosyncratic odor preferences in experiments in which flies chose between filtered, dehumidified clean air and odorants 3-octanol (Fig 1F, left; IS=0.0047, p<0.001), 1-butanol (Fig 1F, middle; IS=0.012, p<0.001), and 2-heptanone (Fig 1F, right; IS=0.015, p<0.001). Importantly, we also confirmed that idiosyncratic preferences persist across days (Fig 1G), as observed for other idiosyncratic fly behaviors [20-22,27]. Retesting flies' odor preference within less than 10 minutes after their initial testing (Fig S1F, r=0.23, p<0.05) yields a trial-to-trial correlation that is lower than retesting after waiting 24 hours. Retesting flies' odor preferences 3 hours after initial testing shows trial-to-trial correlation values that are similar to retesting after 24 hours (Fig S1G, r=0.35, p<0.001). We've evaluated the odor preference of flies up to 96 hours after initial testing, which still yields significant trial-to-trial correlation (Fig S1H).

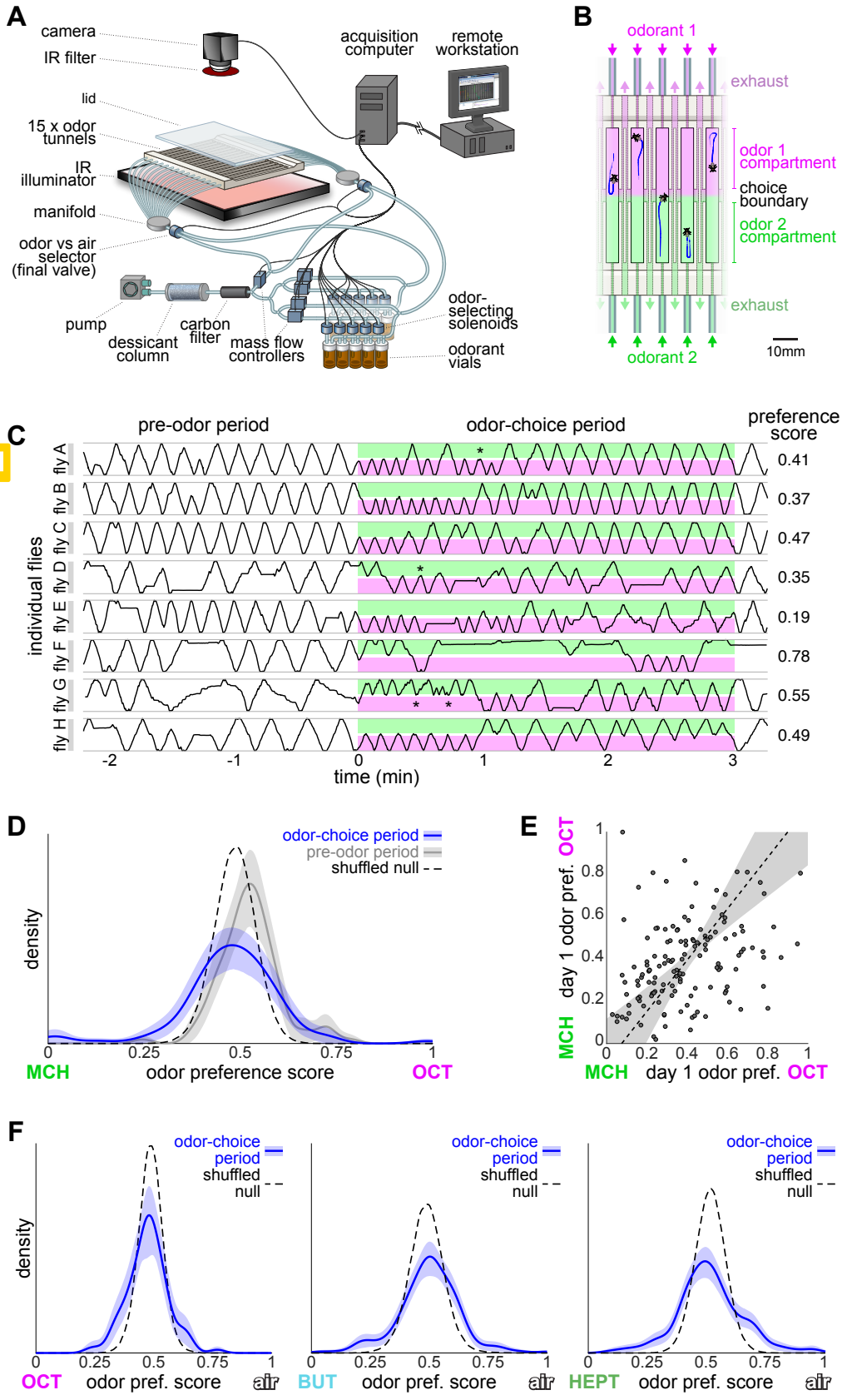

A
camera
IR filter
lid
15 x odor tunnels
IR illuminator
manifold
odor vs air selector (final valve)
pump
dessicant column
carbon filter
mass flow controllers
acquisition computer
remote workstation
odor-selecting solenoids
odorant vials
B
odorant 1
exhaust
odor 1 compartment
choice boundary
odor 2 compartment
exhaust
odorant 2
10mm
C
pre-odor period
odor-choice period
preference score
individual flies
fly A
fly B
fly C
fly D
fly E
fly F
fly G
fly H
0.41
0.37
0.47
0.35
0.19
0.78
0.55
0.49
-2
-1
0
1
2
3
time (min)
D
odor-choice period
pre-odor period
shuffled null
density
0
0.25
0.5
0.75
1
MCH
odor preference score
OCT
E
OCT
day 1 odor pref.
MCH
0
0.2
0.4
0.6
0.8
1
MCH
day 1 odor pref.
OCT
F
odor-choice period
shuffled null
density
OCT
odor pref. score
air
BUT
odor pref. score
air
HEPT
odor pref. score
air

Fig 1 - Individual flies have idiosyncratic odor preferences A) Schematic of the odor-preference experimental apparatus. See Methods. **B)** Schematic of the linear behavioral arenas, into either half of which air odorized with an arbitrary odorant flows. See Methods and Fig S1. Flies typically walk back and forth in these arenas, and the fraction of time spent in a reference odor compartment is their preference score. **C)** Kymographs showing the position in eight individual flies in eight arenas over time. Color blocks indicate the three minute odor-choice period when the two odors, OCT (magenta) and MCH (green), were delivered. Corresponding preference scores are given at right. **D)** Distribution of OCT-MCH preference scores across isogenic wild type animals (iso^{KH11}; see methods). Blue line is the kernel-density estimate of the distribution during the odor-choice period, with shaded area the 95% CI as determined by bootstrapping. Gray line is the kernel-density estimate during the pre-odor period. Dotted-line distribution indicates the distribution expected under the null hypothesis that all flies exhibit behavior drawn from identical distributions. See Methods. The observed distribution is significantly broader than the null distribution ($p<0.001$; by bootstrap resampling). **E)** Scatter plot of individual OCT-MCH odor preferences on day 1 vs day 2. These are significantly correlated ($r=0.35$; $p<0.0001$) indicating that individual odor preferences are stable over days. Line is the best linear fit. Shaded region is the 95% CI of the linear fit. **F)** Distribution of OCT-, 1-butanol- (BUT), and 2-heptanone- (HEPT) vs-air preference scores. Plot elements as in (D). Bootstrapped *p*-values comparing null and observed distributions were all<0.001.

Idiosyncratic behavior presumably has a basis in idiosyncratic patterns of odor-induced neural activity. We hypothesized that such response idiosyncrasies might be observable in the sensory periphery of the olfactory circuit, specifically in the glomeruli of the antennal lobe (AL). To test this hypothesis, we built a stage for delivering the same odorant stimuli from our behavioral instrument to flies being imaged for Ca^{++} activity with a 2-photon microscope (Fig 2A). For each experiment, we stimulated flies with three panels odors (Fig 2B). In the first two panels, 12 different odorants were delivered for 4 seconds each, with a ~80s pause between odors, in a random order. In the third panel, OCT and MCH were delivered in alternation up to 5x times each, with the same timing, starting randomly with OCT or MCH. We took 24 second volumetric recordings across AL glomeruli at ~0.8Hz, acquiring GCaMP6m signal from dendrites of Projection Neurons (PNs; Fig 2C) expressing GH146-Gal4.

As expected, we observed a variety of Ca++ responses in PN dendrites (Fig 2D, E and S2), including excitatory and inhibitory responses to both odor onset and odor offset. As expected, the exact responses depended on the glomerulus (Fig 2D) and the odor (Fig 2E). To characterize the population responses in PNs to each odor, we systematically compared odor responses across many glomeruli using a semi-automated pipeline (see Supplemental Methods) for assigning glomerular labels to recording voxels (Fig 2F-H). Due to variation in transgene expression and mounting geometry, we were not able to identify every glomerulus in every animal. But, we were able to efficiently characterize the odor responses of dozens of animals, to a dozen odors, in 3 to 15 glomeruli (mean=10; Fig S2).

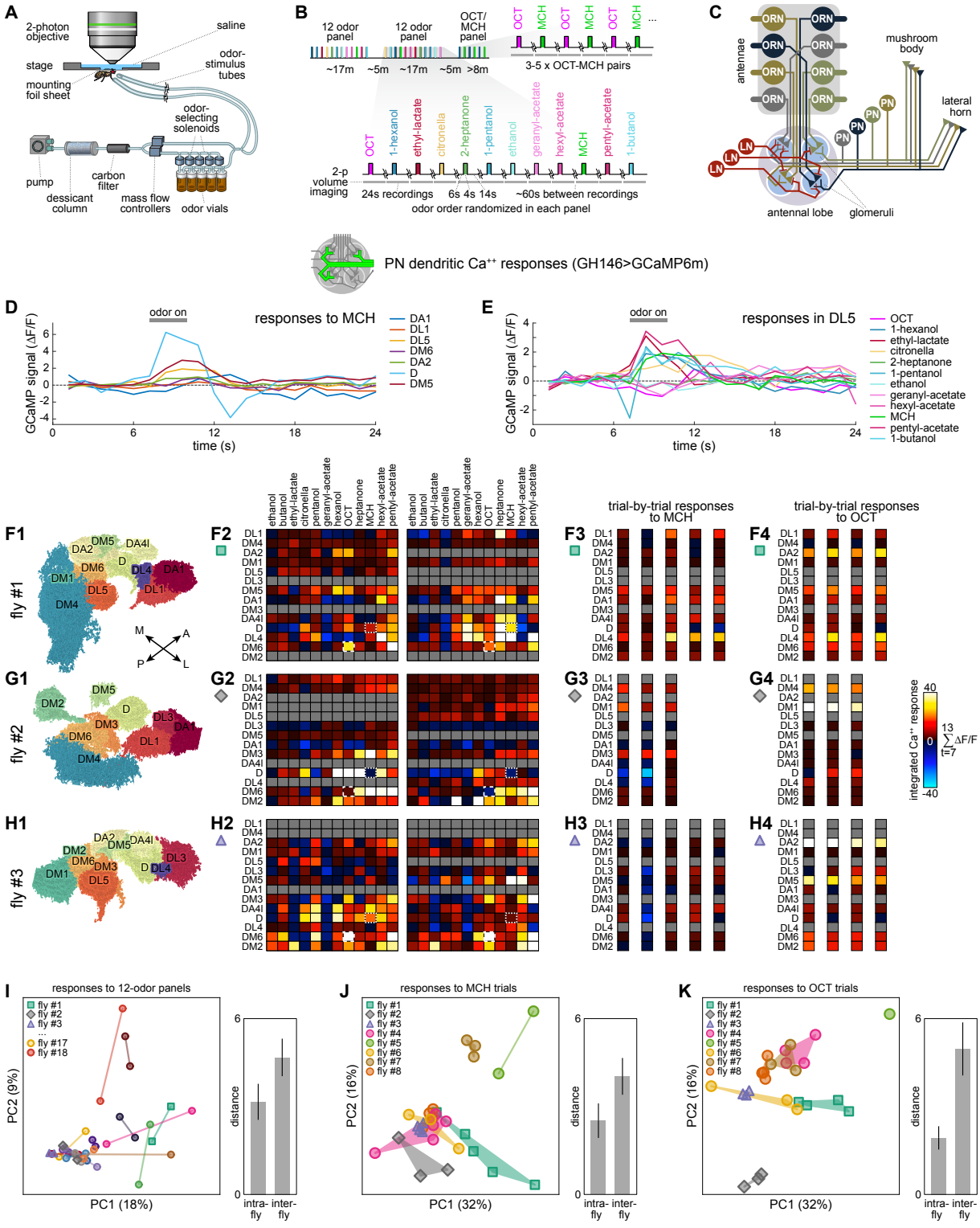

A
2-photon objective
saline
stage
odor-stimulus tubes
mounting foil sheet
odor-selecting solenoids
pump
carbon filter
dessicant column
mass flow controllers
odor vials
B
12 odor panel
12 odor panel
OCT/MCH panel
OCT MCH OCT MCH OCT MCH ...
~17m ~5m ~17m ~5m >8m
3-5 x OCT-MCH pairs
OCT 1-hexanol ethyl-lactate citronella 2-heptanone 1-pentanol ethanol geranyl-acetate hexyl-acetate MCH pentyl-acetate 1-butanol
2-p volume imaging
24s recordings 6s 4s 14s ~60s between recordings
odor order randomized in each panel
C
antennae
ORN
mushroom body
lateral horn
PN
LN
antennal lobe
glomeruli
PN dendritic Ca++ responses (GH146>GCaMP6m)
D
odor on
responses to MCH
GCaMP signal (ΔF/F)
time (s)
DA1 DL1 DL5 DM6 DA2 D DM5
E
odor on
responses in DL5
GCaMP signal (ΔF/F)
time (s)
OCT 1-hexanol ethyl-lactate citronella 2-heptanone 1-pentanol ethanol geranyl-acetate hexyl-acetate MCH pentyl-acetate 1-butanol
F1
fly #1
G1
fly #2
H1
fly #3
M A P L
F2 G2 H2
ethanol butanol ethyl-lactate citronella pentanol geranyl-acetate hexanol OCT heptanone MCH hexyl-acetate pentyl-acetate
F3 G3 H3
trial-by-trial responses to MCH
F4 G4 H4
trial-by-trial responses to OCT
integrated Ca++ response
40
0
-40
13 ∑ ΔF/F t=7
I
responses to 12-odor panels
fly #1 fly #2 fly #3 ... fly #17 fly #18
PC2 (9%)
PC1 (18%)
distance
intra-fly inter-fly
J
responses to MCH trials
fly #1 fly #2 fly #3 fly #4 fly #5 fly #6 fly #7 fly #8
PC2 (16%)
PC1 (32%)
distance
intra-fly inter-fly
K
responses to OCT trials
fly #1 fly #2 fly #3 fly #4 fly #5 fly #6 fly #7 fly #8
PC2 (16%)
PC1 (32%)
distance
intra-fly inter-fly

Fig 2 - Individual flies have idiosyncratic odor Ca^{++} responses in the antennal lobe. A) Schematic of the odor response volumetric imaging set-up. See Methods. **B)** Schematic of the odor stimuli delivered during an imaging session. The order within each 12 odor panel is randomized and each odor was presented for 6 seconds. The identity of the first odor in the OCT/MCH panel is randomized for each trial. OCT-MCH pairs were repeated up to five times. **C)** Schematic of the olfactory circuitry from the olfactory receptor neurons (ORNs) to projection neurons (PNs), which bear odor information to the central brain. LNs are local neurons: predominantly inhibitory interneurons that connect many different sets of glomeruli and inhibit both PNs and LNs. **D)** Ca^{++} responses vs time of seven semiautomatically-segmented glomeruli responding to a pulse of MCH. **E)** Ca^{++} responses vs time of the DC3 glomerulus to the 12 odors of the stimulus panel. **F)** Ca^{++} from one fly (fly #1). F1) Semiautomatically-segmented glomeruli of the antennal lobe. See Methods. Glomerular identity was assigned manually based on the morphology of the glomeruli. F2) Integrated Ca^{++} responses to each odor (columns) of each glomerulus (rows). Two matrices correspond to the two 12-odor panels. Grey cells indicate missing data. Cells with dotted and dashed borders show consistency intra-fly and divergence inter-fly (compare with cells in G and H). F3) Glomerular responses, as in F2, to the MCH trials of the OCT-MCH panel. Colored symbol indicates these data in J) and K). F4) As in F3) but for responses to MCH. Panels F, G and H share the color axis. **G)** As in F), but for fly #2. **H)** As in F), but for fly #3. **I)** Principal components 1 and 2 of individual 12 odor panel responses in the space consisting of odor-glomeruli responses (i.e., the 15 glomerulus x 12 odor=600 dimensional space in which the two matrices of F2 are two data points). Lines connect the two points corresponding to the two 12-odor panels of each fly. Right: average distance among intra-fly trials and inter-fly trials. Bars are +/-SEM calculated by 20,000-replicate bootstrap resampling of individuals. p=0.012 by one-tailed resampling of individual flies. **J)** As in I), but for responses to MCH (projected from the 15 dimensional space in which each column in F3,4 is a data point). Shaded regions are convex hulls containing all the trials from each fly. p=0.002 for intra- vs inter-fly distance comparison. **K)** As in J), but for responses to OCT. Shaded regions are convex hulls containing all the trials from each fly. $p<0.001$ for intra- vs inter-fly distance comparison.

Immediately, we noticed that the responses of some glomeruli were very different across individuals, while appearing consistent across multiple presentations of the odorant within an individual (Fig 2F2-H2). To assess this systematically, we projected the multidimensional glomerulus-odor responses onto their first two principal components (Fig 2I; See S3 for eigenvalues and odor response covariance), where we observed that within-fly responses (i.e., across presentations) were, on average, closer than between-fly responses ($p<0.001$ by bootstrap resampling). This was also true when we examined the responses of OCT and MCH specifically in the space of responses to the OCT/MCH stimulus panel (Fig 2J,K; $p<0.001$ and $p<0.01$,

respectively). Separately, we confirmed that this pattern was not an artifact of in-filling missing data for the PCA, as it was also observed in smaller data sets with no missing data (Fig S4). Thus, neural responses to odors appear to differ significantly across individuals. We assessed whether we can maximize the individuality of flies' responses by selecting for PCs that impart the largest ratio in-terms of the mean inter-fly distance over intra-fly distance in space of responses (Fig S5A). We selected the two PCs (PC1 and PC5) with the highest individuality ratio to project responses onto (Fig S5B). We then assessed whether specific glomerulus-odor combinations may impart more or less individuality than the mean. We calculated the mean ratio of inter-fly over intra-fly distance across all flies in the full space of responses for each odor-glomerulus pair (Fig S5C). We used the same method to calculate whether specific odors (Fig S5D) or specific glomeruli (Fig S5E) impart more or less individuality. It was previously shown that neuromodulators, specifically serotonin, affect the degree of idiosyncrasy in phototaxis behavior [20]. We tested whether neuromodulatory pathways also had an effect on individual odor preferences. We first examined the role of serotonin by feeding flies increasing doses of the serotonin synthesis inhibitor alpha-methyltryptophan (α-MW; 20 or 40mM; [29]). Flies fed α-MW appeared to show a dose-dependent reduction in variability compared to control flies. By contrast, feeding with the serotonin precursor 5-hydroxytryptophan (5-HTP; [29]) had little effect (Fig 3A). While dopamine pharmacological experiments had no effect on phototactic idiosyncrasy [14], the key role of dopamine in olfactory associative conditioning in the mushroom bodies [30,31], led us to hypothesize that opamine may be essential to tune individual odor preferences in an experience-dependent fashion (even in the absence of structured associative training). Flies bearing a mutant allele of the *Dop1R1* dopamine receptor gene (*Dop1R1*^{f02676}, hereafter "*Dop1R1*" [31,32]), also exhibited lower idiosyncrasy (narrower behavioral distributions) than control flies (Fig 3B).

Conversely, flies fed the dopamine precursor L-DOPA [30,31] exhibited higher idiosyncrasy. The lower idiosyncrasy of *Dop1R1* is not explained by anosmia, as these flies exhibited reversal behaviors at the odor boundary during the odor-choice period (Fig S6).

In conducting these experiments, we realized that our experimental manipulations changed not only the apparent variability of behavior, but also its mean, and for our choice of odor preference metric, the mean and variance are coupled. We also suspected that seasonal effects, such as those that affect insect olfactory conditioning [33] might also affect our measured preferences and variabilities. Indeed, variability was higher in the winter — an effect that could be modeled as a linear function of Boston outdoor air temperatures (despite experimental flies being grown in temperature/humidity-controlled incubators and tested in environmental-control rooms; Fig S7A-D). Moreover, we had more confidence in our measure of some individuals' preferences than others — it is hard to characterize the preference of flies that don't walk much in the arenas.

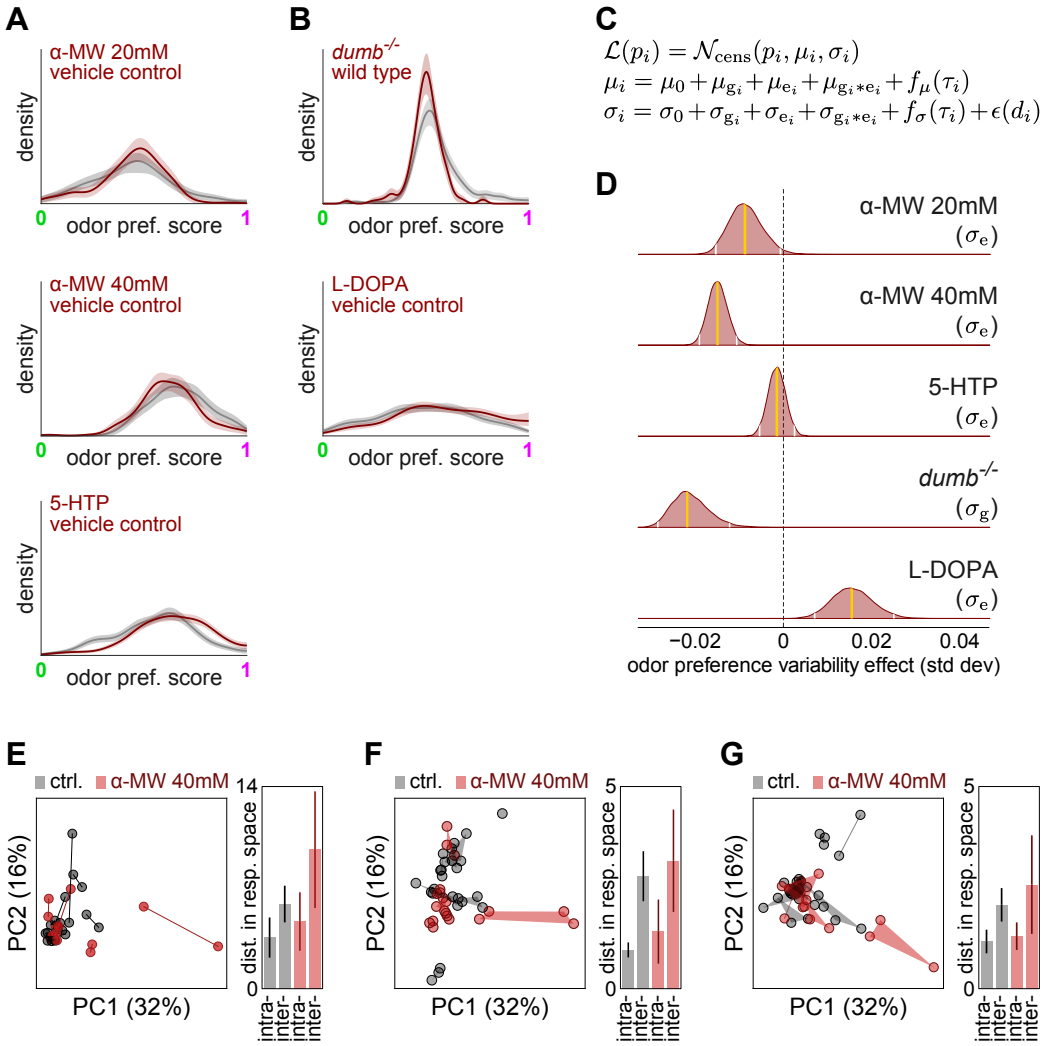
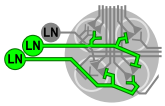


Fig 3 - Neuromodulation of behavioral individuality. A) Representative experimental distributions of OCT-MCH preference scores across isogenic wild type animals in control conditions (gray) and fed pharmacological manipulators of serotonin levels (brown). Lines are kernel density estimates of the distributions; shaded areas are the 95% CIs of the density estimates as determined by bootstrapping. Experiments: flies fed 20mM α-MW for three days (top), 40mM α-MW for three days (middle) and 50mM 5-HTP for three days (bottom). **B)** As in A) for manipulations of dopamine signaling. Top: *Dop1R1*^{f02676} and a genetic control. Bottom: observed distributions for flies fed 5mg/mL L-DOPA or vehicle control for three days. **C)** Model used to estimate the effects on odor preference variability of neuromodulation manipulations. See Methods for full explanation. **D)** Posterior distributions on the model parameters associated with each neuromodulator manipulation. Gold lines indicate the mean of the posterior, and white lines the edges of the 95% credible interval. Posterior distributions heavily overlapping 0 (dotted line) indicate no effect.

We implemented a Bayesian linear modeling framework (Fig 3C) to estimate and control for each of these effects, disentangle the coupling of mean and variance, and assign more weight to inferences based on flies that were active and expressed preference more clearly. See Methods for details and Supplemental Table S1 for effects of experimental factors on various locomotor measures. The output of this analysis was posterior distributions for each parameter of the model (Fig S7E), and we were particularly interested in the posterior distributions on the variance effects of genotype, experimental condition, and genotype-by-experimental condition parameters corresponding to our neuromodulatory manipulations (Fig 3D). Consistent with our observations of single experiments, we found that 5-HTP has no strong effect on variability, while α-MW had a substantial negative, dose-dependent effect (i.e., 0 was above the 95% credible interval for the α-MW effect parameters). Additionally, *Dop1R1* mutation reduced variability substantially, while L-DOPA increased it. We also imaged Ca++ responses in PN dendrites of flies that had been fed α-MW and controls (Fig S8). We again saw the signal of idiosyncratic neural coding (greater between-fly than within-fly distances; Fig S4B, S9A-G), but no significant difference between α-MW-fed and controls (though intra- and inter-fly distances were generally greater in α-MW-fed flies). We confirmed that the drug supplements of 5-HTP or α-MW feeding did increase and decrease, respectively, serotonin concentration in fly heads (Fig S10A), and L-DOPA feeding increased dopamine concentration (respectively) in fly heads (Fig S10B) through using serotonin and dopamine ELISA assays. To evaluate the stability of the drug effect on behavior we fed flies 5-HTP supplemented food for 72 hours, evaluated initial odor preference then retested odor preference after 24 hours on 5-HTP, and found significant correlation between trials (Fig S10C).

Next, we sought to examine the neural circuit basis of the modulatory effects on behavioral variability. We used thermogenetic effectors to activate or inhibit circuit elements within the olfactory system, and recorded the odor preferences of many individuals subject to this manipulation (Fig 4A,B). First we targeted the contralateral serotonin-immunoreactive deutocerebral neurons (CSD; [34]) using two Gal4 lines. These serotonin-positive neurons have post-synaptic compartments distributed widely across the olfactory system and project axons into the AL contralateral to their cell body. Applying a Bayesian framework to infer the effects of these thermogenetic manipulations (Fig 4D; S19), we found that activating CSD neurons with dTRPA1 (an effector that depolarizes neurons at high temperatures; [35]) had no effect on variability (Fig 4E).



thermogenetic manipulation
of LNs and other
modulatory neurons

D

$$\mathcal{L}(p_i) = \mathcal{N}_{\text{cens}}(p_i, \mu_i, \sigma_i)$$
$$\mu_i = \mu_0 + \mu_{g_i} + \mu_{e_i} + \mu_{g_i * e_i} + f_\mu(\tau_i)$$
$$\sigma_i = \sigma_0 + \sigma_{g_i} + \sigma_{e_i} + \sigma_{g_i * e_i} + f_\sigma(\tau_i) + \epsilon(d_i)$$

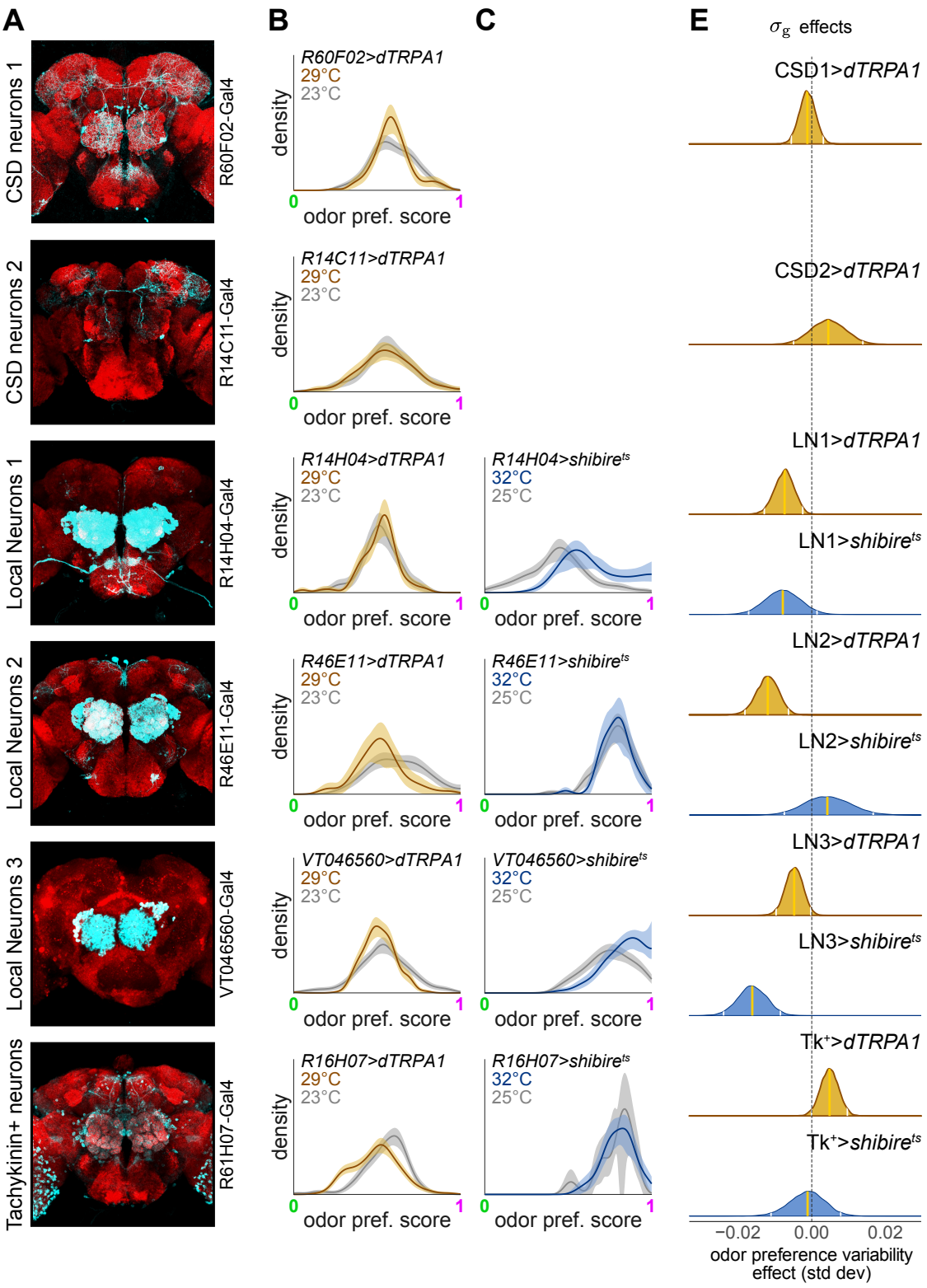


Fig 4 - Local neurons in the antennal lobe modulate individuality of odor preference. A) Confocal micrographs of expression patterns targeting the serotonin-immunoreactive CSD neurons, three different populations of local neurons and tachykinin-positive neurons. Red background stain is anti-nc82 staining synaptic active. (The red channel of the VT046560 image is also stained for anti-DLG [56].) Cyan is mCD8-GFP [57] driven by the Gal4 line denoted. Images of all Janelia FlyLight Gal4 lines (all images except that of VT046560) reproduced and modified with permission from the Janelia FlyLight team. **B)**Kernel density estimates of the distribution of OCT-MCH preference scores for transgenic animals expressing the thermogenetic activator *dTRPA1*. Gray distributions are at the permissive temperature (23°C). Gold distributions are at the restrictive temperature (29°C). **C)** As in B), but for animals expressing *Shibire^{ts}* at permissive (25°C; gray) and restrictive temperatures (32°C; blue). **D)** Model used to estimate the effects on odor preference variability of these neural circuit manipulations. The terms of the model are the same as in Fig 3C. Here, the experimental condition terms (*e*) refers to the temperature of the experimental room, and the genotype terms (*g*) account for animals of the background genotype (iso^{KH11}), parental genotype controls (*Gal4*/+, *UAS-shibire^{ts}*/+ and *UAS-dTRPA1*/+), and experimental F_1s (*Gal4*/*UAS-shibire^{ts}* and *Gal4*/*dTRPA1*). The *g*e* term accounts for the thermogenetic interaction of F_1 genotypes and temperature. **E)** Posterior distributions of the effect on odor preference variability of silencing (blue) or activating (gold) neurons expressed in each Gal4 line using *shibire^{ts}* or *dTRPA1*, respectively. Gold lines indicate the mean of the posterior, and white lines the edges of the 95% credible interval. Posterior distributions heavily overlapping 0 (dotted line) indicate no effect.

While acutely activating CSD may not have an effect on variability, the AL local neurons (LNs) express multiple serotonin receptors [26], and are potential regulators of variability as they have highly variable morphology across individuals [16,36]. We found that activating or inhibiting different populations of LNs often had the effect of reducing behavioral variability. Specifically, the following genotypes had variance-reducing effects at the induced temperature: *R14H04>dTRPA1*, *R14H04>Shibire^{ts}* (probably), *R46E11>dTRPA1*, *VT046560>dTRPA1*, and *VT046560>Shibire^{ts}*. (The Shibire^{ts} effector blocks vesicular release at the restrictive temperature [37].) These Gal4 lines express in different subsets of LNs of varying size and, presumably, varying physiology. Overall, normal neuronal activity in LNs appears to be required acutely for normal levels of behavioral variability. Lastly, we manipulated the activity of tachykinin-expressing (Tk+) neurons (using the R61H07 Gal4 line [38]), which overlap with a specific subset of LNs. We found that activating Tk+ cells with dTRPA1 probably increased variability, while

silencing them had no effect. Thus, the effect of thermogenetically perturbing Tk+ cells appears to be inconsistent with the variability-reducing effect of perturbing LNs. Neuromodulatory dynamics in the AL have been previously implicated in changing odor-induced responses in a satiety-dependent manner [34]. We hypothesized that subjecting flies to environmental stress by switching them from our standard food to a different formulation might induce an increase in behavioral variability, potentially as a bet-hedging response (i.e., when the environment fluctuates, diversify stimulus responses to increase the chance that some individuals implement behaviors suitable to the new environment; [22]). We reared flies on freshly prepared cornmeal/dextrose food before giving them a "food shock" by switching them onto reconstituted flake food (Formula 4-24 from Carolina Biological Supply) for one day. As controls, we switched them to fresh standard food and, alternatively, fed them chronically (for three days) on flake food. These manipulations had significant effects on the mean preference in an OCT-MCH choice assay, but also showed higher variability in the food shock condition (Fig S13A). We used our modeling framework to disentangle (Fig S13B) these effects, and found that food shock increased variability substantially (Fig S13C). In contrast, flies chronically fed on F4-24 flake food since eclosion showed lower variability than controls. Feeding the flies α-MW partially blocked the effects of the food shock, reducing odor preference variability, consistent with our earlier pharmacological experiments (Fig 3A,D).

Discussion

Odors evoke highly individualized perceptions in humans. We set out to study this in a genetic model system, where high throughput behavioral automation and circuit-mapping tools could be

brought to bear. We observed that flies exhibit persistent idiosyncratic preferences when choosing between two monomolecular odors or between an odor and air (Fig 1). The first study to use this style of odor assay reported idiosyncratic naïve odor responses [28], though other studies emphasized consistency in individual responses [39]. A challenge in our analyses was the limited window in which flies expressed an odor preference (roughly three minutes) before appearing to habituate [40] (Fig 1C). The modest day-to-day repeatability of individual odor preferences (r=0.35; Fig 1E) compared to other measures of fly personality [20-22] was likely attributable to this limitation in the amount of data we collected per fly. This constraint partly motivated our use of Bayesian modeling to assess the effects of our manipulations. Despite the well-known anatomical and functional stereotypy in the peripheral olfactory system, we observed individuality in odor coding across glomeruli of the AL (Fig 2). Some of the observed individuality of coding may be due to artifacts of dissection, mounting or variable expression of the Ca++ indicator. Still, the observation of glomerular responses to an odorant that are excitatory in one fly but inhibitory in another (and are consistent within-fly across trials) is not easily attributable to such artifacts. We imaged PN representations, which are more broadly distributed in response space than ORN representations [41], and the circuit dynamics that underlie this broadening may also contribute to distinguishing representations across individuals. Determining the significance of our observed Ca^{++} response differences may ultimately come down to predicting idiosyncratic behaviors from idiosyncratic coding, as a circuit may produce consistent outputs even with idiosyncratic internal states [42]. For now, we believe that the prevailing view that odor responses in the AL are highly stereotyped across individuals should be tempered. Neuromodulatory axes have been previously implicated as affecting the amount of behavioral variability exhibited by isogenic animals; disrupting serotonin increased variability in fly phototaxis [20], while in *C. elegans* it decreased

variability in locomotor activity [43]. Tyramine/octopamine had the opposite effect in worms, so multiple modulatory axes appear to regulate variability. Indeed, we observed that *Dop1R1* mutation strongly decreased odor preference variability (conversely, feeding flies L-DOPA increased variability; Fig 3). Inhibiting serotonin had a dose-dependent effect of decreasing variability in odor preference. The Bayesian framework we used to infer these effects also allowed us to estimate a surprising environmental effect. Odor preference variability was consistently higher in the winter (Fig S6), and this could be modeled as a linear function of the outdoor air temperature in Boston. This effect was large despite our rearing flies in temperature- and humidity-controlled incubators and measuring behavior in temperature- and humidity-controlled environmental rooms. We suspect that outdoor air temperature is only a correlate of the true seasonal cause of fluctuating variability, for which there are many possibilities including plant [44] or yeast [45] volatiles, or barometric pressure [46]. We found that acutely activating the serotonin-immunopositive CSD neurons had no effect on behavioral variability (Fig 4E), in contrast with serotonin pharmacological experiments, but consistent with a reported lack of effect on AL activity [47]. The apparent long timescale of serotonin effects on behavioral variability may reflect a role in regulating circuit structure, consistent with its role in neurodevelopment [36]. Many cell types in the AL express a diversity of serotonin receptors [26] and may be intermediary in the effect of serotonin pharmacological manipulation and behavioral variability. These include the LNs, which, when silenced or activated resulted in lower odor preference variability (Fig 4; and, presumably, a less sparse and regularized pattern of PN activity [48]). This suggests an endogenous role of increasing variability, consistent with their morphological variability across individuals [16]. These effects varied in magnitude by LN subpopulation, perhaps reflecting physiological diversity. In addition to the variability-reducing effect of perturbing LNs, we identified two other

manipulations that reduced variability: serotonin pharmacological manipulation and mutation of *Dop1R1*. These experiments suggest that the endogenous role of these factors is to increase odor preference variability across individuals. *Dop1R1* facilitates synaptic plasticity in the mushroom body in support of associative conditioning [31,49], but we found that thermogenetic manipulations of the mushroom body had no consistent effect on odor preference variability (Fig S11). So perhaps the effect of *Dop1R1* and L-DOPA is in another neuropil, such as the central complex, where it is known to modulate locomotion [50,51]. Indeed, the reversal behavior seen at the odor boundary may be supported by an idiothetic path-integration capacity likely implemented in the central complex [52-54]. Previously, we found that genetic variants [27] and circuit manipulations [8,10] tended to increase variability, as if most endogenous variability-regulating mechanisms suppress it. Here, several manipulations decreased variability, implying an endogenous role increasing variability. This could reflect a bet-hedging strategy [22,24] under the control of the nervous system. Such a strategy could respond rapidly to environmental fluctuations to diversify behavior and allow individuals to exhibit behavioral phenotypes fit for the new environment. We tested this notion by subjecting flies to a rapid change in their food, from their normal cornmeal/dextrose food to a commercial flake food on which flies grow less successfully [55]. This food shock caused an increase in odor preference variability, but only over short timescales. After three days on the flake food, variability went back down. Feeding flies serotonin synthesis inhibitor during this food shock suppressed the increase in variability (Fig 5). Taken together, these findings suggest that odor preference variability is under the acute control of several specific neuron types in the AL, and possibly elsewhere, and over longer timescales by neuromodulation. These axes of flexibility may facilitate bet-hedging strategies by which animals can respond to environmental fluctuations with adaptive changes in their behavioral diversity.

Methods

Fly care and behavior

All transgenic lines were outcrossed to a common isogenic background (iso^{KH11}) 10 generations. Flies were grown on cornmeal/dextrose food in incubators (25°C, 40% RH, 12:12h light:dark cycle) and behavior experiments were conducted on females 3-4 days post-eclosion. Flies were aspirated directly into behavioral arenas without anesthetization. Odors were delivered to each of the behavioral arena using an array of odorant vials, the flow through vialswas was set by computer-controlled solenoids and mass-flow controllers (Figs 1A, S1). Individual preference was measured as the fraction of time each individual spent in the half of the arena with a reference odor. Between day-to-day persistence experiments, flies were housed singly in Fly Plates (FlySorter, LLC).

Imaging and analysis

Flies for Ca^{++} imaging were mounted beneath a foil sheet in a custom stage. Under saline, a needle was used to remove the cuticle over the ALs. After the stage was mounted in our custom 2-photon microscope, odors were delivered to the antennae in a manner similar to the behavioral experiment (Fig 2A). GCaMP6m responses in PNs (driven by GH146-Gal4) were acquire from a volume that included all glomeruli at a rate of 0.833 Hz for 24s for each odor. For most analyses, the response of a glomerulus to a particular odorant was taken as the integrated $\Delta F/F$ for seconds 7-13 of the recording (Fig 2B, D, E).

Behavior modeling

To estimate the effects of environment (pharmacological and nutrient experiments), genotype (Dop1R1 vs wild type) and genotype-by-environment (thermogenetic circuit manipulations) on behavioral variability, we implemented three Bayesian linear models of mean and variance effects (Figs 3C, 4D, 5B). These models accounted for 1) odor preference scores being censored by their [0,1] domain, 2) odor variability changing seasonally (Fig 6) and 3) the odor preference of flies that were less active during the odor-choice period being harder to estimate. These models were fit in the Stan framework in R [58] to estimate posterior distributions on each effect, using weakly informative priors estimated with preliminary experiments.

Pharmacology

Flies fed manipulators of serotonin and dopamine signaling were placed on cornmeal/dextrose media or F4-24 flake food that was made fresh for each experiment by melting the media and mixing it with stock drug to reach the targeted final concentration, or by reconstituting the flake food in drug-containing water.

References

1. Keller A, et al. (2017) Predicting human olfactory perception from chemical features of odor molecules. *Science* 355(6327):820–826.
2. Koulakov AA, Kolterman BE, Enikolopov AG, Rinberg D (2011) In search of the structure of human olfactory space. *Front Syst Neurosci* 5:65.
3. Secundo L, Snitz K, Sobel N (2014) The perceptual logic of smell. *Curr Opin Neurobiol* 25:107–115.
4. Distel H, et al. (1999) Perception of everyday odors--correlation between intensity, familiarity and strength of hedonic judgement. *Chem Senses* 24(2):191–199.
5. Keller A, Hempstead M, Gomez IA, Gilbert AN, Vosshall LB (2012) An olfactory demography of a diverse metropolitan population. *BMC Neurosci* 13:122.
6. Keller A, Vosshall LB (2016) Olfactory perception of chemically diverse molecules. *BMC Neurosci* 17(1):55.
7. Keller A, Zhuang H, Chi Q, Vosshall LB, Matsunami H (2007) Genetic variation in a human odorant receptor alters odour perception. *Nature* 449(7161):468–472.
8. Mainland JD, et al. (2014) The missense of smell: functional variability in the human odorant receptor repertoire. *Nat Neurosci* 17(1):114–120.
9. Menashe I, et al. (2007) Genetic elucidation of human hyperosmia to isovaleric acid. *PLoS Biol* 5(11):e284.
10. Couto A, Alenius M, Dickson BJ (2005) Molecular, anatomical, and functional organization of the Drosophila olfactory system. *Curr Biol* 15(17):1535–1547.
11. Fishilevich E, Vosshall LB (2005) Genetic and functional subdivision of the Drosophila antennal lobe. *Curr Biol* 15(17):1548–1553.
12. Laissue PP, Vosshall LB (2008) The olfactory sensory map in Drosophila. *Adv Exp Med Biol* 628:102–114.

13. Lin H-H, Lai JS-Y, Chin A-L, Chen Y-C, Chiang A-S (2007) A map of olfactory representation in the Drosophila mushroom body. *Cell* 128(6):1205–1217.

14. Jefferis GSXE, et al. (2007) Comprehensive maps of Drosophila higher olfactory centers: spatially segregated fruit and pheromone representation. *Cell* 128(6):1187–1203.

15. Fişek M, Wilson RI (2014) Stereotyped connectivity and computations in higher-order olfactory neurons. *Nat Neurosci* 17(2):280–288.

16. Chou Y-H, et al. (2010) Diversity and wiring variability of olfactory local interneurons in the Drosophila antennal lobe. *Nat Neurosci* 13(4):439–449.

17. Seki Y, Rybak J, Wicher D, Sachse S, Hansson BS (2010) Physiological and morphological characterization of local interneurons in the Drosophila antennal lobe. *J Neurophysiol* 104(2):1007–1019.

18. Tanaka NK, Endo K, Ito K (2012) Organization of antennal lobe-associated neurons in adult Drosophila melanogaster brain. *J Comp Neurol* 520(18):4067–4130.

19. Kim SM, Su C-Y, Wang JW (2017) Neuromodulation of Innate Behaviors in Drosophila. *Annu Rev Neurosci* 40:327–348.

20. Kain JS, Stokes C, de Bivort BL (2012) Phototactic personality in fruit flies and its suppression by serotonin and white. *Proc Natl Acad Sci U S A* 109(48):19834–19839.

21. Buchanan SM, Kain JS, de Bivort BL (2015) Neuronal control of locomotor handedness in Drosophila. *Proc Natl Acad Sci U S A* 112(21):6700–6705.

22. Kain JS, et al. (2015) Variability in thermal and phototactic preferences in Drosophila may reflect an adaptive bet-hedging strategy : BET-HEDGING EXPLAINS THERMOTACTIC VARIABILITY. *Evolution* 69(12):3171–3185.

23. Todd JG, Kain JS, de Bivort BL (2017) Systematic exploration of unsupervised methods for mapping behavior. *Phys Biol* 14(1):015002.

24. Honegger K, de Bivort B (2018) Stochasticity, individuality and behavior. *Curr Biol* 28(1):R8–R12.

25. Linneweber G, Andriatsilavo M, Dutta S, Hellbruegge L (2019) A neurodevelopmental origin of behavioral individuality. *bioRxiv*. doi.org/10.1101/540880.

26. Sizemore TR, Dacks AM (2016) Serotonergic Modulation Differentially Targets Distinct Network Elements within the Antennal Lobe of Drosophila melanogaster. *Sci Rep* 6:37119.

27. Ayroles JF, et al. (2015) Behavioral idiosyncrasy reveals genetic control of phenotypic variability. *Proc Natl Acad Sci U S A* 112(21):6706–6711.

28. Claridge-Chang A, et al. (2009) Writing memories with light-addressable reinforcement circuitry. *Cell* 139(2):405–415.

29. Dierick HA, Greenspan RJ (2007) Serotonin and neuropeptide F have opposite modulatory effects on fly aggression. *Nat Genet* 39(5):678–682.

30. Riemensperger T, et al. (2011) Behavioral consequences of dopamine deficiency in the Drosophila central nervous system. *Proc Natl Acad Sci U S A* 108(2):834–839.

31. Kim Y-C, Lee H-G, Han K-A (2007) D1 dopamine receptor dDA1 is required in the mushroom body neurons for aversive and appetitive learning in Drosophila. *J Neurosci* 27(29):7640–7647.

32. Lebestky T, et al. (2009) Two different forms of arousal in Drosophila are oppositely regulated by the dopamine D1 receptor ortholog DopR via distinct neural circuits. *Neuron* 64(4):522–536.

33. Szyszka P, et al. (2011) Mind the gap: olfactory trace conditioning in honeybees. *J Neurosci* 31(20):7229–7239.

34. Ko KI, et al. (2015) Starvation promotes concerted modulation of appetitive olfactory behavior via parallel neuromodulatory circuits. *Elife* 4. doi:10.7554/eLife.08298.

35. Hamada FN, et al. (2008) An internal thermal sensor controlling temperature preference in Drosophila. *Nature* 454(7201):217–220.

36. Sykes PA, Condron BG (2005) Development and sensitivity to serotonin of Drosophila serotonergic varicosities in the central nervous system. *Dev Biol* 286(1):207–216.

37. Kitamoto T (2001) Conditional modification of behavior in Drosophila by targeted expression of a temperature-sensitive shibire allele in defined neurons. *J Neurobiol*. Available at: https://onlinelibrary.wiley.com/doi/abs/10.1002/neu.1018.

38. Asahina K, et al. (2014) Tachykinin-expressing neurons control male-specific aggressive arousal in Drosophila. *Cell* 156(1-2):221–235.

39. Parnas M, Lin AC, Huetteroth W, Miesenböck G (2013) Odor discrimination in Drosophila: from neural population codes to behavior. *Neuron* 79(5):932–944.

40. Das S, et al. (2011) Plasticity of local GABAergic interneurons drives olfactory habituation. *Proc Natl Acad Sci U S A* 108(36):E646–54.

41. Bhandawat V, Olsen SR, Gouwens NW, Schlief ML, Wilson RI (2007) Sensory processing in the Drosophila antennal lobe increases reliability and separability of ensemble odor representations. *Nat Neurosci* 10(11):1474–1482.

42. Schulz DJ, Goaillard J-M, Marder E (2006) Variable channel expression in identified single and electrically coupled neurons in different animals. *Nat Neurosci* 9(3):356–362.

43. Stern S, Kirst C, Bargmann CI (2017) Neuromodulatory Control of Long-Term Behavioral Patterns and Individuality across Development. *Cell* 171(7):1649–1662.e10.

44. Mansourian S, et al. (2018) Wild African Drosophila melanogaster Are Seasonal Specialists on Marula Fruit. *Curr Biol* 28(24):3960–3968.e3.

45. Becher PG, et al. (2012) Yeast, not fruit volatiles mediate Drosophila melanogaster attraction, oviposition and development. *Funct Ecol* 26(4):822–828.

46. Austin CJ, Guglielmo CG, Moehring AJ (2014) A direct test of the effects of changing atmospheric pressure on the mating behavior of Drosophila melanogaster. *Evol Ecol* 28(3):535–544.

47. Zhang X, Gaudry Q (2016) Functional integration of a serotonergic neuron in the Drosophila antennal lobe. *Elife* 5. doi:10.7554/eLife.16836.

48. Olsen SR, Bhandawat V, Wilson RI (2010) Divisive normalization in olfactory population codes. *Neuron* 66(2):287–299.

49. Qin H, et al. (2012) Gamma neurons mediate dopaminergic input during aversive olfactory memory formation in Drosophila. *Curr Biol* 22(7):608–614.

50. Kong EC, et al. (2010) A pair of dopamine neurons target the D1-like dopamine receptor DopR in the central complex to promote ethanol-stimulated locomotion in Drosophila. *PLoS One* 5(4):e9954.

51. Kottler B, Faville R, Bridi JC, Hirth F (2019) Inverse Control of Turning Behavior by Dopamine D1 Receptor Signaling in Columnar and Ring Neurons of the Central Complex in Drosophila. *Curr Biol* 29(4):567–577.e6.

52. Corfas RA, Dickinson MH (2018) Diverse food-sensing neurons trigger idiothetic local search in Drosophila. *bioRxiv*. Available at: https://www.biorxiv.org/content/10.1101/433771v1.abstract.

53. Stone T, et al. (2017) An Anatomically Constrained Model for Path Integration in the Bee Brain. *Curr Biol* 27(20):3069–3085.e11.

54. Kakaria KS, de Bivort BL (2017) Ring Attractor Dynamics Emerge from a Spiking Model of the Entire Protocerebral Bridge. *Front Behav Neurosci* 11:8.

55. Ormerod KG, et al. (2017) Drosophila development, physiology, behavior, and lifespan are influenced by altered dietary composition. *Fly* 11(3):153–170.

56. Parnas D, Haghighi AP, Fetter RD, Kim SW, Goodman CS (2001) Regulation of postsynaptic structure and protein localization by the Rho-type guanine nucleotide exchange factor dPix. *Neuron* 32(3):415–424.

57. Lee T, Luo L (1999) Mosaic Analysis with a Repressible Cell Marker for Studies of Gene Function in Neuronal Morphogenesis. *Neuron* 22(3):451–461.

58. Stan Development Team (2018) Stan User's Guide Version 2.18. https://mc-stan.org/docs/2_18/stan-users-guide/index.html

This page is intentionally left blank

Chapter II - Loci of individuality in the Drosophila olfactory circuit

Abstract

Behavior varies even among genetically identical animals raised in the same environment[1–10]. However, little is known about the circuit or anatomical underpinnings of this individuality[11,12], though previous work implicates sensory periphery[13,14]. *Drosophila* olfaction presents an ideal model to study the biological basis of behavioral individuality, because while the neural circuit underlying olfactory behavior is well-described[15–18] and highly stereotyped[17], persistent idiosyncrasy in behavior[4], neural coding[4], and neural wiring[19,20] have also been described. Projection neurons (PNs), which relay odor signals sensed by olfactory receptor neurons (ORNs) to deeper brain structures[21–23], exhibit variable calcium responses to identical odor stimuli across individuals, but how these idiosyncrasies relate to individual behavioral responses remains unknown. Here, using paired behavior and two-photon imaging measurements, we show that idiosyncratic calcium dynamics in both ORNs and PNs predict individual preferences for an aversive monomolecular odorant versus air, suggesting that variation at the periphery of the olfactory system determines individual preference for an odor's presence. In contrast, PN, but not ORN, calcium responses predict individual preferences in a two-odor choice assay. Furthermore, paired behavior and immunohistochemistry measurements reveal that variation in ORN presynaptic density also predicts two-odor preference, suggesting this site is a locus of individuality where microscale circuit variation gives rise to idiosyncrasy in behavior. Our results demonstrate how a neural circuit may vary functionally and structurally to produce variable behavior among individuals.

Results

We sought to determine where along the sensorimotor pathway essentially identical sensory stimuli signals are transformed into signals reflecting idiosyncratic behavior — in isogenic individuals reared together in the same environment. We therefore measured idiosyncratic odor preferences and neural responses[4] in the same individuals and asked whether the latter predicted the former (Fig. 1b). To do that, we used inbred strains to express the fluorescent calcium reporter GCamp6m in either of the two most peripheral neural subpopulations of the *Drosophila* olfactory circuit, ORNs or PNs (Fig. 1a, e), and performed head-fixed 2-photon calcium imaging after measuring odor preference in an untethered assay[4] (Fig. 1b-d, Extended Figure 1a). Individual identity was maintained between these experiments by individual housing. We measured volumetric neural responses in the antennal lobe (AL), the site at which ORNs synapse onto PNs in ~50 discrete odor channels (dash here? or in?) microcircuits called glomeruli (Fig. 1a)[23,24]. Flies were exposed to a panel of 12 odors (plus air) and we used *k*-means clustering to automatically segment 5 glomeruli from the resulting 4-D calcium image stacks (Fig. 1e, Extended Figure 2-3, Methods)[23]. We found that both ORN and PN responses varied more across individuals than across multiple trials from a single individual, and that PNs varied more than ORNs (Fig. 1j)[4]. While individual ORN responses are known to vary more than individual PN responses[21], our calcium recordings represent pooled responses across entire ORN or PN subpopulations. This might explain why we find that ORNs exhibit less intra- and inter-individual variation compared to PNs. We also found that PNs exhibited a larger within-individual coding distance measured across left to right ALs compared with trial-to-trial variation within each lobe, whereas ORNs did not (Extended Figure 4c). Finally, we found that a logistic linear classifier could better decode

individual identity from PN responses than ORN (Extended Figure 4d). Together, these data suggest that individuals are more idiosyncratic in their PN than in their ORN responses.

Having maintained the identity of individual flies between measurement of odor preference to neural activity, we first asked which circuit elements, if any, could predict the individual preferences of flies given a choice between an aversive odor (3-octanol, OCT) and air, a choice which results in persistent individuality on time scales from 3 hours up to at least 24 hours (Extended Figure 1b-c). We calculated the peak odor responses for each individual and calculated the principal components (PCs) of PN and ORN neural activity (Figure 1g-i, Extended Figure 4-6). Using each of the first 5 PCs of PN neural activity alone to linearly predict individual preferences, we found that PC 1 explained 16% of preference variance in a training set of 18 flies (Fig. 1k-l). This PC 1-based model also explained 10% of preference variance when evaluated on a held-out set of test flies (n=35 flies) that were not used to construct the original model (Fig. 1m). Similarly, we found that PC 1 of ORN neural activity explained 23% of preference variance (Fig. 1k, n). Therefore, ORN odor responses themselves contain idiosyncrasies which propagate through the olfactory circuit to cause individual behavioral responses to an odor versus air.

We next asked whether the same circuit elements could also predict individual preferences for an aversive monomolecular odorant (OCT) versus another (4-methylcyclohexanol, MCH), a choice which results in persistent individuality on time scales from 3 hours up to at least 24 hours (Extended Figure 1d-e)[4]. As before, we used each of the first 5 PCs of PN neural activity alone to predict individual preferences with a linear model. In this case, we found that a model built from PC 2 explained 15% of preference variance in a training set of 47 flies (Fig. 1o-p). This PC 2-

based model explained 26% of preference variance when evaluated on a held-out set of test flies (n=22 flies) (Fig. 1q). By contrast, we found that no PCs of ORN neural activity could linearly predict odor preference beyond the level of shuffled controls (n=35 flies) (Fig. 1o). We nevertheless selected the single ORN PC that could best predict behavior, PC 1, and observed that the preference predicted from PC 1 could not explain the measured preference (Fig. 1r). We also projected ORN calcium dynamics onto PC 2 of PN dynamics and observed that the fraction of variation explained remained far below that observed in the PN test set (ORN R^2=0.06, PN test R^2=0.26, Extended Figure 9i). Therefore, unlike individual preferences for odor versus air, idiosyncratic PN, but not ORN, responses can predict individual preferences in this two-odor choice paradigm.

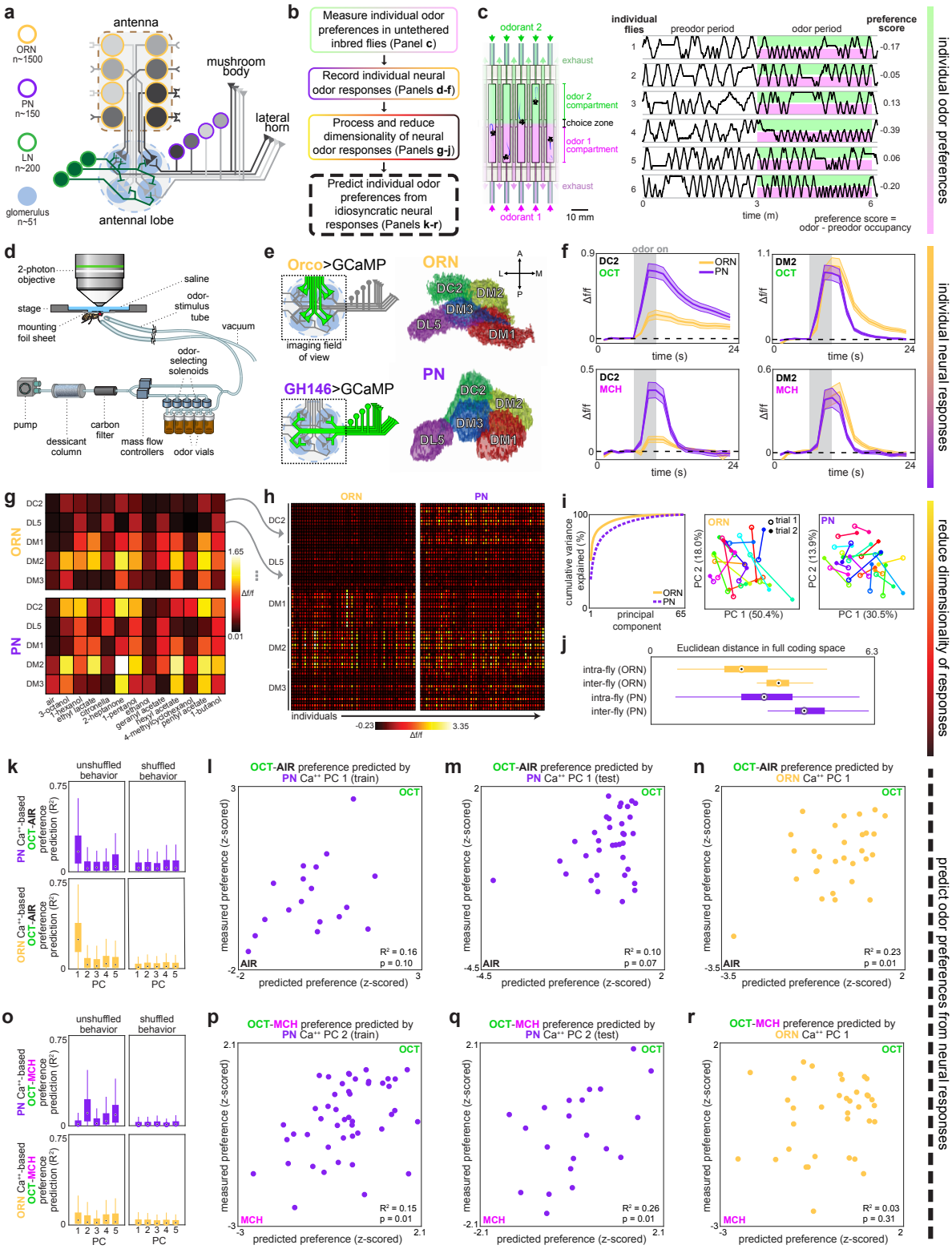

a
antenna
ORN n~1500
PN n~150
LN n~200
glomerulus n~51
mushroom body
lateral horn
antennal lobe
b
Measure individual odor preferences in untethered inbred flies (Panel c)
Record individual neural odor responses (Panels d-f)
Process and reduce dimensionality of neural odor responses (Panels g-j)
Predict individual odor preferences from idiosyncratic neural responses (Panels k-r)
c
odorant 2
exhaust
odor 2 compartment
choice zone
odor 1 compartment
exhaust
odorant 1
10 mm
individual flies
preodor period
odor period
preference score
time (m)
preference score = odor - preodor occupancy
individual odor preferences
d
2-photon objective
saline
odor-stimulus tube
stage
mounting foil sheet
vacuum
odor-selecting solenoids
pump
dessicant column
carbon filter
mass flow controllers
odor vials
e
Orco>GCaMP
imaging field of view
GH146>GCaMP
ORN
PN
DC2
DM2
DM3
DL5
DM1
f
odor on
DC2 OCT
DM2 OCT
DC2 MCH
DM2 MCH
ORN
PN
Δf/f
time (s)
individual neural responses
g
ORN
PN
DC2
DL5
DM1
DM2
DM3
Δf/f
air
3-octanol
1-hexanol
ethyl lactate
citronella
2-heptanone
1-pentanol
ethanol
geranyl acetate
hexyl acetate
4-methylcyclohexanol
benzyl acetate
1-butanol
h
ORN
PN
individuals
Δf/f
i
cumulative variance explained (%)
principal component
ORN
PN
trial 1
trial 2
PC 2 (18.0%)
PC 1 (50.4%)
PC 2 (13.9%)
PC 1 (30.5%)
j
Euclidean distance in full coding space
intra-fly (ORN)
inter-fly (ORN)
intra-fly (PN)
inter-fly (PN)
reduce dimensionality of responses
k
unshuffled behavior
shuffled behavior
PN Ca++-based OCT-AIR preference prediction (R²)
ORN Ca++-based OCT-AIR preference prediction (R²)
PC
l
OCT-AIR preference predicted by PN Ca++ PC 1 (train)
OCT
measured preference (z-scored)
predicted preference (z-scored)
AIR
R² = 0.16
p = 0.10
m
OCT-AIR preference predicted by PN Ca++ PC 1 (test)
R² = 0.10
p = 0.07
n
OCT-AIR preference predicted by ORN Ca++ PC 1
R² = 0.23
p = 0.01
o
unshuffled behavior
shuffled behavior
PN Ca++-based OCT-MCH preference prediction (R²)
ORN Ca++-based OCT-MCH preference prediction (R²)
PC
p
OCT-MCH preference predicted by PN Ca++ PC 2 (train)
MCH
R² = 0.15
p = 0.01
q
OCT-MCH preference predicted by PN Ca++ PC 2 (test)
R² = 0.26
p = 0.01
r
OCT-MCH preference predicted by ORN Ca++ PC 1
R² = 0.03
p = 0.31
predict odor preferences from neural responses

Figure 1: Idiosyncratic calcium dynamics predict individual odor preferences
(a) Olfactory circuit schematic. Olfactory receptor neurons (ORNs, peach outline) and projection neurons (PNs, plum outline) are comprised of ~51 classes corresponding to odor receptor response channels. ORNs of the same class (gray shading) sense odors in the antennae and synapse together on dendrites of PNs of the same class in ball-shaped structures called glomeruli located in the antennal lobe (AL). Local neurons (LNs, green outline) mediate interglomerular cross-talk and presynaptic inhibition, amongst other roles[41,42]. Odor signals are normalized and whitened in the AL before being sent to the mushroom body and lateral horn for further processing. Schematic adapted from [4]. (b) Experiment outline (c) Odor preference behavior tracking setup (reproduced from [4]) and example individual fly ethograms. OCT (green backdrop) and MCH (magenta backdrop) were presented for 3 minutes. (d) Head-fixed 2-photon calcium imaging and odor delivery setup (reproduced from [4]). (e) Orco and GH146 driver expression profiles (left) and example segmentation masks (right) extracted from 2-photon calcium images for a single fly expressing Orco>GCaMP6m (top, expressed in a subset of all ORN classes) or GH146>Gcamp6m (bottom, expressed in a subset of all PN classes). (f) Time-dependent Δf/f for glomerular odor responses in ORNs (peach) and PNs (plum) averaged across all individuals: DC2 to OCT (upper left), DM2 to OCT (upper right), DC2 to MCH (lower left), and DM2 to OCT (lower right). Shaded error bars represent S.E.M. (g) Peak Δf/f for each glomerulus-odor pair averaged across all flies. (h) Individual neural responses measured in ORNs (left) or PNs (right) for 50 flies each. Columns represent the average of up to 4 odor responses from a single fly. Each row represents one glomerulus-odor response pair. Odors are the same as in panel (g). (i) Principal component analysis of individual neural responses. Fraction of variance explained versus principal component number (left). Trial 1 and trial 2 of ORN (middle) and PN (right) responses for 20 individuals (unique colors) embedded in PC 1-2 space. Note the variance explained by each PC is different in the case of ORN and PN responses. (j) Full coding space Euclidean distance within and across flies measured in ORNs (n=65 flies) and PNs (n=122 flies). (k) Bootstrapped R^2 of OCT-AIR preference prediction from each of the first 5 principal components of neural activity measured in PNs (top, training set) or ORNs (bottom, all data). (l) Measured OCT-AIR preference versus preference predicted from PC 1 of PN activity in a training set (n=18 flies). (m) Measured OCT-AIR preference versus preference predicted from PC 1 on PN activity in a test set (n=35 flies) evaluated on a model trained on data from panel (l). (n) Measured OCT-AIR preference versus preference predicted from PC 1 of ORN activity (n=30 flies). (o) Bootstrapped R^2 of OCT-MCH preference prediction from each of the first 5 principal components of neural activity measured in PNs (top, training set) or ORNs (bottom, all data). (p) Measured OCT-MCH preference versus preference predicted from PC 2 of PN activity in a training set (n=47 flies). (q) Measured OCT-MCH preference versus preference predicted from PC 2 on PN activity in a test set (n=22 flies) evaluated on a model trained on data from panel (p). (r) Measured OCT-MCH preference versus preference predicted from PC 1 of ORN activity (n=35 flies).

We next sought to understand the models which predicted odor preference from neural activity. Since our linear models employed the principal components of glomerulus-odor response pairs as predictors, we first plotted PC loadings grouped either by glomerulus or odor, noting that loadings

correlated much more strongly when grouped by glomerulus, suggesting that individual glomeruli, rather than odorant class-sensing groups of glomeruli, may be the more salient substrates of individual variation (Extended Figure 5-6).

Turning our attention to models of OCT-AIR preference, we noted that the loading weights for PC 1 of both ORN and PN neural activity were uniformly positive across glomerulus-odor response dimensions (Fig. 2a, d), indicating that PC 1 approximates each individual's average global response within the glomeruli analyzed in our dataset. Indeed, a linear model built from the average response across all neural coding dimensions (Fig. 2b, e) was able to predict preference for OCT versus air to a similar extent as PC 1 of neural activity in both ORNs and PNs (Fig. 2c, f). The model beta coefficient was negative in both cases, indicating that larger AL responses lead to a higher preference for Air, consistent with the fact that OCT is aversive (Extended Table 1, Extended Figure 8b, d). In other words, flies whose ORNs and PNs respond to odors more strongly are more likely to avoid an aversive odorant.

We next turned our attention to models of OCT-MCH preference. The loadings for PC 2 of PN neural activity, which we found was predictive of preference for OCT versus MCH, exhibited mostly opposing weights for the glomeruli DM2 and DC2 across odors (Fig. 2g), indicating that the relative activation of DM2 and DC2 could predict the likelihood of a fly preferring OCT to MCH. Similarly to a linear model constructed from PC 2 of PN activity, a linear model built from the average of DM2 minus DC2 PN responses (Fig. 2h) could predict individual preference for OCT versus MCH (Fig. 2i). The model beta coefficient was negative, indicating that the relative activations of DM2 and DC2 correlate with preference for MCH and OCT, respectively (Extended

Table 1, Extended Figure 8f). Therefore, the relative responsiveness of DM2 and DC2 PNs determine an individual's preference for MCH or OCT.

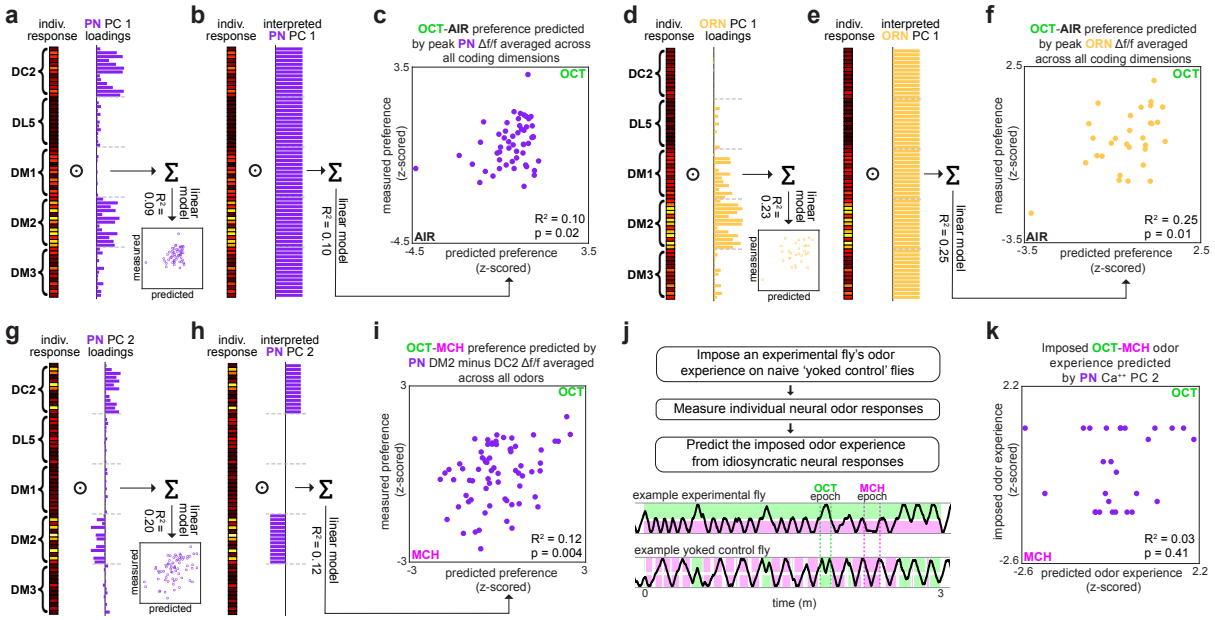


Figure 2: Variation in global and relative glomerular responses explain individual preferences

(a) PC 1 loadings of PN activity for flies tested for OCT-AIR preference (n=53 flies). (b) Interpreted PN PC 1 loadings. (c) Measured OCT-AIR preference versus preference predicted by the average peak response across all PN coding dimensions (n=53 flies). (d) PC 1 loadings of ORN activity for flies tested for OCT-AIR preference (n=30 flies). (e) Interpreted ORN PC 1 loadings. (f) Measured OCT-AIR preference versus preference predicted by the average peak response across all ORN coding dimensions (n=30 flies). (g) PC 2 loadings of PN activity for flies tested for OCT-MCH preference (n=69 flies). (h) Interpreted PN PC 2 loadings. (i) Measured OCT-MCH preference versus preference predicted by the average peak PN response in DM2 minus DC2 across all odors (n=69 flies). (j) Yoked control experiment outline and example behavior traces. Experimental flies are free to move about tunnels permeated with steady state OCT and MCH flowing into either end. Yoked control flies are delivered the same odor at both ends of the tunnel which matches the odor experienced at the nose of the experimental fly at each moment in time. (k) Imposed odor experience versus the odor experience predicted from PC 2 of PN activity (n=27 flies) evaluated on the model trained from data in panel 1p.

Previous work found that PN response transients, rather than fixed points, contain more odor identity information[25]. We therefore asked at which times during odor presentation an individual's neural responses could best predict odor preference. When we built models to predict OCT versus AIR preference from PC 1 of neural activity as a function of time during odor presentation, we

found that behavior prediction generally rose during odor delivery and remained high after odor offset in ORNs, but quickly declined after odor offset in PNs (Extended Figure 7a-b). We observed a similar trend when predicting OCT versus MCH preference from PC 2 of PN activity, whereas in this case ORN responses could not meaningfully predict preference at any point during odor delivery (Extended Figure 7c). The times during which calcium responses could predict individual behavior generally corresponded to the times during which a linear classifier could decode odor identity (Extended Figure 7d), indicating that idiosyncrasies of stereotyped neural responses to odor are predictive of individual preferences. We did note, however, that neural behavior prediction dropped off faster than decoding accuracy after odor offset, suggesting that variations specifically in peak odor responses drive individual preferences.

Our measurements of neural activity occur after behavior measurements acquired ~0-4 hours prior. Past odor experience has been shown to modulate subsequent AL responses[26–28]. Therefore, we asked whether the ability of neural activity to predict odor preference was not a reflection of persistent idiosyncrasy in neural response but rather a persistent imprint of idiosyncratic behavioral experiences on subsequent neural responses. In other words, do persistent idiosyncrasies in neural activity cause unique behavioral experiences, or do unique behavioral experiences cause idiosyncratic neural activity. To address this question, we imposed the individual odor experiences of previously monitored untethered flies given a choice between OCT and MCH on naive "yoked controls" (Fig. 2j). If an individual's odor experience modulated its subsequent neural activity such that the neural activity could predict its previous experience, rather than the underlying persistent neural activity causing the individual's choice behavior and secondarily its odor experience, then the yoked control's experienced odor history should be predictable from its subsequently measured

neural activity. However, in contrast to our ability to predict individual odor preference from PC 2 of PN activity in experimental flies, we were unable to predict the odor experience of yoked controls from their PN activity when evaluated on the same PC 2-based linear model applied in Figure 1p-q (n=27 flies) (Fig. 2k). Therefore, our measurements of idiosyncratic neural activity likely reflect persistent individual differences in neural odor responses which cause individualized odor experiences, not vice versa.

We next investigated how structural variation in the nervous system might underlie the variations in neural activity which we observed could explain idiosyncratic preferences. Because PN, but not ORN, calcium responses could predict individual preference for OCT versus MCH, this raised the possibility that some circuit element residing between the ORN to PN signal transition could confer a behavioral-individuality-inducing idiosyncrasy to PN calcium responses which does not exist in ORNs. We therefore visualized presynaptic T-bar density in ORNs using mStrawberry-tagged Brp-Short and performed immunohistochemistry on brains after measuring individual preference for OCT versus MCH (Fig. 3a, Extended Figure 9)[29].

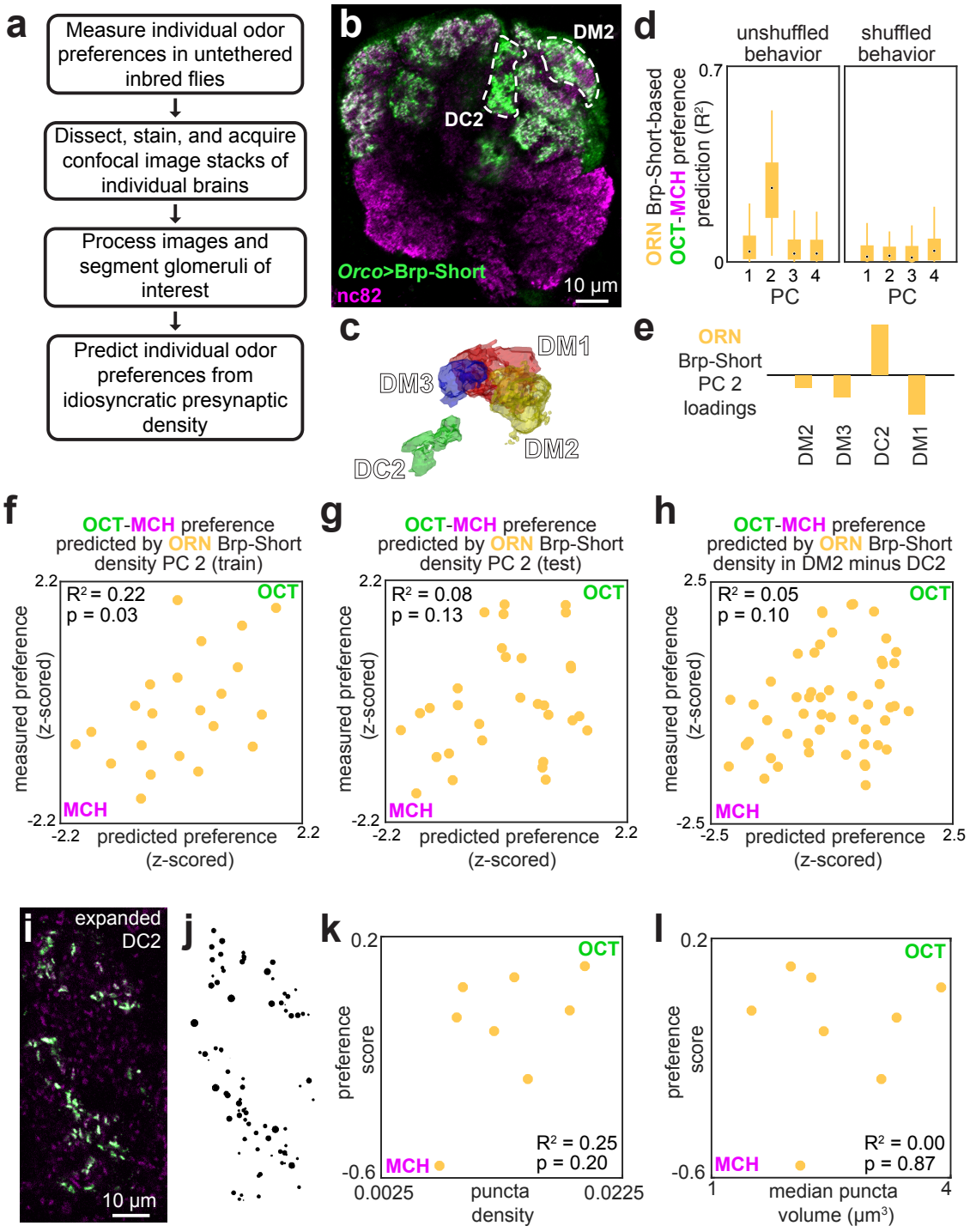


Figure 3: Idiosyncratic presynaptic marker density in DM2 and DC2 predicts OCT-MCH preference (a) Experiment outline. (b) Example slice from a z-stack of the antennal lobe expressing Orco>Brp-Short (green) with DC2 and DM2 visible (white dashed outline). nc82 counterstain (magenta). (c) Example glomerulus segmentation masks extracted from an individual

z-stack. (d) Bootstrapped R^2 of OCT-MCH preference prediction from each of the first 4 principal components of Brp-Short density measured in ORNs (training set, n=22 flies). (e) PC 2 loadings of Brp-Short density. (f) Measured OCT-MCH preference versus preference predicted from PC 2 of ORN Brp-Short density in a training set (n=22 flies). (g) Measured OCT-MCH preference versus preference predicted from PC 2 on ORN Brp-Short density in a test set (n=31 flies) evaluated on a model trained on data from panel (f). (h) Measured OCT-MCH preference versus preference predicted from ORN Brp-Short density in DM2 minus DC2 (n=53 flies). (i) Example expanded AL expressing Or13a>Brp-Short. (j) Imaris-identified spots from the sample in panel (i). (k) OCT-MCH preference score plotted against Brp-Short puncta density in expanded Or13a>Brp-Short samples (n=8 flies). (l) OCT-MCH preference score plotted against Brp-Short median puncta volume in expanded Or13a>Brp-Short samples (n=8 flies).

We used confocal microscopy to image presynaptic T-bars in Orco-expressing ORNs (Fig. 3b). We used semi-automated custom software to segment 4 of the 5 glomeruli (all but DL5) we previously analyzed in calcium recordings. We then quantified the density of Brp-Short staining within each glomerulus (Fig. 3c, Extended Figure 9). To begin building models which predict individual behavior from neural structure, we first calculated the principal components of Brp-Short density and found that PCs 1 and 2 were qualitatively similar to those measured in our calcium imaging experiments in that PC 1 was uniformly positive across glomeruli, reflecting global average staining intensity, and PC 2 exhibited a large magnitude loading for DC2 against negative loadings for the other glomeruli (Fig. 3e, Extended Figure 9g). As in our calcium imaging experiments, we generated linear models to predict individual preference from each individual PC (Fig. 3d). As before for flies given a choice between OCT and MCH, PC 2 predicted preference variation in the training set (Fig. 3f, $R^2 = 0.22$, n=22 flies) and in a held-out test set (Fig. 3g, $R^2 = 0.08$, n=31 flies). We also directly applied our hypothesis from our calcium imaging experiments that the relative activation of DM2 and DC2 should predict behavior and again found that this was the case (Fig. 3h). As before for calcium responses, the beta coefficient of this linear model was negative, indicating that the relative density of DM2 and DC2 presynaptic T-bars correlates with preference for MCH (Extended Table 2). However, the extent of ORN presynaptic density

differences between DM2 and DC2 (-50% to 40%, Extended Figure 8g-h) was less than that of PN calcium response differences (-60% to 100%, Extended Figure 8e-f), suggesting that variable presynaptic density alone cannot fully explain the variable calcium dynamics we observed. This is also consistent with the observation that idiosyncratic presynaptic density also explains less behavioral variation than calcium dynamics (Fig. 2-3). Nevertheless, these results suggest that relative variation in presynaptic input into DM2 and DC2 PNs may cause variation in DM2 and DC2 calcium dynamics, in turn giving rise to individual preferences for OCT versus MCH.

To better understand what variable Brp-Short staining represented on a microstructural level, we performed paired behavior and expansion microscopy in flies expressing Brp-Short specifically in DC2-projecting ORNs. Using expansion microscopy[30,31], we achieved a ~4-fold increase in linear resolution in immunostained samples, allowing us to visualize individual Brp-Short puncta (Fig. 3i-j)[30]. Similar to when quantifying Brp-Short staining density in unexpanded samples, we found that Brp-Short puncta density in DC2-projecting ORNs could predict individual preference (Fig. 3k). By contrast, the median puncta size had no relationship with preference (Fig. 3l). These results show that the density of Brp-Short puncta, but not other idiosyncrasies of presynaptic architecture, predict individual preference for OCT versus MCH. Together, our results suggest that idiosyncrasy in ORN presynaptic density contributes to idiosyncratic activations of PNs stimulated by ORN signals which are agnostic to OCT versus MCH, but not OCT versus Air, preference.

Discussion

Previous work has found mammalian peripheral circuit areas are predictive of individual behavior [13,14,32,33]. Here we show that sensory elements of the *Drosophila* olfactory circuit constitute neural

loci of behavioral individuality (Fig. 4). We have identified two distinct circuit mechanisms underlying individual preferences. Global mean or relative responses measured in the AL predict individual preferences for odor against air or odor against odor, respectively. The variation in the specific circuit elements that cause these differences in neural activity are likely to be different since we have shown that idiosyncratic ORN activity predicts odor against air, but not odor against odor, preferences, whereas PN activity is predictive in both cases. Therefore, variation at distinct sites within the nervous system contributes to different aspects of behavioral individuality.

Our predictions of individual preference from neural activity yield R^2 values in the range of 0.1 to 0.3. It is worth noting that the persistence of individual odor preference is relatively low (R^2=0.1-0.3) on the 3 hour timescale of preference measurement to imaging (Extended Figure 1b-e). To put our behavioral predictions in the context of low persistence, we simulated preferences and neural predictions as a function of the behavioral persistence and neural-behavior prediction R^2 (Extended Figure 10). This model indicates that the fraction of behavioral variation explainable by neural idiosyncrasies is greater than 50% (Fig. 4).

The low persistence of odor preference may be explained by unaccounted factors like neural state or plasticity, both of which would also confound neural predictions of individual preference. Furthermore, it is unclear whether the same circuit elements which vary to predict behavior on average also vary to predict trial-to-trial variations within individuals. In addition, we were unable to jointly measure neural dynamics and neural structure. In the future it will be important to confirm that variation in wiring or synapse density in fact alters calcium dynamics in a manner which predicts individual behavior. Our measurements of idiosyncratic calcium dynamics are

better able to predict behavior than our measurements of synapse density, indicating there is behavioral variation remaining to be explained at the molecular level. Past work has identified local neurons as a particularly variable population[20], so it may be that variation in LN wiring or responsiveness contributes to the variable ORN and PN dynamics we observed.

The fly populations used in our experiments were isogenic and raised under standard laboratory conditions. Unlike enriched environments, which have been shown to result in increased behavioral individuality[34–36], it is unclear how relatively uniform rearing environments like those employed here could generate significant differences in development or experience. Nevertheless, we observed persistent variation in behavior which could be predicted by idiosyncratic neural function and structure. What molecular events account for the neural and behavioral idiosyncrasy we describe? While developing nervous systems are thought to employ various compensation mechanisms to ensure robustness[9,19], the accretion of subtle variations in experience—even in nominally uniform rearing environments—might be responsible for the neural variation we found here to predict individual behavior. Genomic variation between inbred siblings might be an alternative explanation. Beyond genomic and environmental variations, stochasticity in gene expression during development[37,38] governed by thermodynamic noise could result in anatomical variations which underlie coding idiosyncrasies and individual personalities. Development of non-invasive methods to longitudinally assay the fine-scale molecular and anatomical makeup of behaving organisms throughout development and adulthood will be required to further pinpoint the mechanistic origins of individuality.

References

1. Ayroles, J. F. *et al.* Behavioral idiosyncrasy reveals genetic control of phenotypic variability. *Proc. Natl. Acad. Sci. U. S. A.* **112**, 6706–6711 (2015).
2. Stern, S., Kirst, C. & Bargmann, C. I. Neuromodulatory Control of Long-Term Behavioral Patterns and Individuality across Development. *Cell* **171**, 1649–1662.e10 (2017).
3. Pantoja, C. *et al.* Neuromodulatory Regulation of Behavioral Individuality in Zebrafish. *Neuron* **91**, 587–601 (2016).
4. Honegger, K. S., Smith, M. A.-Y., Churgin, M. A., Turner, G. C. & de Bivort, B. L. Idiosyncratic neural coding and neuromodulation of olfactory individuality in. *Proc. Natl. Acad. Sci. U. S. A.* (2019) doi:10.1073/pnas.1901623116.
5. Renart, A. & Machens, C. K. Variability in neural activity and behavior. *Current Opinion in Neurobiology* vol. 25 211–220 (2014).
6. Freund, J. *et al.* Emergence of individuality in genetically identical mice. *Science* **340**, 756–759 (2013).
7. Bierbach, D., Laskowski, K. L. & Wolf, M. Behavioural individuality in clonal fish arises despite near-identical rearing conditions. *Nat. Commun.* **8**, 15361 (2017).
8. Westneat, D. F., Wright, J. & Dingemanse, N. J. The biology hidden inside residual within-individual phenotypic variation. *Biol. Rev. Camb. Philos. Soc.* **90**, 729–743 (2015).
9. Marder, E. Variability, compensation, and modulation in neurons and circuits. *Proc. Natl. Acad. Sci. U. S. A.* **108 Suppl 3**, 15542–15548 (2011).
10. Avitan, L. *et al.* Behavioral signatures of a developing neural code. doi:10.1101/856807.
11. Linneweber, G. A. *et al.* A neurodevelopmental origin of behavioral individuality. doi:10.1101/540880.
12. Skutt-Kakaria, K., Reimers, P., Currier, T. A., Werkhoven, Z. & de Bivort, B. L. A neural

circuit basis for context-modulation of individual locomotor behavior. doi:10.1101/797126.

13. Osborne, L. C., Lisberger, S. G. & Bialek, W. A sensory source for motor variation. *Nature* **437**, 412–416 (2005).
14. Michelson, C. A., Pillow, J. W. & Seidemann, E. Majority of choice-related variability in perceptual decisions is present in early sensory cortex. doi:10.1101/207357.
15. Wang, J. W., Wong, A. M., Flores, J., Vosshall, L. B. & Axel, R. Two-photon calcium imaging reveals an odor-evoked map of activity in the fly brain. *Cell* **112**, 271–282 (2003).
16. Vosshall, L. B., Wong, A. M. & Axel, R. An olfactory sensory map in the fly brain. *Cell* **102**, 147–159 (2000).
17. Wilson, R. I. Transformation of Olfactory Representations in the Drosophila Antennal Lobe. *Science* vol. 303 366–370 (2004).
18. Groschner, L. N. & Miesenböck, G. Mechanisms of Sensory Discrimination: Insights from Olfaction. *Annu. Rev. Biophys.* **48**, 209–229 (2019).
19. Tobin, W. F., Wilson, R. I. & Lee, W.-C. A. Wiring variations that enable and constrain neural computation in a sensory microcircuit. *Elife* **6**, e24838 (2017).
20. Chou, Y.-H. *et al.* Diversity and wiring variability of olfactory local interneurons in the Drosophila antennal lobe. *Nat. Neurosci.* **13**, 439–449 (2010).
21. Wilson, R. I. Early Olfactory Processing inDrosophila: Mechanisms and Principles. *Annual Review of Neuroscience* vol. 36 217–241 (2013).
22. Bhandawat, V., Olsen, S. R., Gouwens, N. W., Schlief, M. L. & Wilson, R. I. Sensory processing in the Drosophila antennal lobe increases reliability and separability of ensemble odor representations. *Nat. Neurosci.* **10**, 1474–1482 (2007).
23. Couto, A., Alenius, M. & Dickson, B. J. Molecular, anatomical, and functional organization

of the Drosophila olfactory system. *Curr. Biol.* **15**, 1535–1547 (2005).

24. Grabe, V., Strutz, A., Baschwitz, A., Hansson, B. S. & Sachse, S. Digital in vivo 3D atlas of the antennal lobe of Drosophila melanogaster. *J. Comp. Neurol.* **523**, 530–544 (2015).
25. Mazor, O. & Laurent, G. Transient dynamics versus fixed points in odor representations by locust antennal lobe projection neurons. *Neuron* **48**, 661–673 (2005).
26. Sachse, S. *et al.* Activity-dependent plasticity in an olfactory circuit. *Neuron* **56**, 838–850 (2007).
27. Golovin, R. M. & Broadie, K. Developmental experience-dependent plasticity in the first synapse of the Drosophila olfactory circuit. *J. Neurophysiol.* **116**, 2730–2738 (2016).
28. Iyengar, A., Chakraborty, T. S., Goswami, S. P., Wu, C.-F. & Siddiqi, O. Post-eclosion odor experience modifies olfactory receptor neuron coding in Drosophila. *Proc. Natl. Acad. Sci. U. S. A.* **107**, 9855–9860 (2010).
29. Mosca, T. J. & Luo, L. Synaptic organization of the Drosophila antennal lobe and its regulation by the Teneurins. *eLife* vol. 3 (2014).
30. Gao, R. *et al.* Cortical column and whole-brain imaging with molecular contrast and nanoscale resolution. *Science* **363**, (2019).
31. Asano, S. M. *et al.* Expansion Microscopy: Protocols for Imaging Proteins and RNA in Cells and Tissues. *Curr. Protoc. Cell Biol.* **80**, e56 (2018).
32. Newsome, W. T., Britten, K. H. & Anthony Movshon, J. Neuronal correlates of a perceptual decision. *Nature* vol. 341 52–54 (1989).
33. Britten, K. H., Newsome, W. T., Shadlen, M. N., Celebrini, S. & Movshon, J. A. A relationship between behavioral choice and the visual responses of neurons in macaque MT. *Vis. Neurosci.* **13**, 87–100 (1996).

34. Körholz, J. C. *et al.* Selective increases in inter-individual variability in response to environmental enrichment in female mice. *Elife* **7**, (2018).

35. Akhund-Zade, J., Ho, S., O'Leary, C. & de Bivort, B. The effect of environmental enrichment on behavioral variability depends on genotype, behavior, and type of enrichment. *J. Exp. Biol.* **222**, (2019).

36. Zocher, S. *et al.* Early-life environmental enrichment generates persistent individualized behavior in mice. doi:10.1101/851907.

37. Raj, A., Rifkin, S. A., Andersen, E. & van Oudenaarden, A. Variability in gene expression underlies incomplete penetrance. *Nature* **463**, 913–918 (2010).

38. Li, H. *et al.* Classifying Drosophila Olfactory Projection Neuron Subtypes by Single-Cell RNA Sequencing. *Cell* **171**, 1206–1220.e22 (2017).

39. Münch, D. & Galizia, C. G. DoOR 2.0--Comprehensive Mapping of Drosophila melanogaster Odorant Responses. *Sci. Rep.* **6**, 21841 (2016).

40. Wu, J. S. & Luo, L. A protocol for dissecting Drosophila melanogaster brains for live imaging or immunostaining. *Nat. Protoc.* **1**, 2110–2115 (2006).

41. Olsen, S. R. & Wilson, R. I. Lateral presynaptic inhibition mediates gain control in an olfactory circuit. *Nature* **452**, 956–960 (2008).

42. Yaksi, E. & Wilson, R. I. Electrical coupling between olfactory glomeruli. *Neuron* **67**, 1034–1047 (2010).

43. Luo, S. X., Axel, R. & Abbott, L. F. Generating sparse and selective third-order responses in the olfactory system of the fly. *Proc. Natl. Acad. Sci. U. S. A.* **107**, 10713–10718 (2010).

This page is intentionally left blank

Chapter III: Idiosyncratic learning performance in flies generalizes across modalities

Abstract

Individuals vary in their innate behaviors, even when they have the same genome and have been reared in the same environment. The extent of individuality in plastic behaviors, like learning, is less well characterized. Also unknown is the extent to which intragenotypic differences in learning generalize: if an individual performs well in one assay, will it perform well in other assays? We investigated this using the fruit fly *Drosophila melanogaster*, an organism long-used to study the mechanistic basis of learning and memory. We found that isogenic flies, reared in identical lab conditions, and subject to classical conditioning that associated odorants with electric shock, exhibit clear individuality in their learning responses. Flies that performed well when an odor was paired with shock tended to perform well when other odors were paired with shock, or when the original odor was paired with bitter taste. Thus, individuality in learning performance appears to be prominent in isogenic animals reared identically, and individual differences in learning performance generalize across stimulus modalities. Establishing these results in flies opens up the possibility of studying the genetic and neural circuit basis of individual differences in learning in a highly suitable model organism.

Introduction

Genetically identical *Drosophila melanogaster* flies display variability in their behaviors even when reared in identical environments (1–8) . Such individuality has been observed in phototaxis

(4), spontaneous locomotor biases (3), thermal preference (2), spontaneous microbehaviors (7), and object-fixated locomotion (8). These differences persist over days and represent something like a fly personality. Work to date has focused exclusively on innate or spontaneous behaviors. But plastic behaviors, such as learning, also have the potential to exhibit individuality, as each animal may have an idiosyncratic propensity to respond to training stimuli (9). Individual variation in learning among genetically identical flies has not been formally characterized.

Here we present evidence that genetically identical flies exhibit individuality in their ability to learn odor associations. In this classical conditioning paradigm, animals are exposed to two stimuli, a conditioned stimulus (CS), to which their behavioral response will change across the conditioning, and an unconditioned stimulus (US), to which their response will remain invariant (10). Typically, the CS is subdivided into two stimuli of the same modality (e.g., two odors) one of which (CS+) is delivered simultaneously with the US, and one of which (CS-) is delivered separately from the US, serving as a control. In a typical *Drosophila* olfactory classical conditioning assay (11), the CS are volatile aversive odorants, often 3-octanol (OCT) and 4-methylcyclohexanol (MCH), and the US is aversive electric shock.

While this assay is normally performed on bulk populations of dozens of flies simultaneously, we individualized it to deliver CS and US to single flies, one per assay chamber. Our implementation also permitted the selection of different CS odorants under computer control and the use of either electric shock or optogenetic activation (12) of negative valence neural circuit elements as US (13). This flexibility over the learning stimuli allowed us to ask high-level questions about individuality in learning. For example, does a fly's performance on one learning task predict its performance on another learning task? We tested this by measuring a fly's ability to relearn the opposite association to which it was recently trained (i.e., swapping the CS+ and CS-

odors). This reversal learning represents a more cognitively demanding form of learning compared to classical conditioning because it requires modification of the previous association. In vertebrates performance on reversal learning tasks has been used as a measure of impulsive and compulsive addiction behaviors (14). In the Drosophila system, reversal learning has been proposed as a metric of cognitive flexibility (15–18). We also measured the correlation in learning responses between OCT-MCH as CS and an entirely novel odor pair.

Correlated learning performance across multiple CS odors might arise by individual variation in the sensory circuits detecting US cues (an animal that is generally insensitive to shock may fail to learn an odor-shock pairing). This scenario is consistent with the observation that training flies with a higher voltage US leads to better performance in a learning assay as compared to training with a lower voltage US (19). We examined individual differences in US encoding by training the same flies across multiple US modalities: shock and optogenetic stimulation of bitter taste receptor neurons. We found a positive correlation in the learning response of flies to shock and bitter stimulation. Thus, individual learning performance appears to generalize across odors as well as unconditioned stimuli. This suggests that higher-order plasticity circuits within the brain, rather than the sensory periphery, may harbor the sites where molecular- or circuit-level variation imparts individuality to learning responses. Mapping such "loci of individuality" (20) is a compelling direction for future work to characterize the basis of variation in learning ability in this model system.

Materials and Methods

All flies were grown on cornmeal/dextrose food in incubators (25C, 40% relative humidity, 12:12 h light:dark cycle). Behavior experiments were conducted females 7-8 days post eclosion. For optogenetic experiments, flies expressing *Gr66a-LexA* in bitter taste receptors were crossed to flies expressing *LexAop-CsChrimson,* the optogenetic activator. In experimental groups receiving the optogenetic US, 10ul of 100mM all-trans-retinal (ATR) was applied to the surface of fly food, and flies were housed on this food for at least 48 hours. Flies were aspirated directly into the behavioral arenas without anesthetization. The arenas consisted of 15 linear tunnels with inlets at either end and a vent at the center (figure 1A-B). A single fly is placed into each tunnel and is allowed to walk freely. Laminar airflow carrying odor stimuli enters the tunnels from either end and meets at the center, forming a sharp boundary. From there, the odorized air is vented to the room (figure 1B). Odors were delivered by flowing clean air over liquid odorants in a series of vials, under the control of solenoids and mass-flow controllers, as described in (6). Within the arena, flies were presented one pair of odors (e.g., MCH vs. octanol or 1-pentanol vs. 2-heptanone). During the training phase, both tunnel halves are filled with a single odor, if the odorant is the CS+ then the US is activated when the tunnel is filled with that odorant. For optogenetic experiments, 685nm red LEDs were used to activate csChrimson. These LEDs were pulsed at 20Hz for 3 seconds delivered triggered at 5 second intervals. For shock experiments, laser cut sheets of indium-tin-oxide (ITO) were installed in the tunnels to deliver 80V DC pulses from a Grass SD9 Pulse Stimulator at 20Hz for 5 seconds delivered at 10 second intervals. An individual's learning score was measured by the normalized magnitude of change in occupancy towards the CS- from pre-training to post-training. This metric has a value of 0 if flies exhibit no learning, 1 if they spend all their time post-training in the CS- compartment, and -1 if they spend all their time post-training in

the CS+ compartment. Normalizing by the pre-training preference score accounts for individual variation in baseline preference (6).

$$\text{Learning score} = \begin{cases} \frac{\text{post-pre}}{\text{1-pre}}, & \text{post - pre} > 0 \\ \frac{\text{post-pre}}{\text{pre}}, & \text{post-pre} <= 0 \end{cases} \quad (1.1)$$

The individual identity of flies whose learning performance was assessed more than once was maintained by housing flies in 96 well plates modified for individual storage (flyPlates, FlySorter, LLC). All learning assays were conducted in a temperature-controlled environmental chamber in total darkness at 25C and 40% relative humidity. Flies were illuminated from below using a modified 15-inch laptop display panel equipped with a high-density infrared LED array for homogenous backlighting, as described in (6). We used a high-resolution CMOS camera (Point Grey Firefly MV) and longpass filter (Kodak Wratten Filter 87C) to collect 60Hz video. Tracking was performed using custom MATLAB scripts that used 2D cross-correlation for tunnel and initial fly identification, and background subtraction to segment fly boundaries. Data analysis was performed using custom MATLAB scripts.

Results

To characterize the learning responses of individual flies, we built an instrument (figure 1A) that could deliver odor conditioned stimuli and optogenetic and electric shock unconditioned stimuli to 15 flies simultaneously. Laminar airflow carrying odorants originates from the tunnel ends and meets at the center of the tunnel to create a sharp odor-choice boundary (figure 1B), as previously described (6). We used a classical conditioning and reversal learning protocol (figure 1C) to form associations between odors and the aversive US. In our first experiments we used MCH and OCT (4-methylcyclohexanol and 3-octanol), standard CS odorants for classical conditioning in flies.

Each training assay consisted of a 2 min pre-training period in which both odorants were present in the tunnels, allowing us to measure flies' naïve, untrained odor preference. Flies were then subjected to a series of training blocks, in which the entire tunnel was filled with one odorant or the other, in alternation. Electric shock (US) was triggered when MCH (CS+) filled the entire tunnel. In a final 2 min post-training phase, both odors were presented again. Flies' preference for OCT was quantified before and after training as the amount of time spent in OCT divided by total time spent in OCT and MCH.

Five minutes after this forward training protocol, flies were subject to the reversal learning protocol, which was structured identically except that OCT was the CS+ odorant. As expected, the classical conditioning and reversal learning assays resulted in significant changes in mean OCT preference across flies (figure 1D). This mean change was not observed in control experiments (e.g., presenting CS only, or breaking its pairing with the US; See figure S1). However, we also observed individual flies that appeared to not learn, with similar preference for OCT pre- and post-training or increased OCT-preference even when OCT was the CS+.

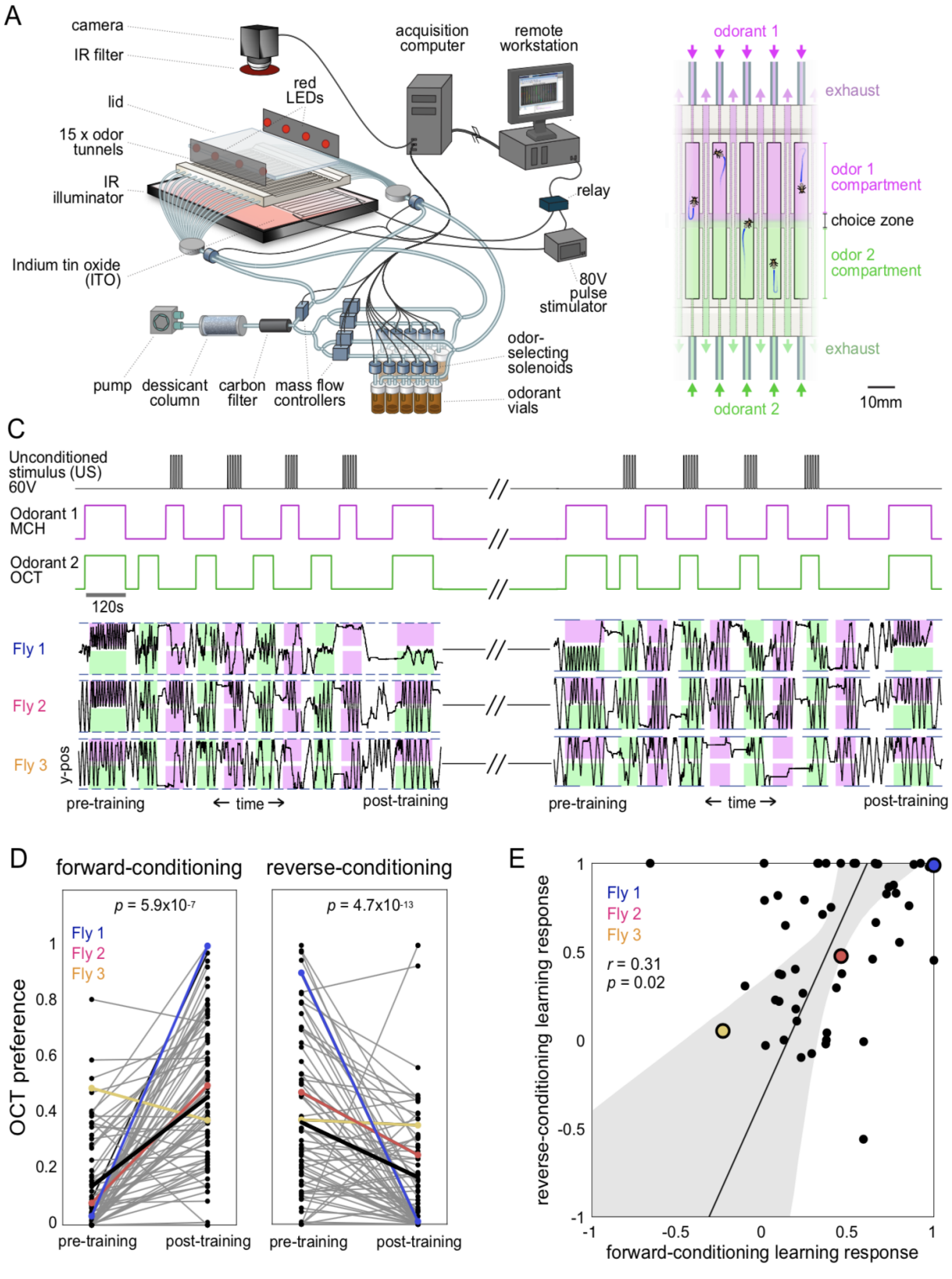

A
camera
IR filter
lid
15 x odor tunnels
IR illuminator
Indium tin oxide (ITO)
red LEDs
acquisition computer
remote workstation
relay
80V pulse stimulator
odor-selecting solenoids
odorant vials
pump
dessicant column
carbon filter
mass flow controllers
odorant 1
exhaust
odor 1 compartment
choice zone
odor 2 compartment
exhaust
odorant 2
10mm
C
Unconditioned stimulus (US) 60V
Odorant 1 MCH
Odorant 2 OCT
120s
Fly 1
Fly 2
Fly 3
y-pos
pre-training
time
post-training
pre-training
time
post-training
D
forward-conditioning
reverse-conditioning
p = 5.9x10-7
p = 4.7x10-13
Fly 1
Fly 2
Fly 3
OCT preference
pre-training
post-training
pre-training
post-training
E
Fly 1
Fly 2
Fly 3
r = 0.31
p = 0.02
reverse-conditioning learning response
forward-conditioning learning response

Figure 1. (A) Schematic of the odor conditioning experimental apparatus. (B) Zoom-in view of the linear behavioral arenas, with odorant flowing into each half. (C) Diagram of training protocol (top). Position in the arena versus time kymographs of three specific flies undergoing conditioning. Magenta and green shading indicate the portions of each arena that are filled with OCT and MCH, respectively. (D) Octanol preference of flies before and after training with MCH as the CS+ (left) and with OCT as the CS+ (right). Points are individual flies. Colored examples correspond to (C). Thick black line represents the mean. (E) Scatterplot of individuals' learning scores for the reverse- vs forward-conditioning trials ($r = 0.31$; $p = 0.02$; $n = 53$). Points are individual flies. Line is the best linear fit and shaded region is the 95%CI of the best-fit line.

These observations could reflect statistical noise, rather than individual variation in learning response. To test this, we examined the correlation between the learning response during the forward-conditioning protocol and the learning response in the reverse-conditioning protocol. This correlation was positive and significant across individual flies ($r = 0.31$, $p = 0.02$), suggesting that individual animals have idiosyncratic learning responses that generalize across the identity of the CS+ odorant. Differences in learning response were not correlated with a fly's activity (distance traveled) during the assay or initial odor preference (figure S2).

The observation that individual performance following forward- and reverse-conditioning is correlated suggests that learning ability may generalize across modalities in flies. To explore this possibility, we designed a two day assay in which flies were forward- and reverse-conditioned with 1-pentanol and 2-heptanone as CS odors, stored for 24 hours, and forward- and reverse-conditioned with MCH and OCT (figure 2A). In addition, we substituted optogenetic stimulation of bitter taste neurons as the US instead of electric shock. This was done by expressing CsChrimson (12) in bitter taste neurons using the *Gr66a-LexA* driver , and exposing flies to 630nm LED illumination in place of the electric shocks. Replacing shock with bitter taste let us assess whether individuality and correlation between forward- and reverse-conditioning performance is US-specific.

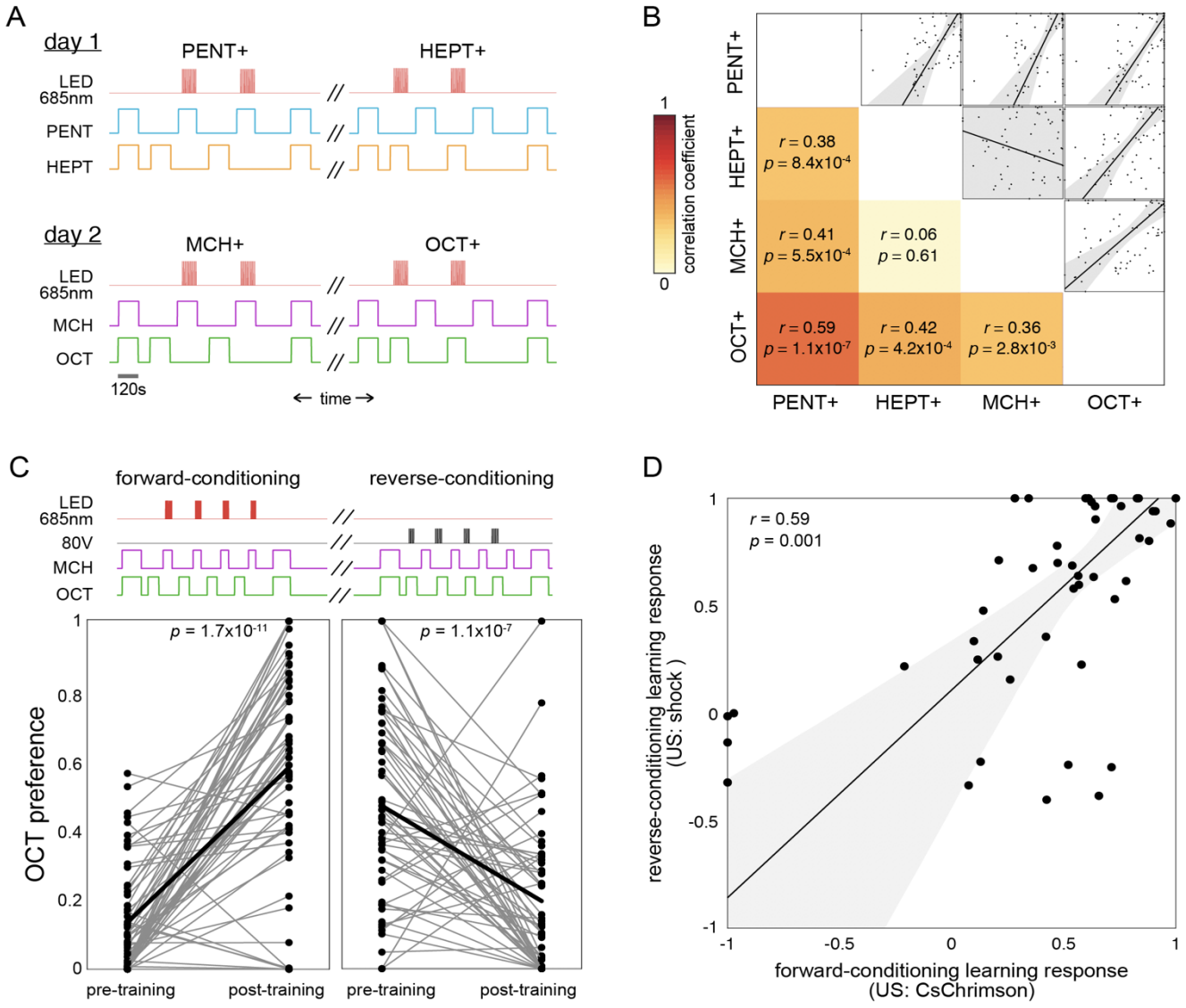


Figure 2. (A) Schematic of the two day conditioning protocol with two different odor pairs and optogenetic US. (B) Correlation matrix for individual fly learning responses for all pairs of the four different learning trials in (A). x- and y-axes of scatter subplots correspond respectively to the learning scores of the CS+ condition indicated by the column and row of the matrix. Points are individual flies. Line is the best linear fit and shaded region is the 95%CI of the best-fit line. (C) Schematic of the back-to-back conditioning paradigms with different US (top). Octanol preference of flies before and after training with shock as the US (left) or optogenetic activation of bitter taste neurons (right). Points are individual flies. Thick black line represents the mean. (D) Scatterplot of learning responses to the shock US trial versus the bitter taste US trial ($r = 0.45$; $p = 0.01$; $n = 47$). Points are individual flies. Line is the best linear fit and shaded region is the 95%CI of the best-fit line.

In addition, by looking at learning performance after 24 h, we could assess whether individual variation in learning performance is stable over time. As we saw with shock-odor conditioning, flies subject to optogenetic bitter-odor conditioning exhibited mean learned avoidance of the CS+ odor (figure S3) as well as individuality in forward- and reverse-conditioning performance (figure S4). We observed significant correlations in individual learning performance among almost all four conditioning variants in this experiment ($0.36 < r < 0.59$; $10^{-5} < p < 3\text{x}10^{-3}$; figure 2B). The exception was MCH+ and 2-heptanone+, for which learning performance was uncorrelated ($r = 0.06$; $p = 0.61$). These results suggest that individuality in learning performance is odor CS- and US-independent and stable over at least 24h.

A possible explanation of these results is individual variation in US encoding. Flies that receive stronger shocks show stronger learning responses (19), so spontaneous variation in the perception of a US (either shock or bitter taste) may affect the learning responses for many CS. We tested this by performing forward- and reverse-conditioning assays with OCT and MCH, but switching between US within the same animals (figure 2C). Both forward- and reverse-conditioning assays show significant mean differences in odor preference (Wilcoxon rank-sum test; $p = 1.7\text{x}10^{-9}$; figure 2C). Comparing across US modalities, we observed a positive correlation in learning responses ($r = 0.59$; $p = 1.4\text{x}10^{-5}$; figure 2D). This suggests that in addition to generalizing across CS odorant identity, individual differences in fly learning performance may generalize across US modalities.

Discussion

Using a training instrument that 1) has versatile control over CS and US and 2) tracks individual learned behavior, we observed that flies are idiosyncratic in their learning performance in classical conditioning paradigms. Flies that perform well for one CS/US pair tend to perform well for other CS and US, suggesting that individual differences in learning performance generalize across stimulus modalities. These results provide a basis upon which to probe the mechanistic basis of individuality in learning. Specifically, our results suggest that the biological basis for such idiosyncrasy in olfactory learning originates more centrally in the brain than sensory circuit elements dedicated to encoding either CS or US. Perhaps there are circuit elements encoding valence generally, which are activated by alternative US and can be paired with alternative CS, that vary stochastically across individuals, accounting for their individual performance (1). Such sites would be "loci of individuality" (20) for learning performance. Mushroom body dopaminergic neurons (DANs; (21, 22)) and output neurons (MBONs; (23)) are strong candidates, but valence might also be encoded broadly across multiple populations of higher-order learning circuit neurons. Bee calcium responses in the antennal lobe (24) and mushroom body (25) show increased neuronal plasticity results in more cognitive flexibility and better performance on learning assays. In bumblebees, performance on a visual learning task and the micro glomerular density in the collar of the mushroom body (26) were correlated across individuals. Circuit elements known to exhibit high developmental stochasticity (8) may also be natural locus of individuality candidates. The wiring between projection neurons and mushroom body kenyon cells is highly stochastic (27). However, that stochasticity may have evolved for the versatile encoding of large odor stimulus spaces, and is distributed over a large population of kenyon cells (~2500). Any single stochastic PN-KC synapse variant may have a vanishing effect

amidst such a large pool of (presumably) independent wiring variations. The mushroom body mediates learning and memory for other sensory modalities including vision. It is unknown if learning performance generalizes across CS sensory modalities in *Drosophila* (i.e., beyond different kinds of odors). Flies may be a promising model for characterizing the circuit basis of individual variation in generalized learning ability, which is evident even when individuals are genetically identical and reared in the same environment.

References

1. K. Honegger, B. de Bivort, Stochasticity, individuality and behavior. *Curr. Biol.* **28**, R8–R12 (2018).

2. J. S. Kain, *et al.*, Variability in thermal and phototactic preferences in Drosophila may reflect an adaptive bet-hedging strategy : BET-HEDGING EXPLAINS THERMOTACTIC VARIABILITY. *Evolution* **69**, 3171–3185 (2015).

3. S. M. Buchanan, J. S. Kain, B. L. de Bivort, Neuronal control of locomotor handedness in Drosophila. *Proc. Natl. Acad. Sci. U. S. A.* **112**, 6700–6705 (2015).

4. J. S. Kain, C. Stokes, B. L. de Bivort, Phototactic personality in fruit flies and its suppression by serotonin and white. *Proc. Natl. Acad. Sci. U. S. A.* **109**, 19834–19839 (2012).

5. J. F. Ayroles, *et al.*, Behavioral idiosyncrasy reveals genetic control of phenotypic variability. *Proc. Natl. Acad. Sci. U. S. A.* **112**, 6706–6711 (2015).

6. K. S. Honegger, M. A.-Y. Smith, M. A. Churgin, G. C. Turner, B. L. de Bivort, Idiosyncratic neural coding and neuromodulation of olfactory individuality in Drosophila. *Proc. Natl. Acad. Sci. U. S. A.* (2019) https:/doi.org/10.1073/pnas.1901623116.

7. J. G. Todd, J. S. Kain, B. L. de Bivort, Systematic exploration of unsupervised methods for mapping behavior. *Phys. Biol.* **14**, 015002 (2017).

8. G. Linneweber, M. Andriatsilavo, S. Dutta, L. Hellbruegge, A neurodevelopmental origin of behavioral individuality. *bioRxiv* (2019).

9. A. Claridge-Chang, *et al.*, Writing memories with light-addressable reinforcement circuitry. *Cell* **139**, 405–415 (2009).

10. R. A. Rescorla, Pavlovian conditioning and its proper control procedures. *Psychol. Rev.* **74**, 71–80 (1967).

11. T. Tully, W. G. Quinn, Classical conditioning and retention in normal and mutantDrosophila melanogaster. *Journal of Comparative Physiology A* **157**, 263–277 (1985).

12. N. C. Klapoetke, *et al.*, Independent optical excitation of distinct neural populations. *Nat. Methods* **11**, 338–346 (2014).

13. A. C. Keene, P. Masek, Optogenetic induction of aversive taste memory. *Neuroscience* **222**, 173–180 (2012).

14. A. Izquierdo, J. D. Jentsch, Reversal learning as a measure of impulsive and compulsive

behavior in addictions. *Psychopharmacology* **219**, 607–620 (2012).

15. B. R. Foley, P. Marjoram, S. V. Nuzhdin, Basic reversal-learning capacity in flies suggests rudiments of complex cognition. *PLoS One* **12**, e0181749 (2017).

16. N. Mancini, *et al.*, Reversal learning in Drosophila larvae. *Learn. Mem.* **26**, 424–435 (2019).

17. Q. Ren, H. Li, Y. Wu, J. Ren, A. Guo, A GABAergic inhibitory neural circuit regulates visual reversal learning in Drosophila. *J. Neurosci.* **32**, 11524–11538 (2012).

18. Y. Wu, Q. Ren, H. Li, A. Guo, The GABAergic anterior paired lateral neurons facilitate olfactory reversal learning in Drosophila. *Learn. Mem.* **19**, 478–486 (2012).

19. C. D. O. Beck, B. Schroeder, R. L. Davis, Learning Performance of Normal and MutantDrosophila after Repeated Conditioning Trials with Discrete Stimuli. *J. Neurosci.* **20**, 2944–2953 (2000).

20. K. Skutt-Kakaria, P. Reimers, T. A. Currier, Z. Werkhoven, B. L. de Bivort, A neural circuit basis for context-modulation of individual locomotor behavior https:/doi.org/10.1101/797126.

21. Y.-C. Kim, H.-G. Lee, K.-A. Han, D1 dopamine receptor dDA1 is required in the mushroom body neurons for aversive and appetitive learning in Drosophila. *J. Neurosci.* **27**, 7640–7647 (2007).

22. K. P. Siju, V. Stih, S. Aimon, J. Gjorgjieva, R. Portugues, Valence and state-dependent population coding in dopaminergic neurons in the fly mushroom body. *bioRxiv* (2019).

23. T. Hige, Y. Aso, M. N. Modi, G. M. Rubin, G. C. Turner, Heterosynaptic Plasticity Underlies Aversive Olfactory Learning in Drosophila. *Neuron* **88**, 985–998 (2015).

24. L. Rath, C. Giovanni Galizia, P. Szyszka, Multiple memory traces after associative learning in the honey bee antennal lobe. *Eur. J. Neurosci.* **34**, 352–360 (2011).

25. J. Haenicke, N. Yamagata, H. Zwaka, M. Nawrot, R. Menzel, Neural Correlates of Odor Learning in the Presynaptic Microglomerular Circuitry in the Honeybee Mushroom Body Calyx. *eNeuro* **5** (2018).

26. L. Li, *et al.*, A possible structural correlate of learning performance on a colour discrimination task in the brain of the bumblebee. *Proc. Biol. Sci.* **284** (2017).

27. S. J. C. Caron, V. Ruta, L. F. Abbott, R. Axel, Random convergence of olfactory inputs in the Drosophila mushroom body. *Nature* **497**, 113–117 (2013).

This page is intentionally left blank

Conclusion:

Throughout my PhD I have investigated the basis of variability in olfactory behaviors in both in naïve and learning contexts within genetically identical *Drosophila melanogaster*. Broadly, our goals were to 1) Determine how behavioral responses to identical stimuli vary across individuals 2) Determine how the neural coding of identical stimuli in a model sensory system varies across individuals and obtain mechanistic understanding of how these differences arise. 3) Examine the extent to which neural differences translate into idiosyncratic differences in behavior. We have largely accomplished these goals through measuring idiosyncratic odor preferences in isogenic Droso*phila melanogaster.* We've found that individual odor preferences are stable across multiple days, representing something akin to a fly personality. Different neural populations and neuromodulators are able to increase and/or decrease the amount of olfactory behavioral variability within a group of isogenic animals. Specifically local interneurons within the antennal lobe reduce overall behavioral variability through both activation and silencing. Pairing animal behavior with 2-photon live Ca++ volumetric imaging we show that idiosyncratic calcium dynamics in both ORNs and PNs predict individual preferences for an aversive monomolecular odorant versus air, suggesting that variation at the periphery of the olfactory system determines individual preference for an odor's presence. In contrast, PN, but not ORN, calcium responses predict individual preferences in a two-odor choice assay. Furthermore, paired behavior and immunohistochemistry measurements reveal that variation in ORN presynaptic density also predicts two-odor preference, suggesting this site is a locus of individuality where microscale circuit variation gives rise to idiosyncrasy in behavior. Lastly, we found that flies display individuality in response to olfactory association tasks, and show a generality in learning performance across US and CS modalities.

Suggesting individual to individual differences in capacity for plasticity dependent events. We believe these results will reveal sources of variation in neural circuits that could function as substrates for natural selection or ecological strategies.

Using our custom odor tunnels we had shown that isogenic flies displayed significant behavioral variability in odor preference. This was a key finding, but supported by work showing significant behavioral variability in various other ecologically relevant *Drosophila* behaviors (1–5). Although individuality in odor preferences exist in humans, the neurobiological and even environmental basis of such individuality is not fully understood. In humans, both sociocultural experience (6) and genetic polymorphisms in odorant receptors (7) explain some individual variation in odor perception, however it remains unclear exactly how this affects downstream odor coding and behavior(8). Our work builds upon these results and demonstrates how inter-animal sensory periphery variability reflects variability in output behavior.

Utilizing the molecular genetic toolkit in Drosophila, we were able to reliably measure odor representations in the early sensory periphery in repeated trials within a fly and compared responses across individual flies. To accomplish this we used fly's that expressed GCaMP6m in 60% of the PNs in the antennal lobe. We coupled volumetric 2-photon scans of the antennal lobe with presentation of 12 different odors. Using a semi-automated pipeline we could identify specific glomerular micro-compartments across flies to compare the response to identical odors. We found that despite the stereotyped anatomy of the antennal lobe, we found idiosyncrasy in response to odors across flies. We determined this through comparing an odor representation of all 12 odors projected into a PCA space. Through presenting the 12-odor panel multiple times to the fly we determined that odor representations are represented uniquely in each fly, and these unique representations are repeatable across trials. We found this to be true for the odor representations

of OCT and MCH, the two odors that we evaluated odor preference behavior of. We thought to evaluate the role of local neurons in generating the idiosyncratic odor behavior. In the presence of excess serotonin, the AL projection neurons become more responsive (9). Our imaging results yielded a similar response increase in responsiveness of PNs for both global decreases and increases of serotonin. This may be an effective mechanism to increase serotonin dependent control over olfactory behavior, through increase in responsiveness in PNs within the antennal lobe, leading to more stereotyped behavioral response.

Serotonin and dopamine, two highly evolutionarily conserved neuromodulators, had an effect on modulating the magnitude of behavioral variability of odor preference. Globally decreasing serotonin levels decreased the amount of individuality in a dose dependent manner, however, the increase of serotonin did not have a significant effect. This agreed with our result of activating the sole serotonergic input into the antennal lobe, the contralaterally-projecting serotonin immunoreceptive deuotocerebral neurons (CSD neurons) (10–12), which did not have an effect on behavioral variability. Our result was surprising, as the CSD neuron has been shown to be a strong modulator of olfactory behavior through releasing high levels of serotonin (13) (14). In mammals, homologous 5-HT receptors are known to motivate, stimulate appetite and mood, suggesting some conservation of function for serotonergic regulation of behaviors (15). A first thought is that the amount of behavioral variability modulated by serotonin is already close to some functional saturation, which would allow a decrease in variability but not increase from any serotonin manipulation. In any case, to resolve the effects of serotonin, specifically in the antennal lobe, we'd need more precise control of serotonin receptor expressing neurons. Interestingly, we found bi-directional modulation of behavioral variability with dopamine, increase and decrease with food supplemented with L-DOPA or a dopamine receptor null mutant, respectively. The

majority of dopamine's role in odor processing occurs in the MB as encoding the valence of the incoming odor information (16). Similar to our serotonin experiment, these were global changes that were made to dopamine throughout the fly, thus we need to perform more precise dopamine manipulations to determine a precise mechanism. We can hypothesize that dopamine facilitating plasticity events could increase individual differences in mushroom body and output (17).

Whether we activated or silenced different LN populations the behavioral variability decreased. We can understand this effect through the LNs potentially working as homeostatic regulators for incoming odor information. The LN population could adjust for idiosyncratic differences across animals in encoding odor information and may adjust signal to some population mean. The LN population represents a core area of individual-to-individual variation in anatomy and physiology within the AL (18, 19). One could image repeating our functional imaging study with GCaMP6m expressed in the LN population. Since the LNs have a significant role in attenuating incoming signals (18, 20), I expect LN activity to predict both odor-odor preference and odor-air preference, however, with lower accuracy than PNs or ORNs.

We paired behavior and two-photon imaging measurements to show that idiosyncratic calcium dynamics in both ORNs and PNs predict individual preferences for an aversive monomolecular odorant versus air, suggesting that variation at the periphery of the olfactory system determines individual preference for an odor's presence. In contrast, PN, but not ORN, calcium responses predict individual preferences in a two-odor choice assay. Furthermore, paired behavior and immunohistochemistry measurements reveal that variation in ORN presynaptic density also predicts two-odor preference, suggesting this site is a locus of individuality where microscale circuit variation gives rise to idiosyncrasy in behavior. Our results demonstrate how a neural circuit may vary functionally and structurally to produce variable behavior among

individuals. Previous work has found mammalian peripheral circuit areas are predictive of individual behavior (21–24). Here we show that sensory elements of the *Drosophila* olfactory circuit constitute neural loci of behavioral individuality. We have identified two distinct circuit mechanisms underlying individual preferences. Global mean or relative responses measured in the AL predict individual preferences for odor against air or odor against odor, respectively. The variation in the specific circuit elements that cause these differences in neural activity are likely to be different since we have shown that idiosyncratic ORN activity predicts odor against air, but not odor against odor, preferences, whereas PN activity is predictive in both cases. Therefore, variation at distinct sites within the nervous system contributes to different aspects of behavioral individuality.

Our predictions of individual preference from neural activity yield R^2 values in the range of 0.1 to 0.3. It is worth noting that the persistence of individual odor preference is relatively low (R^2=0.1-0.3) on the 3 hour timescale of preference measurement to imaging. To put our behavioral predictions in the context of low persistence, we simulated preferences and neural predictions as a function of the behavioral persistence and neural-behavior prediction R^2 . This model indicates that the fraction of behavioral variation explainable by neural idiosyncrasies is greater than 50%. The low persistence of odor preference may be explained by unaccounted factors like neural state or plasticity, both of which would also confound neural predictions of individual preference. Furthermore, it is unclear whether the same circuit elements which vary to predict behavior on average also vary to predict trial-to-trial variations within individuals. In addition, we were unable to jointly measure neural dynamics and neural structure. In the future it will be important to confirm that variation in wiring or synapse density in fact alters calcium dynamics in a manner which predicts individual behavior. Our measurements of idiosyncratic calcium dynamics are

better able to predict behavior than our measurements of synapse density, indicating there is behavioral variation remaining to be explained at the molecular level. Past work has identified local neurons as a particularly variable population(25), so it may be that variation in LN wiring or responsiveness contributes to the variable ORN and PN dynamics we observed.

The fly populations used in our experiments were isogenic and raised under standard laboratory conditions. Unlike enriched environments, which have been shown to result in increased behavioral individuality (26–28), it is unclear how relatively uniform rearing environments like those employed here could generate significant differences in development or experience. Nevertheless, we observed persistent variation in behavior which could be predicted by idiosyncratic neural function and structure. What molecular events account for the neural and behavioral idiosyncrasy we describe? While developing nervous systems are thought to employ various compensation mechanisms to ensure robustness(29, 30), the accretion of subtle variations in experience—even in nominally uniform rearing environments—might be responsible for the neural variation we found here to predict individual behavior. Genomic variation between inbred siblings might be an alternative explanation. Beyond genomic and environmental variations, stochasticity in gene expression during development(31, 32) governed by thermodynamic noise could result in anatomical variations which underlie coding idiosyncrasies and individual personalities. Development of non-invasive methods to longitudinally assay the fine-scale molecular and anatomical makeup of behaving organisms throughout development and adulthood will be required to further pinpoint the mechanistic origins of individuality. Behavior varies even among genetically identical animals raised in the same environment(33–42). However, little is known about the circuit or anatomical underpinnings of this individuality(43, 44), though previous work implicates sensory periphery(45, 46). *Drosophila* olfaction presents an ideal model to study

the biological basis of behavioral individuality, because while the neural circuit underlying olfactory behavior is well-described(47–50) and highly stereotyped(49), persistent idiosyncrasy in behavior(51), neural coding(52), and neural wiring(29, 53) have also been described. Projection neurons (PNs), which relay odor signals sensed by olfactory receptor neurons (ORNs) to deeper brain structures(54–56), exhibit variable calcium responses to identical odor stimuli across individuals, but how these idiosyncrasies relate to individual behavioral responses remains unknown. Here, using paired behavior and two-photon imaging measurements, we show that idiosyncratic calcium dynamics in both ORNs and PNs predict individual preferences for an aversive monomolecular odorant versus air, suggesting that variation at the periphery of the olfactory system determines individual preference for an odor's presence. In contrast, PN, but not ORN, calcium responses predict individual preferences in a two-odor choice assay. Furthermore, paired behavior and immunohistochemistry measurements reveal that variation in ORN presynaptic density also predicts two-odor preference, suggesting this site is a locus of individuality where microscale circuit variation gives rise to idiosyncrasy in behavior. Our results demonstrate how a neural circuit may vary functionally and structurally to produce variable behavior among individuals.

Using a training instrument that 1) has versatile control over CS and US and 2) tracks individual learned behavior, we observed that flies are idiosyncratic in their learning performance in classical conditioning paradigms. Flies that perform well for one CS/US pair tend to perform well for other CS and US, suggesting that individual differences in learning performance generalize across stimulus modalities. These results provide a basis upon which to probe the mechanistic basis of individuality in learning. Specifically, our results suggest that the biological basis for such idiosyncrasy in olfactory learning originates more centrally in the brain than sensory circuit

elements dedicated to encoding either CS or US. Perhaps there are circuit elements encoding valence generally, which are activated by alternative US and can be paired with alternative CS, that vary stochastically across individuals, accounting for their individual performance(57). Such sites would be "loci of individuality"(3) for learning performance. Mushroom body dopaminergic neurons (DANs;(58)) and output neurons (MBONs;(59)) are strong candidates, but valence might also be encoded broadly across multiple populations of higher-order learning circuit neurons. Bee calcium responses in the antennal lobe(60) and mushroom body(61) show increased neuronal plasticity results in more cognitive flexibility and better performance on learning assays. In bumblebees, performance on a visual learning task and the micro glomerular density in the collar of the mushroom body(62) were correlated across individuals. Circuit elements known to exhibit high developmental stochasticity(63) may also be natural locus of individuality candidates. The wiring between projection neurons and mushroom body kenyon cells is highly stochastic(64). However, that stochasticity may have evolved for the versatile encoding of large odor stimulus spaces, and is distributed over a large population of kenyon cells (~2500). Any single stochastic PN-KC synapse variant may have a vanishing effect amidst such a large pool of (presumably) independent wiring variations. The mushroom body mediates learning and memory for other sensory modalities including vision and (65). It is unknown if learning performance generalizes across CS sensory modalities in *Drosophila* (i.e., beyond different kinds of odors). Flies may be a promising model for characterizing the circuit basis of individual variation in generalized learning ability, which is evident even when individuals are genetically identical and reared in the same environment.

These findings change our perspective on individuality of behavior, and we have identified sources of variation in neural circuits that could function as substrates for natural

selection or ecological strategies. We've shown that such individuality is, in part, the result of differences in odor coding within the peripheral nervous system in invertebrates, specifically the projection neurons. While activity within olfactory receptor neurons predicts odor-air sensitivity. We've also shown that learning within isogenic animals exhibits individuality that generalizes across modalities, both US and CS. We believe that there are substantial and interesting directions from this collection of works that will continue to contribute significantly to the field, and hope that our work will encourage the field to focus on individual differences in future studies.

1. J. F. Ayroles, *et al.*, Behavioral idiosyncrasy reveals genetic control of phenotypic variability. *Proc. Natl. Acad. Sci. U. S. A.* **112**, 6706–6711 (2015).

2. S. M. Buchanan, J. S. Kain, B. L. de Bivort, Neuronal control of locomotor handedness in Drosophila. *Proc. Natl. Acad. Sci. U. S. A.* **112**, 6700–6705 (2015).

3. K. Skutt-Kakaria, P. Reimers, T. A. Currier, Z. Werkhoven, B. L. de Bivort, A neural circuit basis for context-modulation of individual locomotor behavior https:/doi.org/10.1101/797126.

4. K. S. Kakaria, B. L. de Bivort, Ring Attractor Dynamics Emerge from a Spiking Model of the Entire Protocerebral Bridge. *Front. Behav. Neurosci.* **11**, 8 (2017).

5. J. S. Kain, *et al.*, Variability in thermal and phototactic preferences in Drosophila may reflect an adaptive bet-hedging strategy : BET-HEDGING EXPLAINS THERMOTACTIC VARIABILITY. *Evolution* **69**, 3171–3185 (2015).

6. A. Keller, M. Hempstead, I. A. Gomez, A. N. Gilbert, L. B. Vosshall, An olfactory demography of a diverse metropolitan population. *BMC Neurosci.* **13**, 122 (2012).

7. J. D. Mainland, *et al.*, The missense of smell: functional variability in the human odorant receptor repertoire. *Nat. Neurosci.* **17**, 114–120 (2014).

8. D. Pita, B. Collignon, J. Halloy, E. Fernández-Juricic, Collective behaviour in vertebrates: a sensory perspective. *R Soc Open Sci* **3**, 160377 (2016).

9. A. M. Dacks, D. S. Green, C. M. Root, A. J. Nighorn, J. W. Wang, Serotonin modulates olfactory processing in the antennal lobe of Drosophila. *J. Neurogenet.* **23**, 366–377 (2009).

10. X. Zhang, Q. Gaudry, Functional integration of a serotonergic neuron in the Drosophila antennal lobe. *Elife* **5** (2016).

11. C. Pantoja, *et al.*, Neuromodulatory Regulation of Behavioral Individuality in Zebrafish. *Neuron* **91**, 587–601 (2016).

12. T. R. Sizemore, A. M. Dacks, Serotonergic Modulation Differentially Targets Distinct Network Elements within the Antennal Lobe of Drosophila melanogaster. *Sci. Rep.* **6**, 37119 (2016).

13. L. Xu, *et al.*, A Single Pair of Serotonergic Neurons Counteracts Serotonergic Inhibition of Ethanol Attraction in Drosophila. *PLOS ONE* **11**, e0167518 (2016).

14. K. Vogt, *et al.*, Internal state configures olfactory behavior and early sensory processing in Drosophila larva. *bioRxiv*, 2020.03.02.973941 (2020).

15. I. S. Ebenezer, M. J. Arkle, R. M. Tite, 8-Hydroxy-2-(di-N-propylamino)-tetralin (8-OH-DPAT) inhibits food intake in fasted rats by an action at 5-HT1A receptors. *Methods and Findings in Experimental and Clinical Pharmacology* **29**, 269 (2007).

16. K. P. Siju, V. Stih, S. Aimon, J. Gjorgjieva, R. Portugues, Valence and state-dependent population coding in dopaminergic neurons in the fly mushroom body. *bioRxiv* (2019).

17. S. Yamamoto, E. S. Seto, Dopamine dynamics and signaling in Drosophila: an overview of genes, drugs and behavioral paradigms. *Exp. Anim.* **63**, 107–119 (2014).

18. Y.-H. Chou, *et al.*, Diversity and wiring variability of olfactory local interneurons in the Drosophila antennal lobe. *Nat. Neurosci.* **13**, 439–449 (2010).

19. N.-F. Liou, *et al.*, Diverse populations of local interneurons integrate into the Drosophila adult olfactory circuit. *Nat. Commun.* **9**, 2232 (2018).

20. M. Fişek, R. I. Wilson, Stereotyped connectivity and computations in higher-order olfactory neurons. *Nat. Neurosci.* **17**, 280–288 (2014).

21. C. A. Michelson, J. W. Pillow, E. Seidemann, Majority of choice-related variability in perceptual decisions is present in early sensory cortex https:/doi.org/10.1101/207357.

22. L. C. Osborne, S. G. Lisberger, W. Bialek, A sensory source for motor variation. *Nature* **437**, 412–416 (2005).

23. W. T. Newsome, K. H. Britten, J. Anthony Movshon, Neuronal correlates of a perceptual decision. *Nature* **341**, 52–54 (1989).

24. K. H. Britten, W. T. Newsome, M. N. Shadlen, S. Celebrini, J. A. Movshon, A relationship between behavioral choice and the visual responses of neurons in macaque MT. *Vis. Neurosci.* **13**, 87–100 (1996).

25. Y.-H. Chou, *et al.*, Diversity and wiring variability of olfactory local interneurons in the Drosophila antennal lobe. *Nat. Neurosci.* **13**, 439–449 (2010).

26. J. C. Körholz, *et al.*, Selective increases in inter-individual variability in response to environmental enrichment in female mice. *Elife* **7** (2018).

27. J. Akhund-Zade, S. Ho, C. O'Leary, B. de Bivort, The effect of environmental enrichment on behavioral variability depends on genotype, behavior, and type of enrichment. *J. Exp. Biol.* **222** (2019).

28. S. Zocher, *et al.*, Early-life environmental enrichment generates persistent individualized behavior in mice https:/doi.org/10.1101/851907.

29. W. F. Tobin, R. I. Wilson, W.-C. A. Lee, Wiring variations that enable and constrain neural computation in a sensory microcircuit. *Elife* **6**, e24838 (2017).

30. E. Marder, Variability, compensation, and modulation in neurons and circuits. *Proc. Natl. Acad. Sci. U. S. A.* **108 Suppl 3**, 15542–15548 (2011).

31. A. Raj, S. A. Rifkin, E. Andersen, A. van Oudenaarden, Variability in gene expression underlies incomplete penetrance. *Nature* **463**, 913–918 (2010).

32. H. Li, *et al.*, Classifying Drosophila Olfactory Projection Neuron Subtypes by Single-Cell RNA Sequencing. *Cell* **171**, 1206–1220.e22 (2017).

33. J. F. Ayroles, *et al.*, Behavioral idiosyncrasy reveals genetic control of phenotypic variability. *Proc. Natl. Acad. Sci. U. S. A.* **112**, 6706–6711 (2015).

34. S. Stern, C. Kirst, C. I. Bargmann, Neuromodulatory Control of Long-Term Behavioral Patterns and Individuality across Development. *Cell* **171**, 1649–1662.e10 (2017).

35. C. Pantoja, *et al.*, Neuromodulatory Regulation of Behavioral Individuality in Zebrafish. *Neuron* **91**, 587–601 (2016).

36. K. S. Honegger, M. A.-Y. Smith, M. A. Churgin, G. C. Turner, B. L. de Bivort, Idiosyncratic neural coding and neuromodulation of olfactory individuality in. *Proc. Natl. Acad. Sci. U. S. A.* (2019) https:/doi.org/10.1073/pnas.1901623116.

37. A. Renart, C. K. Machens, Variability in neural activity and behavior. *Current Opinion in Neurobiology* **25**, 211–220 (2014).

38. J. Freund, *et al.*, Emergence of individuality in genetically identical mice. *Science* **340**, 756–759 (2013).

39. D. Bierbach, K. L. Laskowski, M. Wolf, Behavioural individuality in clonal fish arises despite near-identical rearing conditions. *Nat. Commun.* **8**, 15361 (2017).

40. D. F. Westneat, J. Wright, N. J. Dingemanse, The biology hidden inside residual within-individual phenotypic variation. *Biol. Rev. Camb. Philos. Soc.* **90**, 729–743 (2015).

41. E. Marder, Variability, compensation, and modulation in neurons and circuits. *Proc. Natl.*

Acad. Sci. U. S. A. **108 Suppl 3**, 15542–15548 (2011).

42. L. Avitan, *et al.*, Behavioral signatures of a developing neural code https:/doi.org/10.1101/856807.

43. G. A. Linneweber, *et al.*, A neurodevelopmental origin of behavioral individuality https:/doi.org/10.1101/540880.

44. K. Skutt-Kakaria, P. Reimers, T. A. Currier, Z. Werkhoven, B. L. de Bivort, A neural circuit basis for context-modulation of individual locomotor behavior https:/doi.org/10.1101/797126.

45. L. C. Osborne, S. G. Lisberger, W. Bialek, A sensory source for motor variation. *Nature* **437**, 412–416 (2005).

46. C. A. Michelson, J. W. Pillow, E. Seidemann, Majority of choice-related variability in perceptual decisions is present in early sensory cortex https:/doi.org/10.1101/207357.

47. J. W. Wang, A. M. Wong, J. Flores, L. B. Vosshall, R. Axel, Two-photon calcium imaging reveals an odor-evoked map of activity in the fly brain. *Cell* **112**, 271–282 (2003).

48. L. B. Vosshall, A. M. Wong, R. Axel, An olfactory sensory map in the fly brain. *Cell* **102**, 147–159 (2000).

49. R. I. Wilson, Transformation of Olfactory Representations in the Drosophila Antennal Lobe. *Science* **303**, 366–370 (2004).

50. L. N. Groschner, G. Miesenböck, Mechanisms of Sensory Discrimination: Insights from Olfaction. *Annu. Rev. Biophys.* **48**, 209–229 (2019).

51. K. S. Honegger, M. A.-Y. Smith, M. A. Churgin, G. C. Turner, B. L. de Bivort, Idiosyncratic neural coding and neuromodulation of olfactory individuality in. *Proc. Natl. Acad. Sci. U. S. A.* (2019) https:/doi.org/10.1073/pnas.1901623116.

52. K. S. Honegger, M. A.-Y. Smith, M. A. Churgin, G. C. Turner, B. L. de Bivort, Idiosyncratic neural coding and neuromodulation of olfactory individuality in. *Proc. Natl. Acad. Sci. U. S. A.* (2019) https:/doi.org/10.1073/pnas.1901623116.

53. Y.-H. Chou, *et al.*, Diversity and wiring variability of olfactory local interneurons in the Drosophila antennal lobe. *Nat. Neurosci.* **13**, 439–449 (2010).

54. R. I. Wilson, Early Olfactory Processing inDrosophila: Mechanisms and Principles. *Annual Review of Neuroscience* **36**, 217–241 (2013).

55. V. Bhandawat, S. R. Olsen, N. W. Gouwens, M. L. Schlief, R. I. Wilson, Sensory processing in the Drosophila antennal lobe increases reliability and separability of ensemble odor representations. *Nat. Neurosci.* **10**, 1474–1482 (2007).

56. A. Couto, M. Alenius, B. J. Dickson, Molecular, anatomical, and functional organization of the Drosophila olfactory system. *Curr. Biol.* **15**, 1535–1547 (2005).

57. K. Honegger, B. de Bivort, Stochasticity, individuality and behavior. *Curr. Biol.* **28**, R8–R12 (2018).

58. Y.-C. Kim, H.-G. Lee, K.-A. Han, D1 dopamine receptor dDA1 is required in the mushroom body neurons for aversive and appetitive learning in Drosophila. *J. Neurosci.* **27**, 7640–7647 (2007).

59. T. Hige, Y. Aso, M. N. Modi, G. M. Rubin, G. C. Turner, Heterosynaptic Plasticity Underlies Aversive Olfactory Learning in Drosophila. *Neuron* **88**, 985–998 (2015).

60. L. Rath, C. Giovanni Galizia, P. Szyszka, Multiple memory traces after associative learning in the honey bee antennal lobe. *Eur. J. Neurosci.* **34**, 352–360 (2011).

61. J. Haenicke, N. Yamagata, H. Zwaka, M. Nawrot, R. Menzel, Neural Correlates of Odor Learning in the Presynaptic Microglomerular Circuitry in the Honeybee Mushroom Body Calyx. *eNeuro* **5** (2018).

62. L. Li, *et al.*, A possible structural correlate of learning performance on a colour discrimination task in the brain of the bumblebee. *Proc. Biol. Sci.* **284** (2017).

63. G. Linneweber, M. Andriatsilavo, S. Dutta, L. Hellbruegge, A neurodevelopmental origin of behavioral individuality. *bioRxiv* (2019).

64. S. J. C. Caron, V. Ruta, L. F. Abbott, R. Axel, Random convergence of olfactory inputs in the Drosophila mushroom body. *Nature* **497**, 113–117 (2013).

65. K. Vogt, *et al.*, Shared mushroom body circuits underlie visual and olfactory memories in Drosophila. *Elife* **3**, e02395 (2014).

This page is intentionally left blank

Appendix I – Chapter I Supplemental Material:

Fly stocks

The following stocks were obtained from the Bloomington *Drosophila* Stock Center: P{GMR14C11-GAL4}attP2 (BDSC #49256), P{GMR60F02-GAL4}attP2 (#48228), P{GMR61H07-GAL4}attP2 (#39282), P{GMR14H04-GAL4}attP2 (#48665), P{GMR46E11-GAL4}attP2 (#50272), UAS-dTrpA1 (#26263), and P{20XUAS-IVS-GCaMP6m}attP40 (#42748). The VT046650-GAL4 (VDRC ID #204702) driver was obtained from Vienna *Drosophila* Resource Center, and the GH146-GAL4 and *Dop1R1* lines were generously provided by Y. Zhong and J. Dubnau, respectively. The PBac{20XUAS-TTS—shi[ts1]-p10}attP2 line and the split-GAL4 line "MB010B" (13F02-p65ADZp/CyO; 52H09-ZpGdbd) were generously provided by G. Rubin and Y. Aso.

Isogenic line iso^{KH11}

Our main control strain, the isogenic *Drosophila* line iso^{KH11}, was created by inbreeding the balancer-isogenized *w(isoCJ1)* strain of w^{1118} ([1]; shared by J. Dubnau) for 10 generations with full-sibling crosses. To equilibrate genetic background, all mutant and transgenic lines listed above were outcrossed to the iso^{KH11} line for at least 10 generations before being used in any imaging or odor preference experiments.

Fly rearing

Unless otherwise indicated, experimental flies were reared in a *Drosophila* incubator (Percival Scientific DR-36VL) under controlled conditions (25°C, 40% RH, 12:12h light:dark cycle) and

fed a standardized cornmeal/dextrose medium [2] supplemented with activated yeast. Flies used for behavior were cultured under low-density conditions by allowing ~10 mated females 48-72 hours to lay eggs in a 500ml culture bottle containing folded Kimwipes and ~200ml medium.

Behavioral apparatus

The custom designed behavioral apparatus was constructed of Accura 60 plastic using stereolithography (In'Tech Industries) fabrication. Stainless steel hypo tubing (Small Parts) was used to connect the apparatus with Teflon odor tubes (ID: 0.7mm). The apparatus consisted of 15 parallel tunnels (50mm long, 5mm wide, 1.3mm tall), separated by 5mm spacers. Odorized or clean air was delivered through inlet ports at each end of the tunnel and streams vented to the room through exhaust ports in the center choice zone. An active vacuum was not applied to the exhaust ports, and the tunnels operated close to atmospheric pressure throughout the experiment. Clear acrylic was used as a base and lid for the apparatus. The lid was clamped in place above the apparatus to ensure an air-tight seal during odor presentation. Odors were presented using proportional air blending to control odor concentration. Air dilutions could be made independently for each side of the apparatus. A custom 15-way PEEK manifold was used on each side to split the odorized flow equally between 15 tunnel inlets. A final valve (SH360T041; NResearch) was used immediately upstream of each manifold to quickly switch between pure dehumidified air and the odorized stream. Based on simulation results (details below), airflow through the tunnels is expected to be laminar, and to form a sharp boundary between the two odor compartments at the middle of the corridor.

To maintain a consistent molar flux of odorant at different experimental temperatures, we used digital mass flow controllers to deliver 0.1SLPM air to the end of each tunnel. Because the density of a gas is a function of temperature, the volumetric flow of air increases with temperature to maintain a constant mass flow. Therefore, the velocity of air flowing through the tunnels increases with temperature, but the molar flux of odorant over the fly stays constant (ignoring changes in vapor pressure). The laminar air velocity in the direction of the center port was approximately 2.6cm/sec at 25°C, well within the range of wind speeds experienced by insects in a natural environment [3].

A three-dimensional Computational Fluid Dynamics (CFD) analysis was performed using Autodesk CFD (Autodesk, Inc., San Rafael, CA) software to model the flow of gas through the tunnels. CFD analysis revealed that flow through most of the length of each tunnel is laminar, with some turbulent flow in the center and near the inlet ports on each end (Figure S1A). A scalar mixing simulation, using a simulated tracer gas, revealed a steep mixing gradient for odor concentration, limited almost entirely to the center choice zone where the opposing odor streams meet (Figure S1B). These results are in general agreement with the behavior we observe.

Odor delivery

For imaging experiments, odors were delivered using a 12-channel serial-air-dilution olfactometer described in [4]. For behavioral experiments, odors were presented using a dual-path odor delivery system integrated into the behavioral apparatus. In both devices, desiccated air was filtered through an activated carbon trap (Agilent HT-200) before passing through digital mass flow controllers (MFCs; Alicat Scientific). For each odorant, 5ml of pure odorant was placed with a folded strip of

filter paper in a 40ml glass vial fitted with a custom PTFE cap with inert fittings. The saturated headspace from these vials was combined with a variable carrier stream to produce between 10% and 20% saturated vapor, the range in which we observe a linear input-output relationship. All tubing was pure PTFE or PTFE coated for inertness. A photoionization detector (200B miniPID, Aurora Scientific) was used to periodically monitor the concentrations of test odors being delivered. The following odorants were obtained from Sigma-Aldrich: 2-heptanone (CAS#: 110-43-0), 1-pentanol (71-41-0), 3-octanol (589-98-0), hexyl-acetate (142-92-7), 4-methylcyclohexanol (589-91-3), pentyl-acetate (628-63-7), 1-butanol (71-36-3), ethyl-lactate (97-64-3), geranyl acetate (105-87-3), and 1-hexanol (111-27-34). Citronella and peppermint essential oils were purchased from Aura Cacia (items #191112 and #188840), and 200 proof ethanol from Decon Labs (V1001).

Behavior imaging

Flies were illuminated from beneath using a modified 15-inch laptop display panel (LP150X2; LG Philips) equipped with a high-density infrared LED array (peak emission 880nm). This approach produces homogeneous backlighting for high-contrast silhouette detection at a wavelength not visible to the fly. The screen was placed approximately 4cm below the behavioral apparatus to avoid heating the flies. We used a high-resolution CMOS camera (Point Grey Firefly MV USB) equipped with a zoom lens and longpass filter (Kodak Wratten Filter #87C) to collect images at 60Hz.

Behavior-tracking software

Custom MATLAB (The MathWorks, Inc.) routines were used to record and analyze the behavior of flies and control odor delivery. Tunnels and flies were automatically detected using 2D cross-correlation to align tunnel and fly outlines to template images. During an odor experiment, each frame was background subtracted to yield the silhouettes of the flies being assayed. For each time point, the centroid position, orientation, and major axis length of each silhouette were calculated and stored for offline analysis.

Behavioral experiments

Flies to be assayed for behavior were collected within 24 hours of eclosing and placed into a fresh vial containing fresh cornmeal/dextrose medium. Strictly, only females were used for behavior and imaging experiments. Vials each contained approximately 30 female flies, and were kept in the temperature and humidity-controlled incubator for 3 days, so that all flies were 3-4 days post-exclusion when tested. Flies were individually aspirated into the behavioral apparatus through a small hole in the lid. No anesthesia was used at any point on flies used in behavioral experiments. To minimize external causes of behavioral variability, odor preference assays were performed in an isolated temperature-controlled environmental chamber in total darkness. Behavioral assays began immediately after all flies were loaded and the lights were turned off. Each odor preference experiment ran for a total of 6 minutes and 30 seconds: 3 minutes of clean air, 3 minutes of air mixed with odorant, and 30 seconds of clean air post-odorant. The apparatus was partially disassembled and wiped down with absolute ethanol between experiments to remove any fly-deposited contamination. Prior to running behavioral experiments we adjusted odor concentrations so that the mean odor preference for OCT would be near 0.4. This was done by measuring the

mean odor preference of a small number of *iso*^{KH11} flies prior to the behavior experiment, then adjusting concentrations via flow controllers and remeasuring mean preference.

Preference persistence experiments

Several experiments required storing and maintaining identities of individual flies across multiple days. For this we used FlyPlates (FlySorter LLC, Seattle, WA), which are modified 96-well plates with a mesh top and bottom. The plates were placed on a bed of cornmeal/dextrose fly medium and individual flies were aspirated into and out of each well, allowing identities to be maintained across multiple days. The food was replaced daily. To remove any potential contribution of between-tunnel differences in stimulus delivery to the across-day correlation, the tunnel assignment for each fly was randomly chosen each day.

Gal4 expression pattern images

Panels modified with permission from FlyLight images (Figure 4A) were downloaded from http://flweb.janelia.org/cgi-bin/flew.cgi. Confocal micrographs of expression patterns targeting, the red is the background stain for anti-nc82, and cyan is mCD8-GFP. The red channel of the VT046560 image is also stained for anti-DLG [5].) Cyan is mCD8-GFP [6] driven by the Gal4 line denoted.

Calcium imaging fly prep

Flies were collected from population bottles within 24 hours of eclosion. Those flies were put into vials with standard cornmeal/dextrose fly food for approximately 72 hours. Prior to mounting, single flies were cold anesthetized by being sealed in a plastic tube and submerged in ice. The

anesthetized fly was then placed into a custom platform that exposed the fly head for removal of the cuticle and calcium imaging of the antennal lobe while keeping the antennae dry and exposed beneath the platform. The platform was a 3D printed 80mm diameter circle with a 5mm by 5mm square recessed into the center. At the bottom of the recess was a thin aluminum sheet (0.5mm) with a laser cut hole which allowed for the fly's head and thorax to be wedged between to stabilize the fly without damage. The fly's head was fixed to the stage by applying a small amount of UV (Loctite AA 3972) curing glue around the edge of both eyes to secure it the stage. The proboscis was then carefully extended and waxed to the bottom of the stage to further prevent movement of the head. We used a saline solution, as described in the methods of [7], to cover the exposed fly head and thorax and filling the small recessed section of the mounting stage. We used a sharpened 32-gauge needle to cut the cuticle of the fly and expose the antennal lobe.

Calcium imaging

GCaMP6m-expressing flies were imaged using a custom-built galvanometer-scanning two-photon microscope and ultrafast Ti:sapphire laser (Spectra-Physics Mai Tai) tuned to 930 nm. The microscope was controlled with a customized build of ScanImage 3.8 software (Vidrio Technologies, [8]). Custom MATLAB scripts were used to control stimulus delivery during imaging. Fast volume-scanning was performed using a piezoelectric objective scanner (Physik Instrumente PIFOC PD72Z4), capable of continuous sawtooth movement in the Z dimension. Each volume was imported as a tiff stack and smoothed with a 3-dimensional gaussian kernel with standard deviation of 3 in all dimensions. A background was selected for every odor presentation per fly by pooling all volumes and taking pixels with intensity below the 25th percentile. At each time point, the mean of the background was calculated to generate a value for background

subtraction. The resultant volumes were linearized into 1xn vectors and concatenated across time to create a matrix for *k*-means clustering (n-voxels by *k*-time points). Each voxel was *z*-scored across time, and *k*-means clustering was run using MATLAB R2018a's default KMEANS function with $k = 36$ and replicates = 15. For each cluster output by *k*-means, we applied a lenient size criterion that included only clusters composed of between 300 and 30,000 voxels. We then manually sorted through the remaining clusters to pick those that look reasonable in terms of geometry, size, and location, using a 3-dimensional *in-vivo Drosophila* antennal lobe atlas as a guide [9]. The selected clusters represented the glomeruli for each fly. This glomerulus mask was applied to the fly's odor block to yield ΔF/F traces for each glomerulus-odor pair within the fly. Within a single fly, separate *k*-means glomeruli masks were generated and applied for each odor presentation panel (12-odor panel-1, 12-odor panel-2, and the panel of OCT/MCH presentations). The matrix for principal component analysis was created by taking the integrated sum of ΔF/F for seconds 7-13 for each glomerulus-odor pair in an odor panel presentation, and z-scoring across flies. Whenever a glomerulus cannot be identified within a fly, the associated glomerulus-odor values for that fly are considered missing data. For our PCA matrix, we replaced any missing data within a fly with the mean across all flies of that specific odor-glomerulus value.

Thermogenetics

The thermogenetic effectors, UAS-shibire^{ts} and UAS-dTrpA1, were obtained from Bloomington Stock Center and backcrossed for at least ten generations into our isogenic line *iso^{KH11}*. For behavioral experiments, each effector was crossed to a GAL4 driver line and F_1s were used for the experiment. TrpA1 F_1s were tested at 23°C (permissive temperature control condition) or 29°C (restrictive; TRPA1 active). Shibire^{ts} F_1s were tested at 25°C (permissive temperature control

condition) or at 32°C (restrictive; Shibire^{ts} blocking vesicle release). Animals in the restrictive condition were incubated for 30 minutes at 32°C prior to testing.

Pharmacology

Flies used for drug treatment experiments were placed on food that was supplemented with either α-MW, 5-htp, or L-DOPA. To create the drug food mixture, the drug was mixed into water solution and diluted to the appropriate concentration with melted cornmeal/dextrose standard medium or F4-24 flake food, then placed into an empty plastic vial (Genesee scientific 32-116). The flies were flipped onto freshly made drug-supplemented food daily for the 72 hours post eclosion.

Food-induced environmental stress

Formula 4-24 (F4-24) prepared food mix was purchased from Carolina Biological Supply Company (item #173120). Portions of this dry media mix were processed in a coffee grinder to achieve a uniform density and mixed with tap water with a ratio of 1:1. For the food shock experiments we placed newly eclosed flies onto cornmeal/dextrose medium for 48 hours, then switched to F4-24 food for the remaining 24 hours prior to evaluating behavior.

Behavioral analysis

All behavioral analyses were performed using R-3.5.1 [8] or MATLAB R2018b. Behavioral analyses consisted of both model-based (estimating effects of experimental manipulations) and non model-based (individuality scores and distribution visualizations) inference. For non model-based analyses we included only flies that met a minimum activity threshold of 25 cm of distance traveled during the odor period, since highly inactive flies can substantially skew the analysis. For

model-based analyses we adjust for group differences in activity level, so we included all flies that entered the choice zone of the tunnel at least once during the experiment.

Individuality scores were calculated as Var_{obs} - Var_{null}. Though MAD as a measure of dispersion is preferable to variance, as discussed below, we used variance to estimate individuality because its additive property makes the numerical difference between observed and null a meaningful quantity. The individuality score is interpretable as the amount of additional variance, supplied by stable inter-fly preference differences, beyond that expected from sampling error alone.

The expected "null model" variance was estimated from a distribution derived by Monte Carlo simulation. Briefly, we calculated a transition matrix representing the proportion of times flies crossed from one odor into the other, or entered the choice zone and then returned to the side they came from. Then we segmented tunnel position traces into a series of bout times - the time between entering an odorized portion of the tunnel and leaving it, and pooled them together according to odor. For a given group of flies, the collection of odor bouts preserves the overall mean preference, but discards the correlation of bouts observed within a fly. A population of virtual "Markov flies" equal to the number of observed flies was generated and each virtual fly was assigned an initial "odor choice." For each virtual fly, a Markov chain of choices was generated from the empirical transition matrix, and each virtual choice was paired with an occupancy time sampled from the pool of bout times for its respective odor. Samples were repeatedly taken from the chain until 3 minutes of simulated behavior was collected for each fly. From each Markov fly's simulated time series, we calculated the proportion of time spent in the reference odor and collected these preference scores across the virtual population. This procedure was repeated 1,000 times and the

variance of simulated scores across each virtual population was calculated. From this distribution of simulated variances, 10,000 bootstrap replicates were taken and used to estimate confidence intervals and p-values of the null hypothesis test of no difference between the variance of the observed and the simulated preference scores.

Modeling of behavioral effects

Our goal was to measure the effect size of specific experimental manipulations on inter-fly odor preference variability. Isolating these effects is difficult for several reasons. First, observed behavioral variance is confounded by sampling error. To minimize the impact of sampling error, we could simply sample odor responses for a longer period of time; however, after several minutes, most flies adapt to the stimuli and behaviorally habituate. Second, manipulating environmental temperature and neural activity may produce changes in overall locomotor activity. Effects on some of these locomotor features are shown in Table S1. This issue directly impacts the sampling error issue, since less active animals will have fewer chances to cross the center and sample both odors, thus biasing preference scores toward extreme values (though, notably, the mean preference is unaffected [Fig S12]). Third, our measure of preference, a proportion, is bounded on [0,1], which tends to artificially deflate estimates of dispersion. Indeed, variance is a poor measure of dispersion on bounded distributions because it is not robust to accumulated observations at the extrema. Furthermore, we believe that it is unlikely that two flies with a measured odor preference of e.g., 1, truly have the exact same magnitude of preference. Rather, our assay is incapable of resolving these differences because of sampling limitations, a phenomenon generally known as data censoring. These issues are further exacerbated when the mean is far from 0.5, causing more flies to accumulate at values of 0 or 1, thereby producing an artificial dependence of dispersion on the

central tendency. Thus, we must be concerned that experimental manipulations which affect the mean can amplify the censoring effect and produce spurious apparent effects on variance. One possible way to address these concerns is to use non-parametric measure of dispersion, e.g., MAD or IQR, as done previously [10]. However, that only addresses the issue of measuring dispersion in a robust way. To address the other issues we must control for the confounding effects of overall locomotor activity on measured preference.

We used a linear modeling approach to address these challenges by jointly modeling the main effects of experimental manipulations, their interactions, and confounding "nuisance" parameters on both the mean and variance of odor preference scores. We developed a novel censored heteroscedastic regression model, where experimental and environmental factors exert their effects on odor preference distribution independently and in combination. For example, preference variability in experiments utilizing thermogenetic reagents was potentially affected by two factors we would like to control for (genotype and experimental temperature) and by their interaction, which is the effect size we are actually interested in estimating [11]. The likelihood, *L,* of observing a particular odor preference, p_i, is calculated from a censored Normal distribution:

$$\mathcal{L}(p_i) = \mathcal{N}_{cens}(p_i, \mu_i, \sigma_i)$$

which assumes that the odor preference is a latent continuous variable and that observed values of 0 and 1 are really censored observations of preference values that extend beyond the observable range [0,1]. The formulation of odor preference as a censored latent variable makes the estimation of variance in the model insensitive to changes in the mean. The expected mean, μ, and standard deviation, σ, of odor preference for fly *i*:

$$\mu_i = \mu_0 + \mu_{g_i} + \mu_{e_i} + \mu_{g_i * e_i} + f_\mu(\tau_i)$$

$$\sigma_i^2 = \sigma_0^2 + \sigma_{g_i}^2 + \sigma_{e_i}^2 + \sigma_{g_i * e_i}^2 + f_\sigma(\tau_i) + \epsilon(d_i)$$

depend on animal *i*'s genotype, environment, the interaction of genotype and environment (coded as binary indicator variables), and a term to account for seasonal effects of external air temperature (a scaled continuous variable). The standard deviation has an offset term, ε, defined for a given fly as:

$$\epsilon_i = a * dist_i^b + c$$

that depends on the distance, *dist*, traveled by fly *i* during the odor period and accounts for the increased uncertainty in estimating odor preference for inactive flies. The relationship between ε and *dist* was determined empirically by fitting a function, of the form shown in Eq. 3, to the pre-odor variance-by-distance plot of a pilot dataset (Figure S1D). The coefficient values used in all three models were a = 2.365, b = -0.651, c = -0.0077.

As shown above, we included two nuisance terms in the model to adjust for uncontrolled sources of variability: an offset to the variance based on the distance traveled during the odor period, and an additional uncontrolled environmental variable (the average air temperature in Boston) that was observed to have a significant association with preference variability (Figure S7B,D). Air temperature data recorded at the Boston Logan International Airport weather station (WBAN:14739) were downloaded from the NOAA Climate Data Online website [11] for the time period encompassing our behavior experiments. Temperature values were scaled to have a mean of 0 and a standard deviation of 1. We suspect that outdoor air temperature is only a correlate of the true seasonal cause of fluctuating variability, for which there are many possibilities including plant [12] or yeast [13] volatiles, or barometric pressure [14].

Bayesian model fitting

The model described above may be fit using maximum likelihood estimation or by using Markov Chain Monte Carlo (MCMC) simulation within a Bayesian framework. We chose to use the Bayesian approach, since the inclusion of reasonable prior expectations can provide parameter regularization and aid in model identifiability. Models were programmed in the Stan modeling language [15,16] and implemented using the RStan library [17] for R [18]. Model fitting was performed on the Odyssey cluster supported by the FAS Division of Science, Research Computing Group at Harvard University.

For each model, 32 MCMC chains were run in parallel using the No-U-Turn-Sampler implementation of the Hamiltonian Monte Carlo algorithm [19]. Briefly, 1,500 samples were drawn from each chain, and the first 1,000 warm-up samples were discarded. The remaining 500 samples from each chain were aggregated, for a total of 16,000 samples taken from the joint posterior. Several within-chain and between-chain diagnostic criteria were monitored for each model, in accordance with current best practices [20]. These diagnostics did not indicate any pathological MCMC behaviors for any of the models reported.

A series of pilot experiments using the control genotype (iso^{KH11}) under baseline conditions was used to update an initial set of vague priors on the mean intercept, variance intercept, and environmental air temperature coefficient terms in the model (n = 3,722 flies total). The posterior standard deviations (multiplied by a factor of ten to reflect more uncertainty) and means from this model were used as prior parameter values for their corresponding terms in subsequent models:

$$\mu_g \sim \mathcal{N}(0, 0.2)$$
$$\mu_e \sim \mathcal{N}(0, 0.2)$$
$$\mu_{g*e} \sim \mathcal{N}(0, 0.2)$$
$$\sigma_g^2 \sim \mathcal{N}(0, 0.01)$$
$$\sigma_e^2 \sim \mathcal{N}(0, 0.01)$$
$$\sigma_{g*e}^2 \sim \mathcal{N}(0, 0.01)$$
$$\mu_0 \sim \mathcal{N}(0.5, 0.25)$$
$$\sigma_0^2 \sim \mathcal{N}(0.012, 0.01)$$
$$f_\mu \sim \mathcal{N}(-0.034, 0.03)$$
$$f_\sigma \sim \mathcal{N}(-0.008, 0.01)$$

For all regression coefficient priors, we used a Normal distribution, centered at 0, and selected weakly-informative, but reasonable, values for the scale:

$$\mu_g \sim \mathcal{N}(0, 0.2)$$
$$\mu_e \sim \mathcal{N}(0, 0.2)$$
$$\mu_{g*e} \sim \mathcal{N}(0, 0.2)$$
$$\sigma_g^2 \sim \mathcal{N}(0, 0.01)$$
$$\sigma_e^2 \sim \mathcal{N}(0, 0.01)$$
$$\sigma_{g*e}^2 \sim \mathcal{N}(0, 0.01)$$
$$\mu_0 \sim \mathcal{N}(0.5, 0.25)$$
$$\sigma_0^2 \sim \mathcal{N}(0.012, 0.01)$$
$$f_\mu \sim \mathcal{N}(-0.034, 0.03)$$
$$f_\sigma \sim \mathcal{N}(-0.008, 0.01)$$

The overall goal for selecting priors was simply to provide some degree of regularization for parameter estimates and to aid in model identifiability, rather than to influence posterior estimates based on any prior expectations about specific effects. We fit a total of three separate regression models for: 1) neuromodulation experiments shown in Figures 3 and 5 (n = 5,327 flies total); 2)

thermogenetic experiments using the *dTrpA1* effector in Figure 4 (n = 5,285); and 3) thermogenetic experiments using the shi^{ts1} effector in Figure 4 (n = 2,027).

Kernel Density Estimates (KDE) of odor preference distributions

The KDEs of odor preference were estimated in MATLAB using the KSDENSITY function with a Gaussian kernel. Kernel bandwidth was automatically chosen using the default optimal method for normal densities, and censoring was applied at values of 0 and 1, the upper and lower bounds of observable odor preference scores.

Measuring neurotransmitter concentration in fly head homogenates

The concentrations of serotonin and dopamine were measured in fly head homogenates using ELISA kits (Enzo Life Sciences Serotonin ELISA kit ADI-900-175) and (Abnova Dopamine ELISA kit KA1887). Flies spent 72 hours on drug supplemented food (α-MW, 5-HTP, or L-DOPA) or control food. Then flies were moved into an empty plastic vial (Genesee scientific 32-116) and placed in a -80C freezer to rapidly freeze, then heads were separated by forceps and pooled into groups of 10-15 heads in a 1.5mL microcentrifuge tube in 250uL of the kit ELISA assay buffer and homogenized using a pestle. The microcentrifuge tubes were spun down at 14,000rpm for 1 minute, and 2x 100uL of the supernatant was removed and placed into 2x microcentrifuge tubes to be used for the ELISA assay. The ELISA kit protocol, which include normalization steps for the number of loaded heads per sample, was then followed. All standards and samples were prepared in duplicate. The resultant plates were read at absorbance of 450nm (Dopamine ELISA) and 405nm (Serotonin ELISA). A standard curve was generated for both

assays by applying a linear fit to the log concentration of the standards provided in each assay, with r2=0.91 and r2=0.98 for dopamine and serotonin standards respectively.

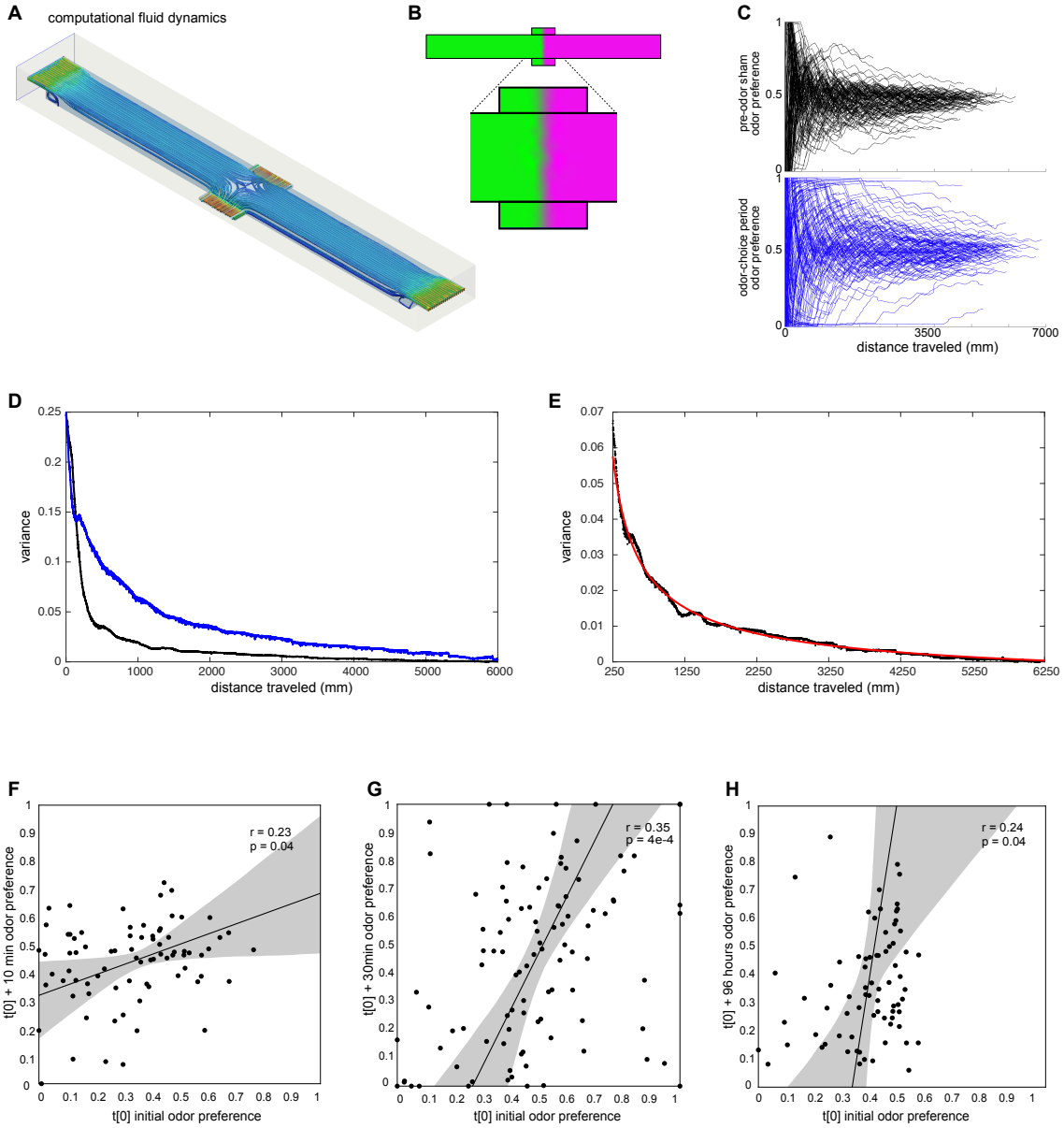

A
computational fluid dynamics
B
C
pre-odor sham odor preference
odor-choice period odor preference
distance traveled (mm)
D
variance
distance traveled (mm)
E
variance
distance traveled (mm)
F
r = 0.23
p = 0.04
t[0] + 10 min odor preference
t[0] initial odor preference
G
r = 0.35
p = 4e-4
t[0] + 30min odor preference
t[0] initial odor preference
H
r = 0.24
p = 0.04
t[0] + 96 hours odor preference
t[0] initial odor preference

Figure S1 — Dynamics of odor stimuli and behavioral variability. A) Computational Fluid Dynamics (CFD) simulation of steady state airflow through a single linear behavioral arena. Note the largely laminar flow along the length of the tunnel and the sharp flow boundary created in the center choice zone. Warmer colors indicate higher flow rates. **B)** CFD scalar mixing simulation showing the distribution of odor concentration at steady state. The scenario simulated the flow of an odorized stream (magenta) in one end of the arena (outlined in black) and clean air (green) in the other. A steep gradient is observed in the center choice zone, with little diffusion into the opposite arm. **C)** The running odor preference scores of 120 control (iso^{KH11}) flies as a function of distance traveled in the arena. Each line depicts the preference score trajectory of an individual fly. During the pre-odor period (top) most scores rapidly converge toward 0.5, but preference trajectories during the odor-choice period (bottom) are considerably more divergent. **D)** Across-fly variance of the trajectories depicted in S1C as a function of distance traveled. During the pre-odor period (black) variance rapidly converges toward 0 as most flies approach a preference of 0.5, but during the odor-choice period (blue) across-fly variance stays much higher as flies exhibit preference for an odor. **E)** Pre-odor period variance as a function of distance (black) fitted by the function var = 2.365 * $distance^{-0.651}$ - 0.0077 (red, R^2 = 0.96 for the region shown). This power-law relationship was used to calculate the activity-based variance offset for each fly. **F)** Correlation plot of individual fly odor preference 10 minutes after initial test versus during initial test. Pearson correlation r = 0.23, and p = 0.04. Line is the best fit as determined by minimizing orthogonal residuals using PCA (i.e., no explicit dependent or independent variables). Shaded are is the 95%CI of the regression line. **G)** As in F) except retested 3 hours later. Pearson correlation r = 0.35, and p = 4e-4. **H)** As in F) except retested 96 hours later. Pearson correlation r = 0.24, and p = 0.04.

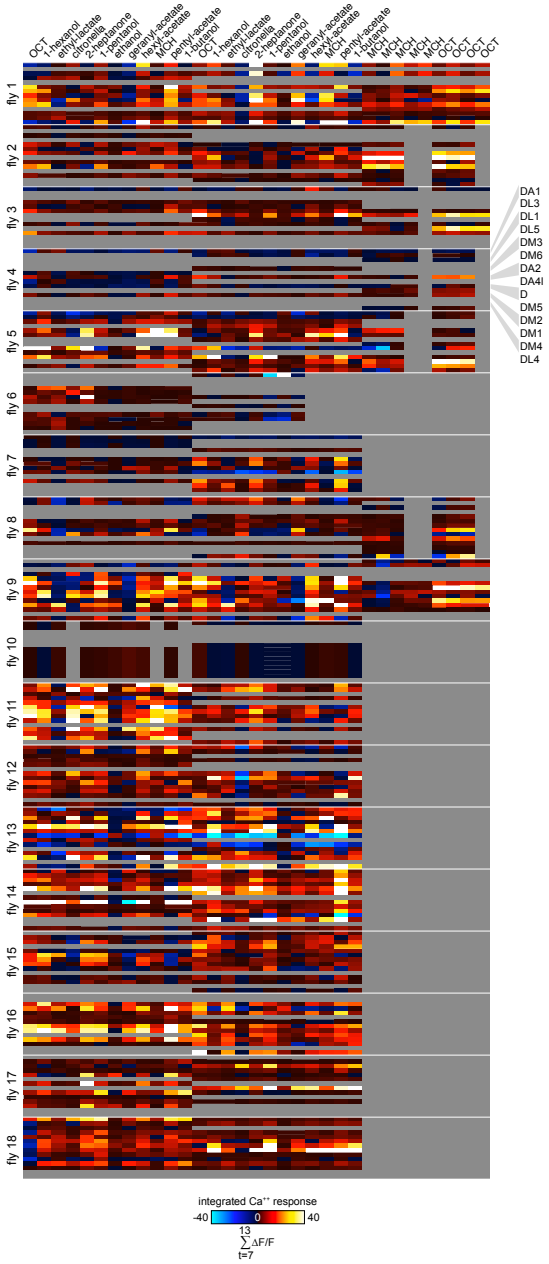


Figure S2 — Odor Ca++ response matrix for flies expressing GCaMP6m in GH146-Gal4 PNs. Integrated ΔF/F during and after the odor-stimulus period, by odor across the two 12 odor panels and OCT/MCH panel (columns). Rows are organized by individual fly and glomeruli.

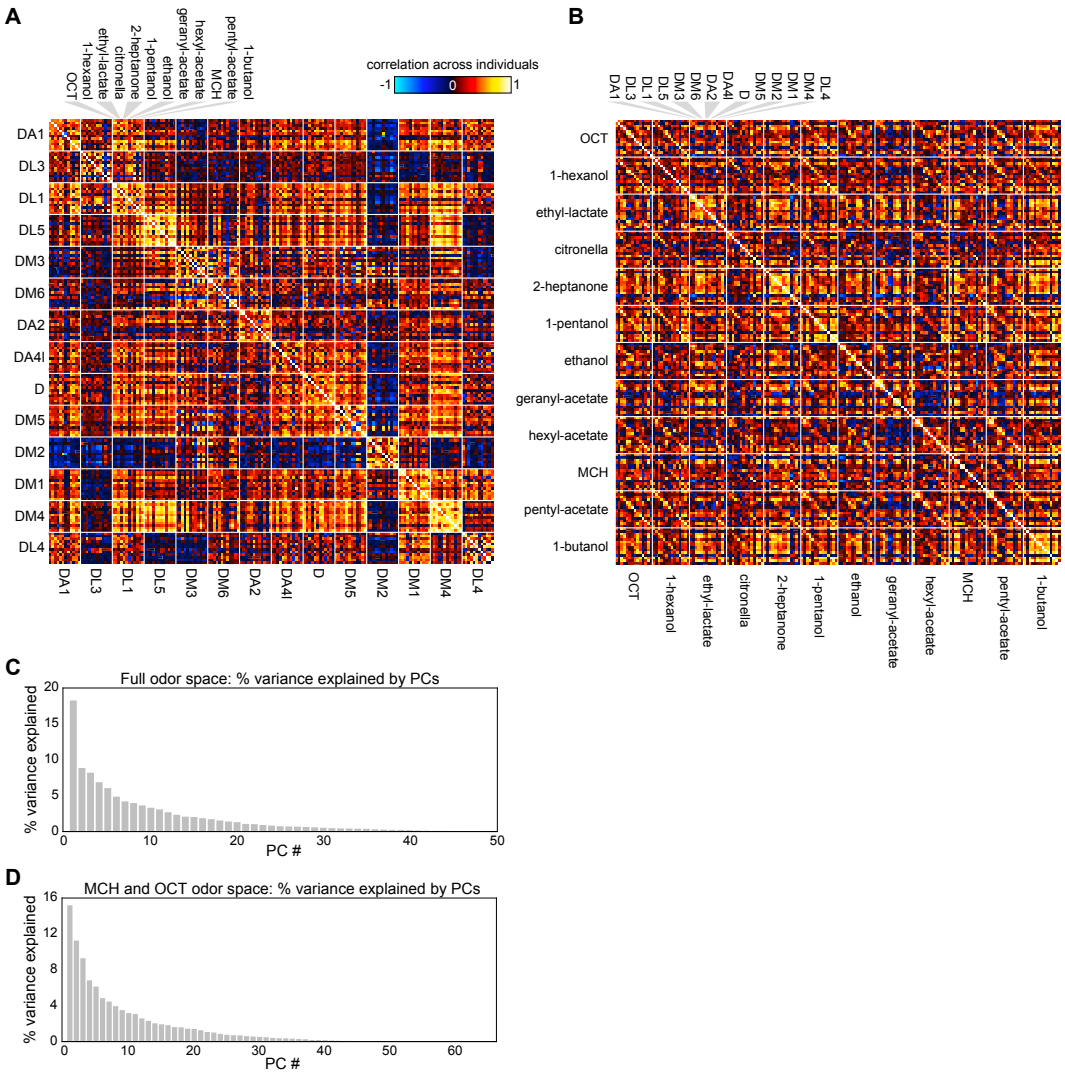


Figure S3 — Structure of odor response covariance. **A)** Correlation matrix of Ca^{++} responses across individual flies. Rows and columns are organized by glomerulus and then odor. Here all responses for each odor are averaged within each fly. I.e., OCT and MCH values reflect the average of up to nine values (two values from the 12 odor panels, and the remainder from the OCT/MCH trials). The values for all other odorants are the average of the two responses per fly in the 12 odor panels. **B)** As in A), except rows and columns are organized by odor and then glomerulus.
C) Ranked eigenvalues of the principle components of a Ca^{++} response space in which individual 12 odor panel trials are points and glomerulus-odor pairs are dimensions (corresponding to Figure 2I).**D)** As in C) except for a Ca^{++} response space in which individual OCT or MCH trials are points and glomeruli are dimensions (corresponding to Figure 2J,K).

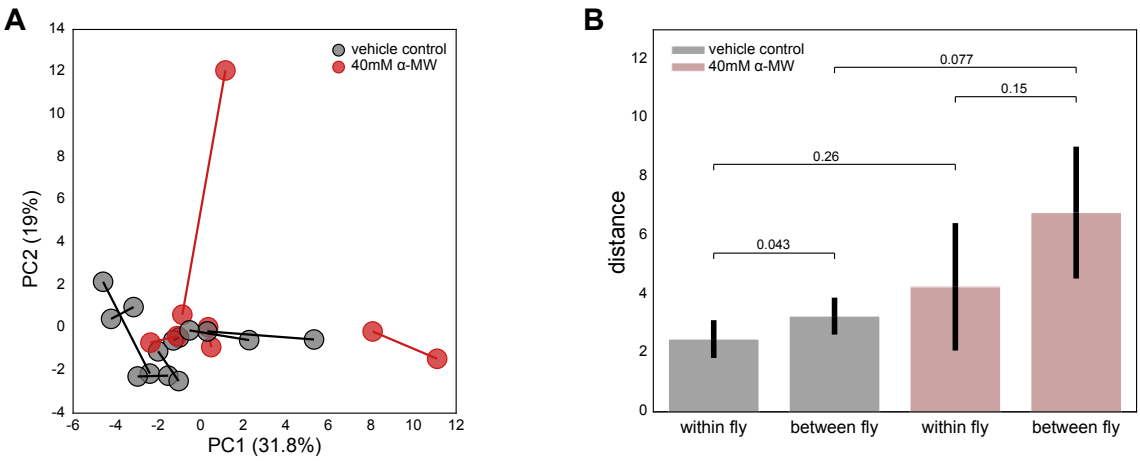


Figure S4 — PCA of odor responses in a data set with no missing values. A) PCA embedding of 12 odor panel trials for a data set with no missing values, i.e., the largest complete data set that can be made from the values in Figure S8 (containing 6 control flies and 4 α-MW-fed flies, with responses to two 12 odor panels across four glomeruli each. See Figure S8 and S9 for data from α-MW-feeding experiment). Projection onto PC1 and PC2 of the two 12 odor panel responses. Lines connect paired panels for each individual. **B)** Distance within and between flies in PC1-PC2 space for the data set used in A). Error bars are +/-1 standard error as determined by bootstrapping of individual flies. *P*-values within conditions reflect one-tailed resampling tests that the distance between flies is greater than the distance within. P-values between conditions reflect one-tailed resampling tests that α-MW distances are greater than control.

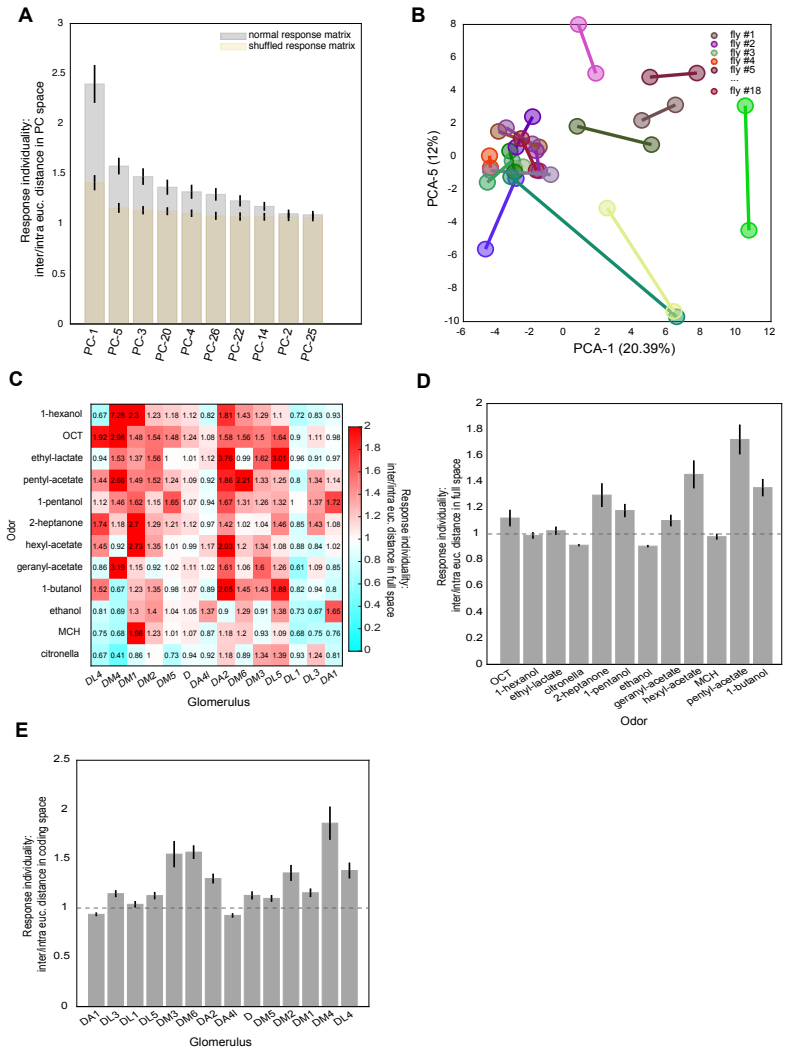


Figure S5 — Response individuality by odor and glomerulus. A) Individuality of odor responses on each principal component of response variation. Individuality was calculated by performing PCA on the original matrix of N-flies by 168 odor-glomerulus combinations. We then calculated inter-fly and intra-fly values using the same method as in Fig 2I), but only using a single indicated PC for each value. **B)** Scatter plot of odor panel responses on the two PCs with the highest individuality values, PC1 versus PC5. **C)** Matrix of individuality for each odor-glomerulus pair (i.e., each single dimension of the odor panel data set). Individuality was calculated by the ratio of inter-fly distance to intra-fly distance for each odor-glomerulus pair. **D)** Individuality by odor. Individuality was calculated by the inter-fly distance over intra-fly distance for all glomeruli responding to each odor as follows. For each odor, a response matrix of size 36 (18 flies, 2 trials each) X 14 glomerular responses was computed. Then the inter-fly distance and intra-fly distance was calculated using the same methods as in Figure 2I. Bars are +/-SEM calculated by 500-replicate bootstrap resampling of individuals. **E)** Individuality by glomerulus. Same as above in S5D), but estimating individuality of each glomerulus response across all 12 odors.

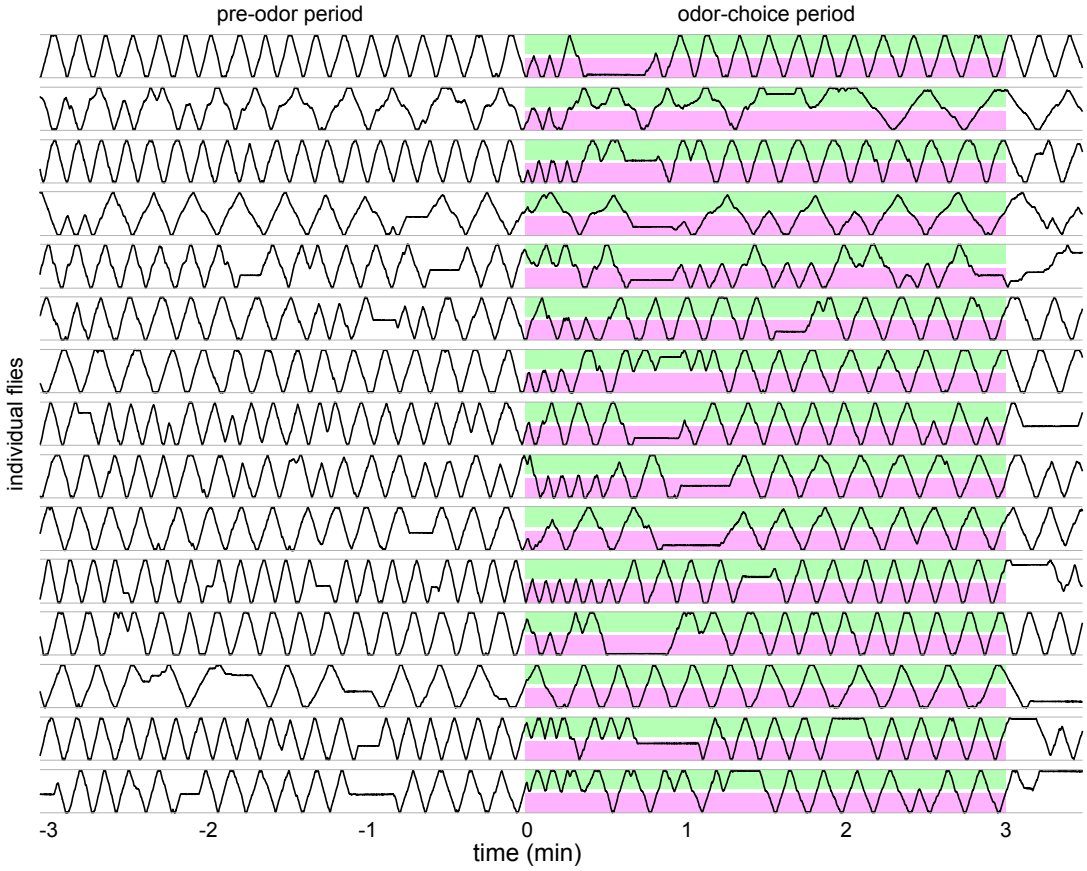


Figure S6 — Sample individual kymographs of odor behavior for *Dop1R1* flies. Reversals (turning around at the odor boundary) during the odor-choice period, indicate that the flies are detecting the odorants. Magenta = OCT, green = MCH.

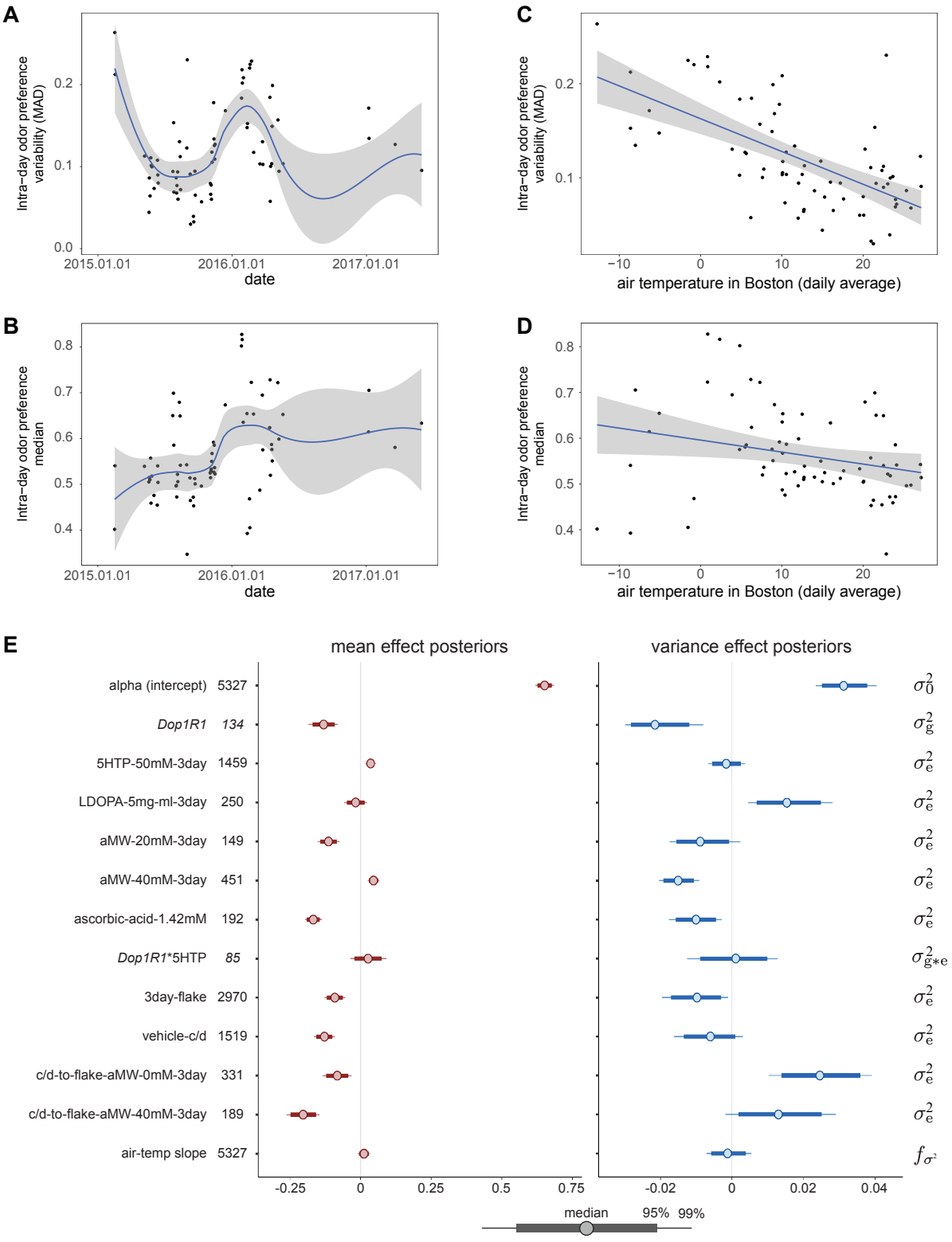

A
Intra−day odor preference variability (MAD)
0.0
0.1
0.2
2015.01.01
2016.01.01
2017.01.01
date
B
Intra−day odor preference median
0.4
0.5
0.6
0.7
0.8
2015.01.01
2016.01.01
2017.01.01
date
C
Intra−day odor preference variability (MAD)
0.1
0.2
−10
0
10
20
air temperature in Boston (daily average)
D
Intra−day odor preference median
0.4
0.5
0.6
0.7
0.8
−10
0
10
20
air temperature in Boston (daily average)
E
mean effect posteriors
variance effect posteriors
alpha (intercept) 5327
Dop1R1 134
5HTP-50mM-3day 1459
LDOPA-5mg-ml-3day 250
aMW-20mM-3day 149
aMW-40mM-3day 451
ascorbic-acid-1.42mM 192
Dop1R1*5HTP 85
3day-flake 2970
vehicle-c/d 1519
c/d-to-flake-aMW-0mM-3day 331
c/d-to-flake-aMW-40mM-3day 189
air-temp slope 5327
-0.25
0
0.25
0.5
0.75
-0.02
0
0.02
0.04
median
95%
99%
σ_0^2
σ_g^2
σ_e^2
σ_e^2
σ_e^2
σ_e^2
σ_e^2
σ_{g*e}^2
σ_e^2
σ_e^2
σ_e^2
σ_e^2
f_{σ^2}

Figure S7 — Parameters of the Bayesian model of odor preference. A) MAD (median absolute deviation) of wild type odor preferences measured daily (points) vs date. Blue line is a LOESS regression (span = 0.7), and grey region is the 95% CI. $n = 3722$. **B)** As in B) for the daily median of odor preference. **C)** MAD of wild type odor preferences measured daily (points) vs average daily temperature, as measured at the WBAN:14739 NOAA (Boston Logan International Airport) weather station. Blue line is a linear regression, and grey region is the 95% CI. $n = 3722$. **D)** As in D) for the daily median of odor preference. **E)** Forest plot of the posterior distributions for all parameters of the neuromodulation and food-shock model (Figures 3C and 5B). Labels at left indicate which type of coefficient each parameter is in the term for variability (σ^2). Numbers by parameter labels indicate the "marginal sample size," i.e., the number of flies available to fit each parameter. c/d indicates cornmeal/dextrose media; flake indicates F4-24 food.

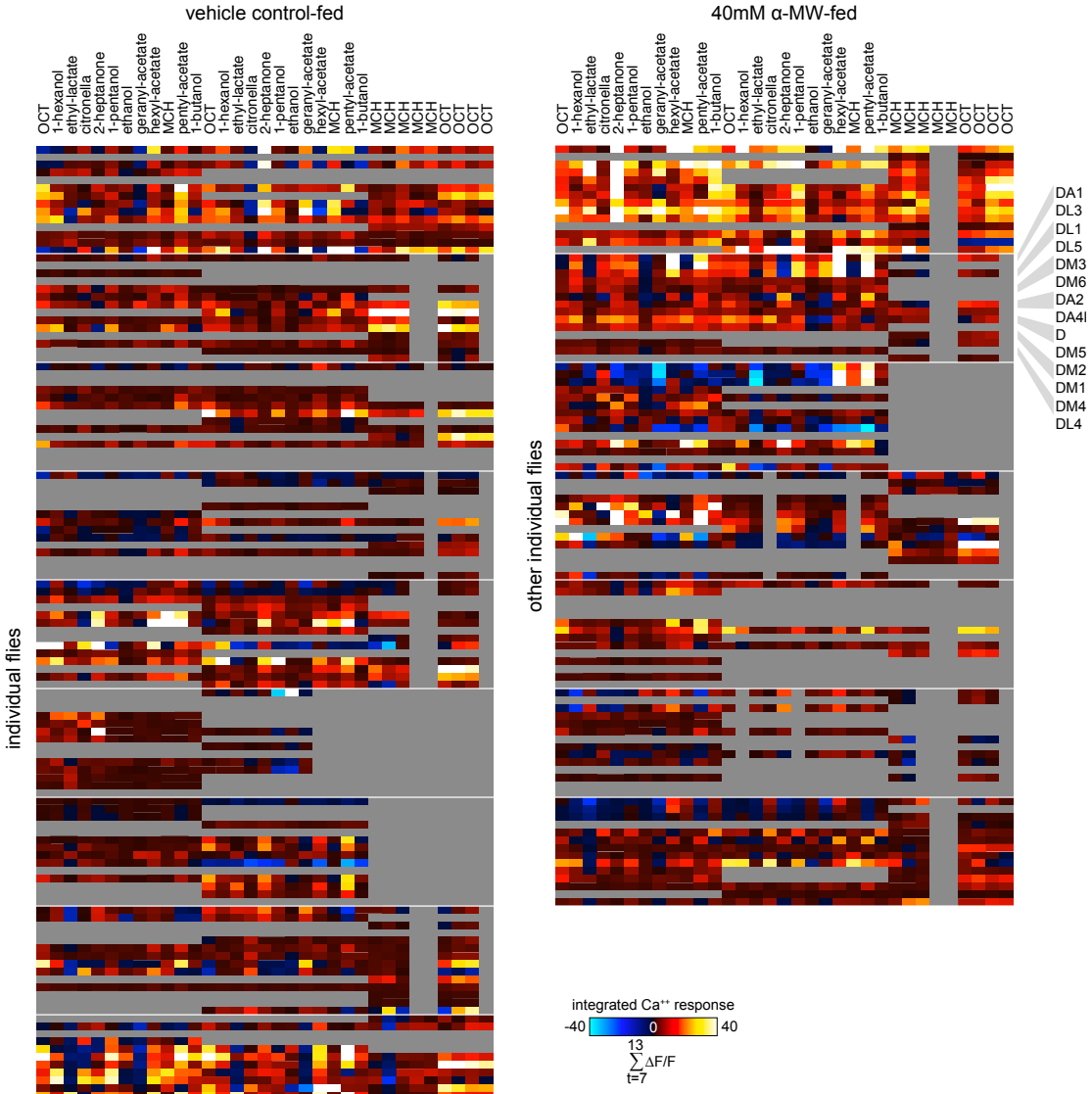


Figure S8 — Odor Ca^{++} response matrices for control (left) and α-MW-fed (right) flies expressing GCaMP6m in GH146-Gal4 PNs. Integrated ΔF/F during and after the odor-stimulus period, by odor across the two 12 odor panels and OCT/MCH panel (columns). Rows are organized by individual fly and glomeruli.

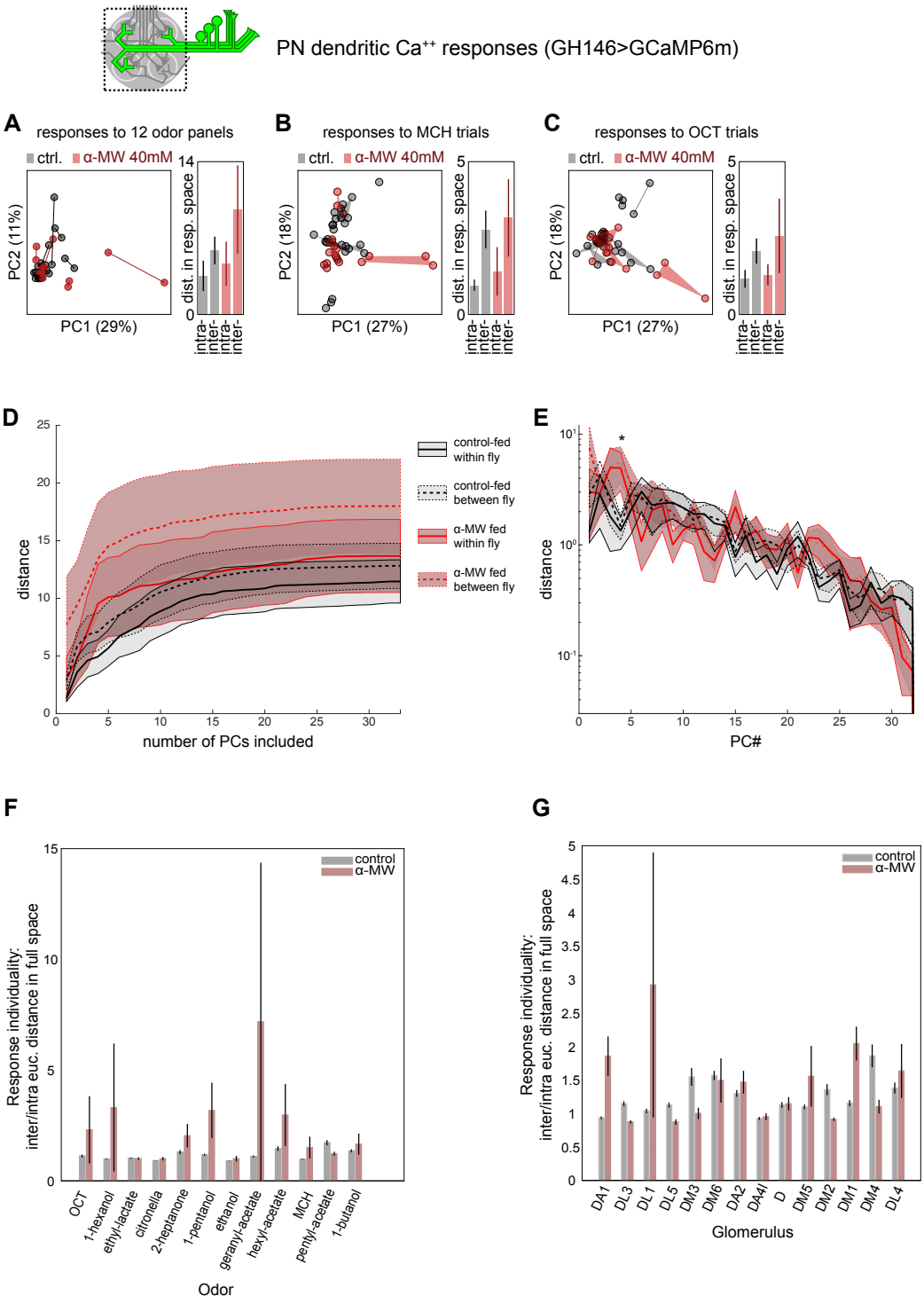

PN dendritic Ca++ responses (GH146>GCaMP6m)
A
responses to 12 odor panels
ctrl.
α-MW 40mM
PC2 (11%)
PC1 (29%)
dist. in resp. space
intra-
inter-
intra-
inter-
B
responses to MCH trials
PC2 (18%)
PC1 (27%)
C
responses to OCT trials
D
distance
number of PCs included
control-fed within fly
control-fed between fly
α-MW fed within fly
α-MW fed between fly
E
PC#
F
Response individuality: inter/intra euc. distance in full space
control
α-MW
OCT
1-hexanol
ethyl-lactate
citronella
2-heptanone
1-pentanol
ethanol
geranyl-acetate
hexyl-acetate
MCH
pentyl-acetate
1-butanol
Odor
G
DA1
DL3
DL1
DL5
DM3
DM6
DA2
DA4l
D
DM5
DM2
DM1
DM4
DL4
Glomerulus

Figure S9 — PN dendrite Ca^{++} responses in α-MW-fed flies and controls. A) Left: Principal components 1 and 2 of individual panel responses in the space of odor-glomeruli responses (as in Figure 2I-K). Right: average distance among intra-fly trials and inter-fly trials. Bars indicate +/- SEM calculated by 20,000-replicate bootstrap resampling of individuals. The means within each treatment (intra- vs. inter-) are significantly different (p=0.011 and p=0.024) by one-tailed resampling. The means between treatments means are not statistically significant ($0.25 < p < 0.35$). Black indicates control flies, brown flies fed 40mM α-MW for three days. B) As in E) but with points representing responses to MCH in the 15 glomerular space containing MCH and OCT responses (as in Figure 2J and K). Intra- vs. inter- means are significantly different within control treatment ($p = 0.004$) but not statistically significant within α-MW treatment ($p = 0.093$). Differences in means between treatments means are not statistically significant ($0.34 < p < 0.40$). C) As in F) but with points representing responses to OCT in the 15 glomerular space containing MCH and OCT responses (as in Figure 2J and K). Means are significantly different within ($p < 0.001$) but not between ($0.34 < p < 0.39$) treatments. **D)** From the whole data set used in C, distance between control-fed and α-MW-fed trials as a function of the dimensionality of the projected PC space in which distances are calculated. Shaded areas represent +/- standard error as calculated by bootstrap resampling. **E)** As in F), but for distances (on a log y-axis) on just one PC at a time. α-MW-fed trials are significantly farther apart on PC4 than control trials (asterisk). $p = 0.028$ by bootstrapping based t-test comparing control and α-MW-fed inter-fly distances, and $p = 0.026$ for intra-fly distances. **F)** Individuality of Ca++ responses for each odor, for control and α-MW treated flies. (See Figure S3.) **G)** Individuality of Ca++ responses for each glomerulus, for control and α-MW treated flies. (See Figure S3.)

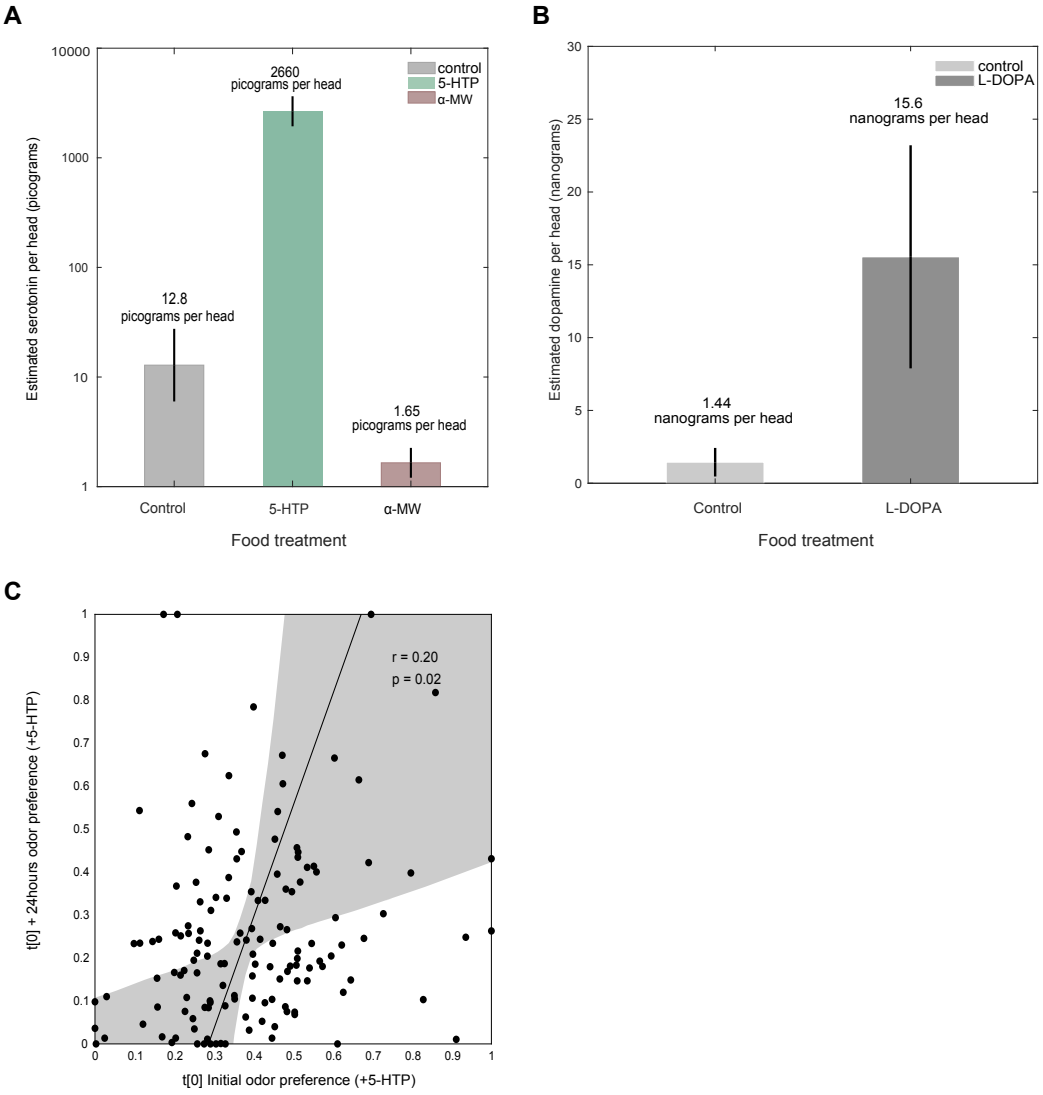


Figure S10 — Effects of 5-HTP, α-MW, and L-DOPA on neurotransmitter concentration in brain and day-to-day persistence of behavior. A) Estimation of the effect of α-MW and 5-HTP drug supplement on serotonin concentration per fly head via ELISA serotonin assay. For each assay, fly heads were pooled and homogenized to increase serotonin amounts to within the detectable range of the assay, as further described in the methods. Flies grow on control media yield an estimate of 12.8 picograms of serotonin per fly head. Flies grown on media supplemented with 5-HTP yield an estimate of 2660 picograms of serotonin per fly head. Flies grown on media supplemented with α-MW yield an estimate of 1.65 picograms of serotonin per fly head. We found that our estimate of serotonin per fly head after 5-HTP feeding is ~10x larger than that reported by (Claridge-Chang et al., Cell 2009), as detected using HPLC. We believe our larger estimate is due to the cross-reaction of 5-HTP with the serotonin ELISA assay, which the assay manual reports. It is likely 0.4% of 5-HTP present in the samples was misidentified as serotonin. **B)** Same as in S8A) but for the effect of L-DOPA on dopamine concentration per fly head via ELISA dopamine assay. **C)** Correlation plot of individual fly odor preference 24 hours after initial test versus during initial

test. Pearson correlation $r = 0.20$, and $p = 0.02$. Line is the best fit as determined by minimizing orthogonal residuals using PCA (i.e., no explicit dependent or independent variables). Shaded are is the 95%CI of the regression line.

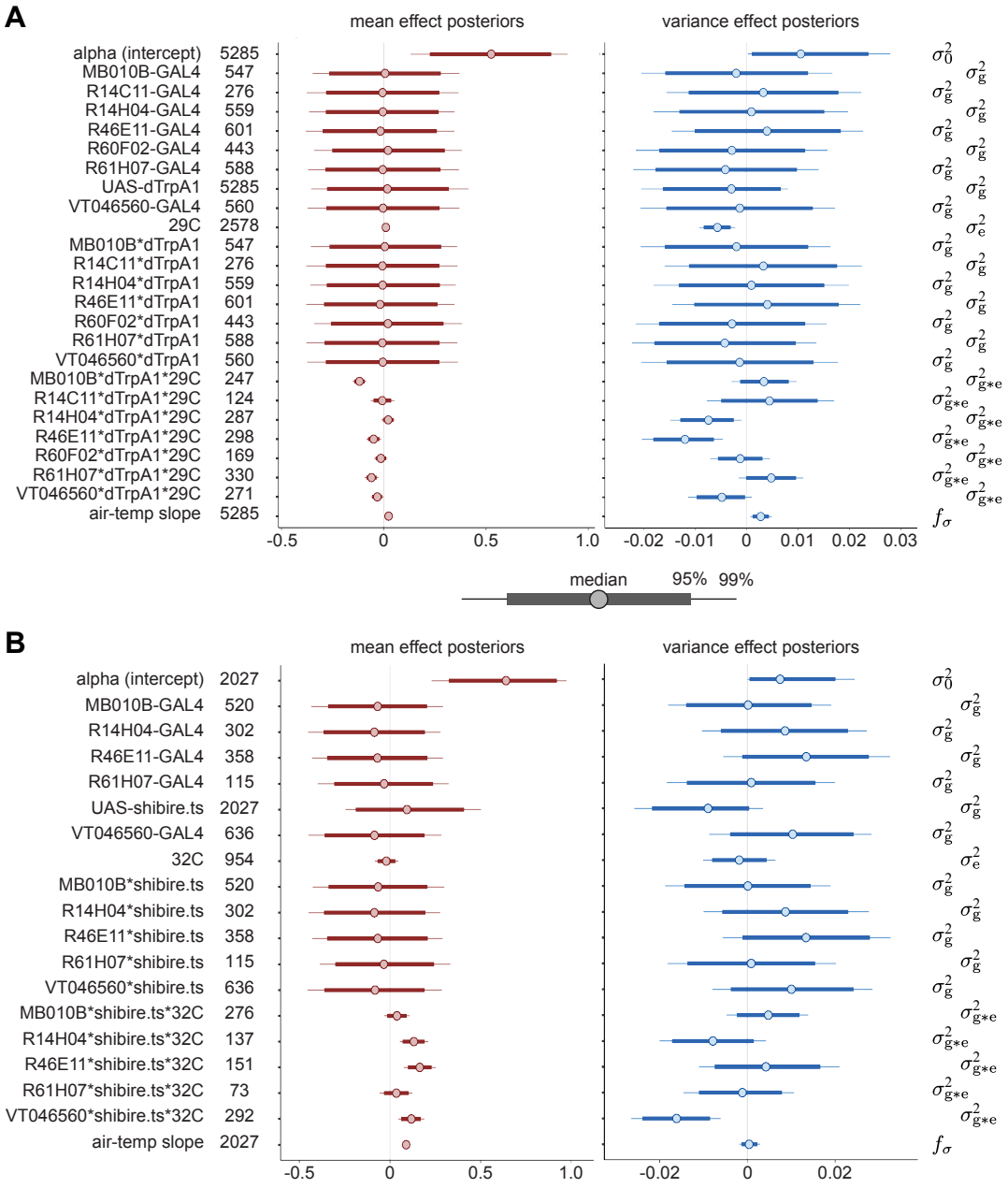


Figure S11 — Model parameters for thermogenetic experiments. A) Forest plot of the posterior distributions for all parameters of the neural circuit dTRPA1 activation model (Figure 4D). Labels at left indicate which type of coefficient each parameter is in the term for variability (σ^2). Numbers by parameter labels indicate the "marginal sample size," i.e., the number of flies available to fit each parameter. **B)** As in A), for Shibire^{ts} experiments.

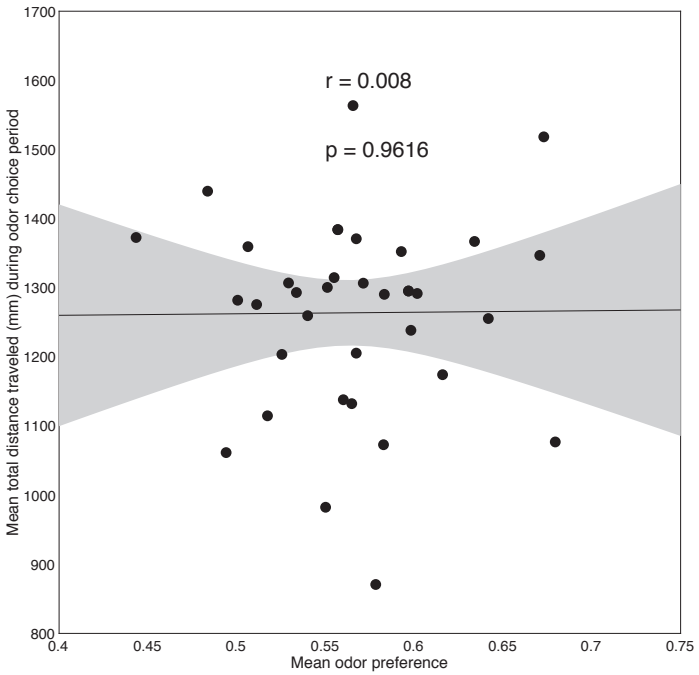


Figure S12 — Mean odor preference is independent of locomotor activity. Each point is the mean odor preference and mean total distance traveled within a single experimental factor (those listed in Figs S7 and S11). Factors estimated from fewer than 200 flies were excluded.

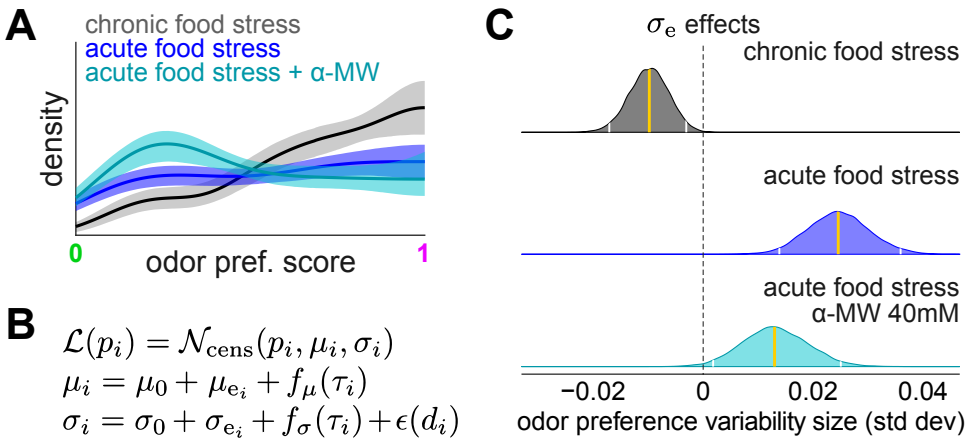


Figure S13 - Variability of odor preference is modulated by changes in diet. A) Kernel-density estimates of the behavioral distribution of iso^{KH11} flies grown chronically on F4-24 flake food (gray), subject to a food stress treatment in which flies were transferred from cornmeal/dextrose food to F4-24 flake food (blue), and flies subject to the same food stress treatment but with 40mM α-MW in both food sources (teal). Shaded areas are 95% CIs. **B)** Model used to estimate the effects on odor preference variability of diet manipulations. Each terms can be compared to those in Figs 3C and 4D. **C)** Posterior distributions of the effect of diet manipulations. Gold lines indicate the mean of the posterior, and white lines the edges of the 95% credible interval. Posterior distributions heavily overlapping 0 (dotted line) indicate no effect.

Supplementary References

1. Yin JC, et al. (1994) Induction of a dominant negative CREB transgene specifically blocks long-term memory in Drosophila. *Cell* 79(1):49–58.
2. Brent MM, Oster II (1974) Nutritional substitution: a new approach to microbial control for Drosophila cultures. *Drosoph Inf Serv* 155:157.
3. Budick SA, Dickinson MH (2006) Free-flight responses of Drosophila melanogaster to attractive odors. *J Exp Biol* 209(Pt 15):3001–3017.
4. Honegger KS, Campbell RAA, Turner GC (2011) Cellular-resolution population imaging reveals robust sparse coding in the Drosophila mushroom body. *J Neurosci* 31(33):11772–11785.
5. Parnas D, Haghighi AP, Fetter RD, Kim SW, Goodman CS (2001) Regulation of postsynaptic structure and protein localization by the Rho-type guanine nucleotide exchange factor dPix. *Neuron* 32(3):415–424.
6. Lee T, Luo L (1999) Mosaic Analysis with a Repressible Cell Marker for Studies of Gene Function in Neuronal Morphogenesis. *Neuron* 22(3):451–461.
7. Hige T, Aso Y, Modi MN, Rubin GM, Turner GC (2015) Heterosynaptic Plasticity Underlies Aversive Olfactory Learning in Drosophila. *Neuron* 88(5):985–998.
8. Pologruto TA, Sabatini BL, Svoboda K (2003) ScanImage: flexible software for operating laser scanning microscopes. *Biomed Eng Online* 2:13.
9. Grabe V, et al. (2016) Elucidating the Neuronal Architecture of Olfactory Glomeruli in the Drosophila Antennal Lobe. *Cell Rep* 16(12):3401–3413.

10. Kain JS, Stokes C, de Bivort BL (2012) Phototactic personality in fruit flies and its suppression by serotonin and white. *Proc Natl Acad Sci* 109(48):19834–19839.

11. Nieuwenhuis S, Forstmann BU, Wagenmakers E-J (2011) Erroneous analyses of interactions in neuroscience: a problem of significance. *Nat Neurosci* 14(9):1105–1107.

12. Mansourian S, et al. (2018) Wild African Drosophila melanogaster Are Seasonal Specialists on Marula Fruit. *Curr Biol* 28(24):3960–3968.e3.

13. Becher PG, et al. (2012) Yeast, not fruit volatiles mediate Drosophila melanogaster attraction, oviposition and development. *Funct Ecol* 26(4):822–828.

14. Austin CJ, Guglielmo CG, Moehring AJ (2014) A direct test of the effects of changing atmospheric pressure on the mating behavior of Drosophila melanogaster. *Evol Ecol* 28(3):535–544.

15. Stan Development Team (2018) Stan User's Guide Version 2.18. https://mc-stan.org/docs/2_18/stan-users-guide/index.html

16. Carpenter B, et al. (2017) Stan: A probabilistic programming language. *J Stat Softw* 76(1). Available at: https://www.osti.gov/biblio/1430202.

17. Stan Development Team (2018) RStan: the R interface to Stan. R package version 2.18.2. http://mc-stan.org/.

18. R Core Team. (2019) R: A Language and Environment for Statistical Computing. *R Foundation for Statistical Computing.*

19. Hoffman MD, Gelman A (2014) The No-U-Turn sampler: adaptively setting path lengths in Hamiltonian Monte Carlo. *J Mach Learn Res* 15(1):1593–1623.

20. Gabry J, Simpson D, Vehtari A, Betancourt M, Gelman A (2019) Visualization in Bayesian workflow. *J R Stat Soc A* 182(2):389–402.

This page is intentionally left blank

Appendix II - Chapter II Supplemental Material

Fly rearing

Experimental flies were reared in a *Drosophila* incubator (Percival Scientific DR-36VL) at 22° C, 40% relative humidity, and 12:12h light:dark cycle. Flies were fed cornmeal/dextrose medium, as previously described[4]. Mated female flies aged 3 days post-eclosion were used for all behavioral persistence experiments. Mated female flies aged 7 to 15 days post-eclosion were used for all paired behavior-calcium imaging and immunohistochemistry experiments.

Fly stocks

The following stocks were obtained from the Bloomington *Drosophila* Stock Center: P{20XUAS-IVS-GCaMP6m}attP40 (BDSC #42748), w[*]; P{w[+mC]=Or13a-GAL4.F}40.1 (BDSC #9945), w[*]; P{w[+mC]=Or19a-GAL4.F}61.1 (BDSC #9947), w[*]; P{w[+mC]=Or22a-GAL4.7.717}14.2 (BDSC #9951), w[*]; P{w[+mC]=Orco-GAL4.W}11.17; TM2/TM6B, Tb[1] (BDSC #26818). As described previously, GH146-Gal4 was a gift provided by Y. Zhong[4]. w; UAS-Brp-Short-mStrawberry; UAS-mCD8-GFP; + was a gift of Timothy Mosca and was not outcrossed to the isokh11 background[29]. Unless otherwise indicated, all transgenic lines were outcrossed to the isogenic line isokh11[4] for at least 5 generations prior to being used in any experiments.

Odor delivery

As previously described, odor delivery during behavioral tracking and neural activity imaging were controlled with isolation valve solenoids (NResearch Inc.)[4]. Saturated headspace from 40

ml vials containing 5 ml pure odorant were serially diluted via carbon-filtered air to generate a variably (10-25%) saturated airstream controlled by digital flow controllers (Alicat Scientific) and presented to flies at total flow rates of ~100 mL/min. The odor panel used for imaging was comprised of the following odorants: 2-heptanone (CAS #110-43-0, Millipore Sigma), 1-pentanol (CAS #71-41-0, Millipore Sigma), 3-octanol (CAS #589-98-0, Millipore Sigma), hexyl-acetate (CAS #142-92-7, Millipore Sigma), 4-methylcyclohexanol (CAS #589-91-3, Millipore Sigma), pentyl acetate (CAS #628-63-7, Millipore Sigma), 1-butanol (CAS #71-36-3, Millipore Sigma), ethyl lactate (CAS #97-64-3, Millipore Sigma), geranyl acetate (CAS #105-87-3, Millipore Sigma), 1-hexanol (CAS #111-27-34, Millipore Sigma), citronella java essential oil (191112, Aura Cacia), and 200 proof ethanol (V1001, Decon Labs).

Odor preference behavior

Odor preference was measured at 25°C and 20% relative humidity. As previously described[4], individual flies confined to custom-fabricated tunnels were illuminated with infrared light and behavior was recorded with a digital camera (Basler) and zoom lens (Pentax). The odor choice tunnels were 50 mm long, 5 mm wide, and 1.3 mm tall. Custom real-time tracking software written in Matlab was used to track centroid, velocity, and principal body axis angle throughout the behavioral experiment, as previously described[4]. After a 3-minute acclimation period, odorants were delivered to either end of the tunnel array for 3 minutes. Odor preference score was calculated as the fraction of time spent in the reference side of the tunnel during odor-on period minus the time spent in the reference side of the tunnel during the pre-odor acclimation period.

Behavioral preference persistence measurements

After measuring odor preference, flies were stored in individual housing fly plates (FlySorter, LLC) under otherwise standard food, temperature, humidity, and lighting conditions. Odor preference of the same individuals was measured 3 and/or 24 hours later. In some cases, fly tunnel position was randomized between measurements, although we observed that randomization had little effect on preference persistence.

Calcium imaging

Flies expressing GCaMP6m in defined neural subpopulations were imaged using a custom-built two-photon microscope and ultrafast Ti:Sapphire laser (Spectra-Physics Mai Tai) tuned to 930 nm, as previously described[4]. For paired behavior and imaging experiments, the time elapsed between behavior measurement and imaging ranged from 0 to 4 hours. Flies were anesthetized on ice and immobilized in an aluminum sheet with a female-fly-sized hole cut in it. The head cuticle between the antennae and ocelli was removed along with the tracheae to expose the ALs from the dorsal side. Volume scanning was performed using a piezoelectric objective mount (Physik Instrumente). ScanImage 2013 software (Vidrio Technologies) was used to coordinate galvanometer laser scanning and image acquisition. Custom Matlab (Mathworks) scripts were used to coordinate image acquisition and control odor delivery. 256 by 192 (x-y) pixel resolution 16-bit tiff images were recorded. The piezo travel distance was adjusted between 70 and 90 μm so as to cover most of the AL. We varied the number of z-sections acquired between 7 and 12, but the number acquired was held constant within a given odor panel delivery. Volume images were acquired at a rate of 0.833 Hz. Odor delivery occurred during seconds 6 through 9.6 of the recording.

Each fly experienced up to four deliveries of the odor panel. The antennal lobe being recorded (left or right) was alternated after each successful completion of an odor panel. Odors were delivered in randomized order. In cases where baseline fluorescence was very weak or no obvious odor responses were visible, not all four panels were delivered.

Glomerulus segmentation and labelling

Putative glomerular segmentation masks were extracted from raw image stacks using a K-means clustering algorithm based on time-varying voxel fluorescence intensities, as previously described[4]. Each image stack, corresponding to a single odor panel delivery, was processed individually. Time-varying voxel fluorescence values for each odor delivery were concatenated to yield a voxel-by-time matrix consisting of each voxel's recorded value during the course of all 13 odor deliveries of the odor panel. After z-scoring, principal component analysis was performed on this matrix and 75% of the variance was retained to reduce dimensionality. Next, K-means (k=80, 50 replicates with random starting seeds) was performed to produce 50 distinct voxel cluster assignment maps which we next used to calculate a consensus map. Using multiple cluster assignment maps to calculate a consensus (rather than using the output from a single K-means replicate) resulted in glomerular segmentation masks which better matched those that would would have been produced by manual inspection.

Of the 50 generated voxel cluster assignment maps, the top 5 were selected by choosing those maps with the lowest average within-cluster sum of distances. The remaining maps were discarded. Next, all isolated voxel islands in each of the top 5 maps were identified and pruned

based on size (minimum size = 100 voxels, maximum size = 10000 voxels). Finally, consensus clusters were calculated by finding voxel islands with significant overlap across all 5 of the pruned maps. Voxels which fell within a given cluster across all 5 pruned maps were added to the consensus cluster. This process was repeated for all clusters until the single consensus cluster map was complete. In some cases we found by manual inspection that some individual glomeruli were clearly split into two discrete clusters. These splits were remedied by automatically merging all consensus clusters whose centroids were separated by a physical distance of less than 30 voxels and whose peak odor response Spearman correlation was greater than 0.8. Finally, glomeruli were manually labelled based on anatomical position, morphology, and size[24]. We focused our analysis on 5 glomeruli (DM1, DM2, DM3, DL5, and DC2) which could be observed in most of our recordings. However, not all 5 glomeruli were identified in all recordings (Extended Figure 4). Glomeruli which have been failed to be identified from a recording were considered missing data, and their data was later mean imputed.

Calcium image data analysis

All data was processed and analyzed in Matlab. Calcium responses for each voxel were calculated as $\Delta f/f = [f(t) - F]/F$, where $f(t)$ and F are the instantaneous and average fluorescence, respectively. Each glomerulus' time-dependent calcium response was calculated as the mean $\Delta f/f$ across all voxels falling within the glomerulus' automatically-generated segmentation mask during a single volume acquisition . Time-varying odor responses were normalized to baseline by subtracting the median of pre-odor $\Delta f/f$ from each trace. Peak odor response was calculated as the maximum fluorescence signal within the glomerulus during seconds 7.2 through 10.8 (images 6 through 9) of the recording.

To extract principal components from calcium dynamics, each fly's complement of odor panel responses (a 5 glomeruli by 13 odors = 65-dimensional vector) was concatenated. Some flies exhibited missing values due to missing glomeruli in some odor panel recordings. Missing glomerulus-odor response pairs were filled in with the mean value for that pair across all fly recordings for which the data was not missing (Extended Figure 4). After mean imputation, principal component analysis was carried out with individual odor panel deliveries as observations and glomerulus-odor response pairs as features (Figure 1, Extended Figure 4, 6).

In a subset experiments in which we imaged PN calcium activity, some solenoids failed to open, resulting in the failure of odor delivery in a small number of trials. In these cases, we identified trials in which glomeruli failed to respond and set all glomerulus-odor response pairs to missing for that trial. These glomerulus-odor responses pairs were mean imputed as described above. Add number of flies, and number of odor trials that were missing?

For all predictive models constructed, the average principal component score or glomerulus-odor $\Delta f/f$ response across odor panel deliveries was used per individual; that is, each fly contributed one data point to the relevant model. Linear models were constructed from behavior scores and the relevant predictor (principal component, average $\Delta f/f$ across dimensions, specific glomerulus measurements) as described in the text and Extended Tables 1-2.

To predict behavior as a function of time during odor delivery, we analyzed data as described above, with the exception that we considered only $\Delta f/f$ during a single time point. Mean filling

and PCA were performed and a linear model was constructed as described above. This procedure was repeated for each time point of the recording (Extended Figure 7a-c).

To decode individual identity from neural responses, we first performed PCA on individual odor panel peak responses. We retained principal component scores constituting specified fractions of variance (Extended Figure 4d) and trained a linear logistic classifier to predict individual identity from single odor panel deliveries.

To decode odor identity from neural responses, each of the 5 recorded glomeruli were used as features, and the calcium response of each glomerulus to a specific odor at a specified time point were used as observations (PNs, n=5317 odor deliveries; ORNs, n=2704 odor deliveries). A linear logistic classifier was trained to predict the known odor identity using 2-fold cross-validation. That is, a model was trained on half the data and evaluated on the remaining half, and then this process was repeated with the train and test half reversed. The decoding accuracy was quantified as the fraction of odor deliveries in which the predicted odor was correct.

DoOR data

DoOR data for the glomeruli and odors relevant to our study was downloaded from http://neuro.uni-konstanz.de/DoOR/default.html[39].

Imposed odor experience experiments

We selected six flies for which both odor preference and neural activity were recorded to serve as the basis for imposed odor experiences for yoked control flies. The experimental flies were

chosen such to represent a diversity of preference scores. Each experimental fly's odor experience was binned into discrete odor bouts to represent experience of either MCH or OCT based on its location in the tunnel as a function of time (Figure 2j). Odor bouts lasting less than 100 ms were omitted due to limitations on odor-switching capabilities of the odor delivery apparatus. To deliver a given experimental fly's odor experience to yoked controls, we set both odor streams (on either end of the tunnel apparatus) to deliver the same odor experienced by the experimental fly at that moment during the odor-on period. No odor was delivered to yoked controls during time points in which the experimental fly resided in the tunnel choice zone (central 5 mm). See Figure 2j for an example pair of experimental fly and yoked control behavior and odor experience.

Immunohistochemistry

After measuring odor preference behavior and 7-15 day-old flies were anesthetized on ice and brains were dissected in phosphate buffered saline (PBS). Dissection and immunohistochemistry were carried out as previously reported[40]. The experimenter was blind to the behavioral scores of all individuals throughout dissection, imaging, and analysis. Individual identities were maintained by fixing, washing, and staining each brain in an individual 0.2 mL PCR tube using fluid volumes of 100 uL per brain (Fisher Scientific). Primary incubation solution contained mouse anti-nc82 (1:40, DSHB), chicken anti-GFP (1:1000, Aves Labs), rabbit anti-mStrawberry (1:1000, biorbyt), and 5% normal goat serum (NGS, Invitrogen) in PBT (0.5% Triton X-100 in PBS). Secondary incubation solution contained Atto 647N-conjugated goat anti-mouse (1:250, Millipore Sigma), Alexa Fluor 568-conjugated goat anti-rabbit (1:250), Alexa Fluor 488-conjugated goat anti-chicken (1:250, ThermoFisher), and 5% NGS in PBT. Primary and

secondary incubation times were 2 and 3 overnights, respectively, at 4° C. Stained samples were mounted and cleared in Vectashield (H-1000, Vector Laboratories) between two coverslips (12-568B, Fisher Scientific). Two reinforcement labels (5720, Avery) were stacked to create a 0.15 mm spacer.

Expansion microscopy

Immunohistochemistry for expansion microscopy was carried out as described above, with the exception that antibody concentrations were modified as follows: mouse anti-nc82 (1:40), chicken anti-GFP (1:200), rabbit anti-mStrawberry (1:200), Atto 647N-conjugated goat anti-mouse (1:100), Alexa Fluor 568-conjugated goat anti-rabbit (1:100), Alexa Fluor 488-conjugated goat anti-chicken (1:100). Expansion of stained samples was performed as previously described[30,31]. Expanded samples were mounted in coverslip-bottom petri dishes (MatTek Corporation) and anchored by treating the coverslip with poly-l-lysine solution (Millipore Sigma) as previously described[31].

Confocal imaging

All confocal imaging was carried out at the Harvard Center for Biological Imaging. Unexpanded samples were imaged on an LSM700 (Zeiss) inverted confocal microscope equipped with a 40x oil-immersion objective (1.3 NA, EC Plan Neofluar, Zeiss). Expanded samples were imaged on an LSM880 (Zeiss) inverted confocal microscope equipped with a 40x water-immersion objective (1.1 NA, LD C-Apochromat, Zeiss). Acquisition of Z-stacks was automated with Zen Black software (Zeiss).

Standard confocal image analysis

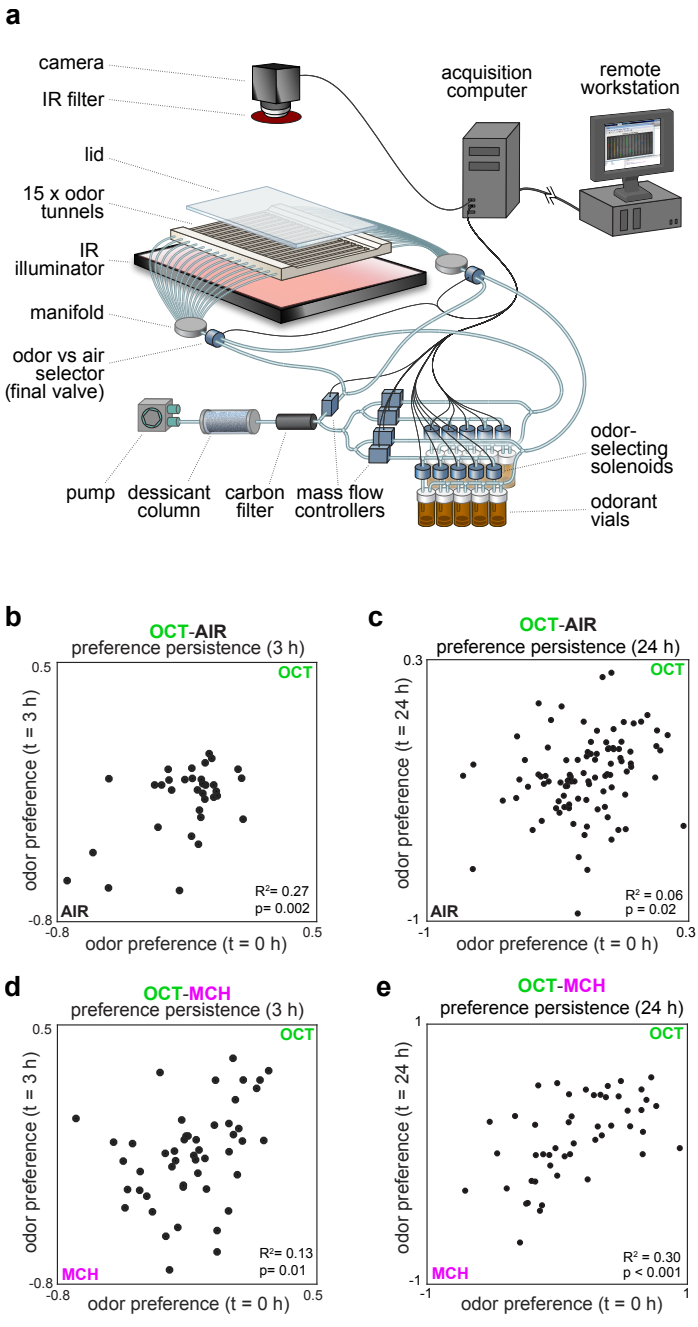
We used custom semi-automated code to generate glomerular segmentation masks from confocal z-stacks of unexpanded Orco>Brp-Short brains. Using Matlab, each image channel was median filtered (σ_x, σ_y, σ_z = 11, 11, 1 pixels) and downsampled in x and y by a factor of 11. Next, an ORN mask was generated by multiplying and thresholding the Orco>mCD8 and Orco>Brp-Short channels. Next, a locally normalized nc82 and Orco>mCD8 image stack were multiplied and thresholded, and the ORN mask was applied to remove background and other undesired brain structures. This pipeline resulted in a binary image stack which maximized the contrast of the glomerular structure of the antennal lobe. We then applied a binary distance transform and watershed transform to generate discrete subregions which aimed to represent segmentation masks for each glomerulus tagged by Orco-Gal4.

However, this procedure generally resulted in some degree of under-segmentation; that is, some glomerular segmentation masks were merged. To split each merged segmentation mask, we convolved a ball (whose radius was proportional to the cube root of the volume of the segmentation mask in question) across the mask and thresholded the resulting image. The rationale of this procedure was that 2 merged glomeruli would exhibit a mask shape resembling two touching spheres, and convolving a similarly-sized sphere across this volume followed by thresholding would split the merged object. After ball convolution, we repeated the distance and watershed transform to once more generate discrete subregions representing glomerular segmentation masks. This second watershed step generally resulted in over-segmentation; that is, by visual inspection it was apparent that many glomeruli were split into multiple subregions. Therefore, we finally manually agglomerated the over-segmented subregions to generate single

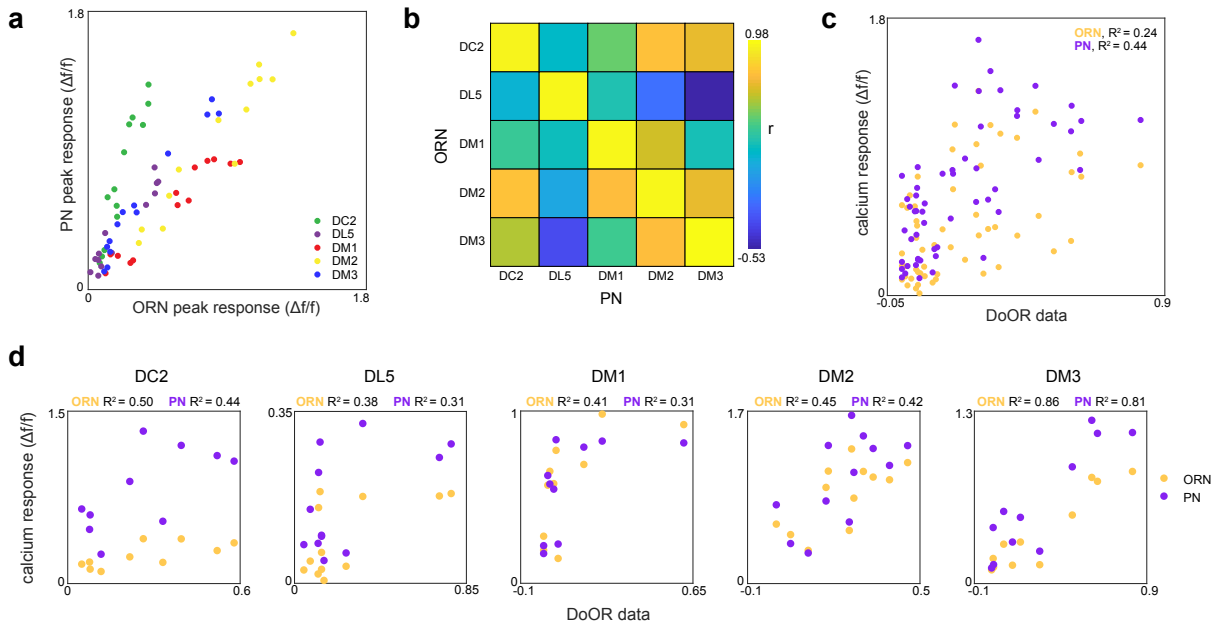
segmentation masks for each glomerulus of interest. We used a published atlas to aid manual identification of glomeruli[24]. The total Brp-Short fluorescence signal within each glomerulus was determined and divided by the volume of the glomerulus' segmentation mask to calculate Brp-Short density values.

Expansion microscopy image analysis

The spots function in Imaris 9.0 (Bitplane) was used to identify individual Brp-Short puncta in expanded sample image stacks of Or13a>Brp-Short samples[29]. The spot size was set to 0.5 um, background subtraction and region-growing were enabled, and the default spot quality threshold was used for each image stack. Identified spots were used to mask the Brp-Short channel and the resultant image was saved as a new stack. In Matlab, a glomerular mask was generated by smoothing (σ_x, σ_y, σ_z = 40, 40, 8 pixels) and thresholding (92.5th percentile) the raw Brp-Short image stack. The mask was then applied to the spot image stack to remove background spots. Finally, the masked spot image stack was binarized and spot number and properties were quantified.

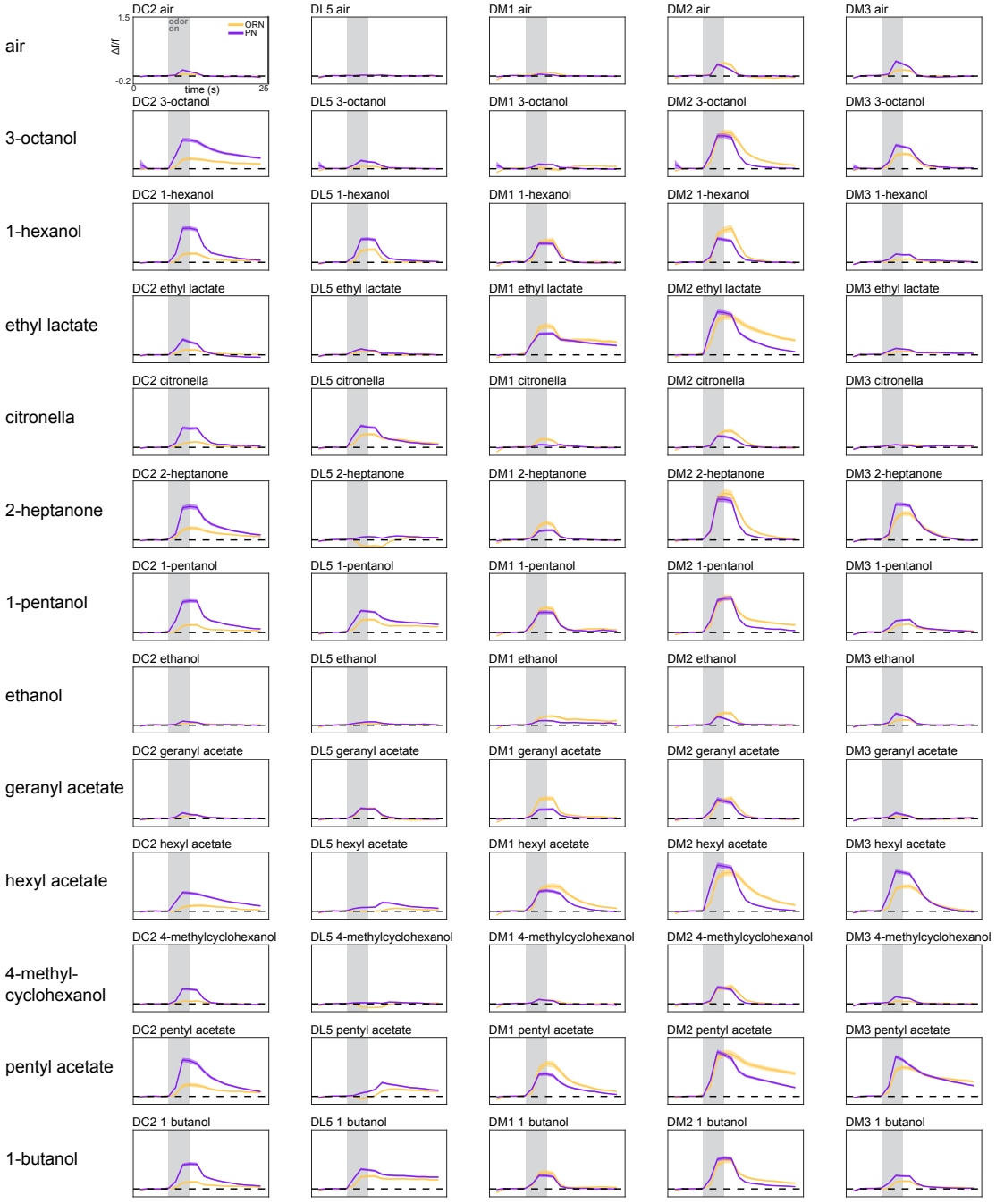


Extended Figure 1: Behavioral measurements and individual preference persistence A) Behavioral measurement apparatus (adapted from [4]). **B)** Odor preference persistence over 3 hours for flies given a choice between 3-octanol and air (n=34 flies). **C)** Odor preference persistence over 24 hours for flies given a choice between 3-octanol and air (n=97 flies). **D)** Odor preference persistence over 3 hours for flies given a choice between 3-octanol and 4-methylcyclohexanol (n=51 flies). **E)** Odor preference persistence over 24 hours for flies given a choice between 3-octanol and 4-methylcyclohexanol (n=49 flies).

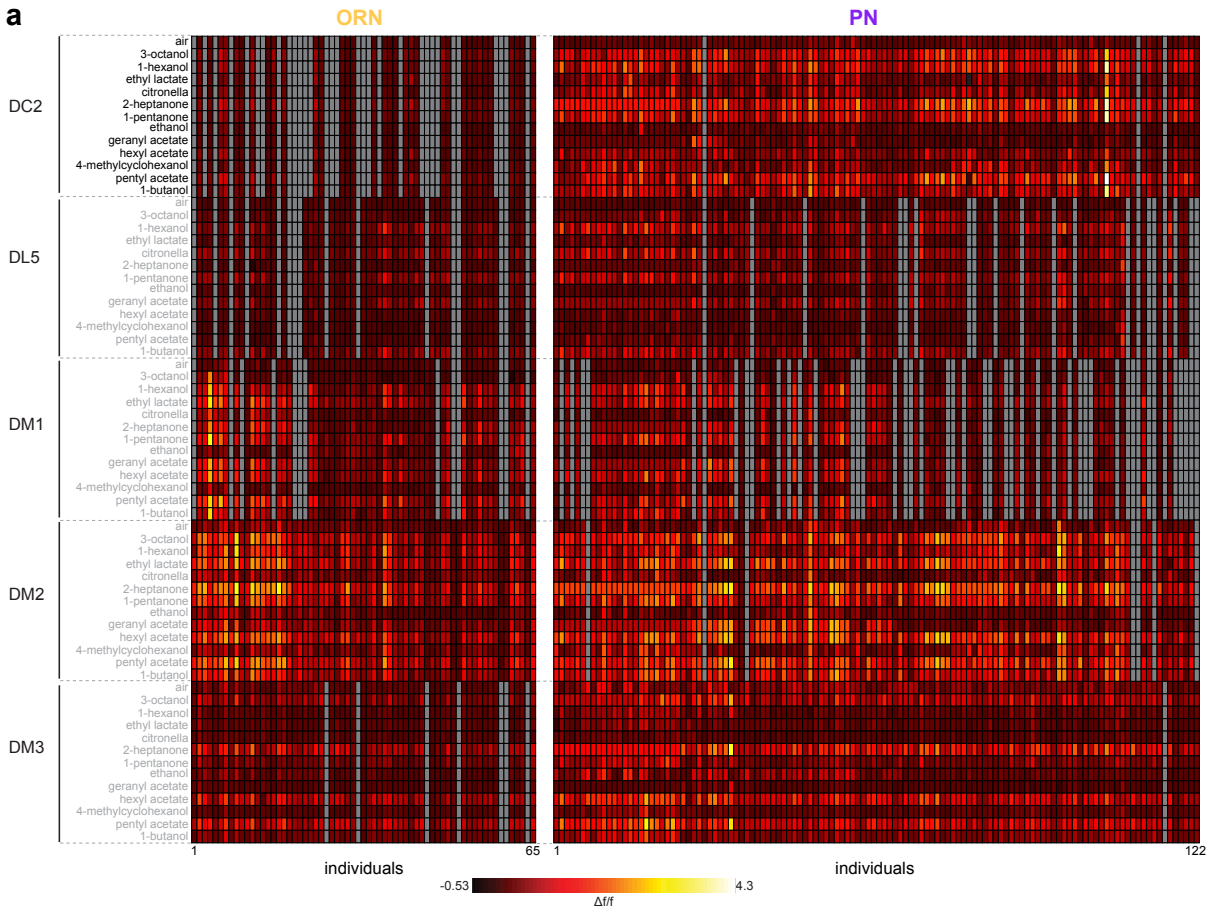


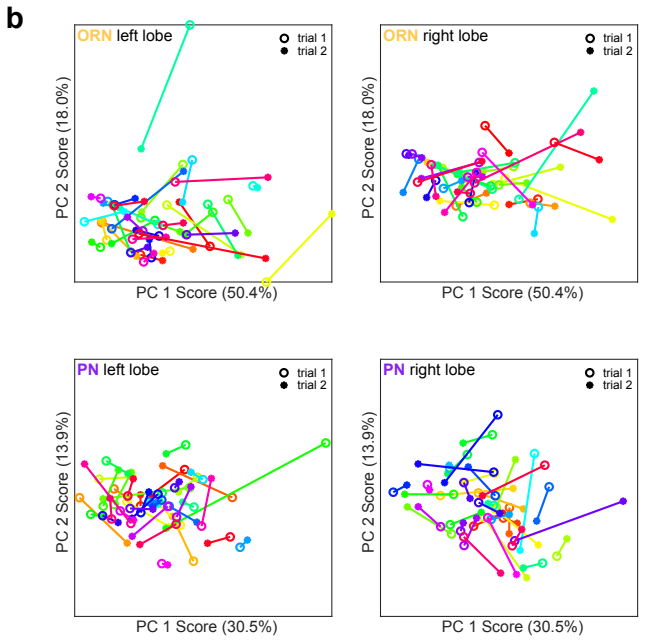
Extended Figure 2: Glomerulus identification

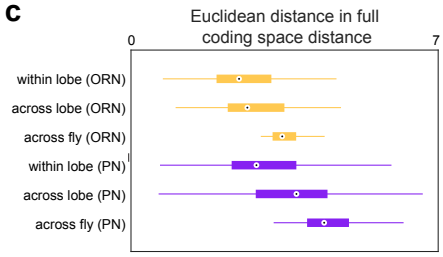
A) Glomerulus odor responses measured in PNs versus those measured in ORNs. Odors are the same as those listed in Figure 1j. **B)** Correlation matrix between glomerular odor responses in ORNs and PNs. **C)** Peak calcium responses for each glomerulus-odor pair measured in this study plotted against those recorded in the DoOR dataset[39]. **D)** Peak calcium responses for each individual glomerulus plotted against those recorded in the DoOR dataset.

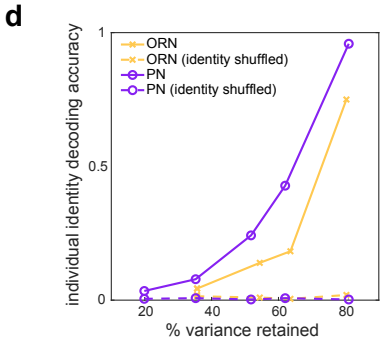


Extended Figure 3: Average glomerulus odor responses. Time-dependent responses of each glomerulus identified in our study to the 13 odors in our odor panel. Data represents the average across flies (ORN, peach curves, n=65 flies; PN, plum curves, n=122 flies). Shaded error bars represent S.E.M.

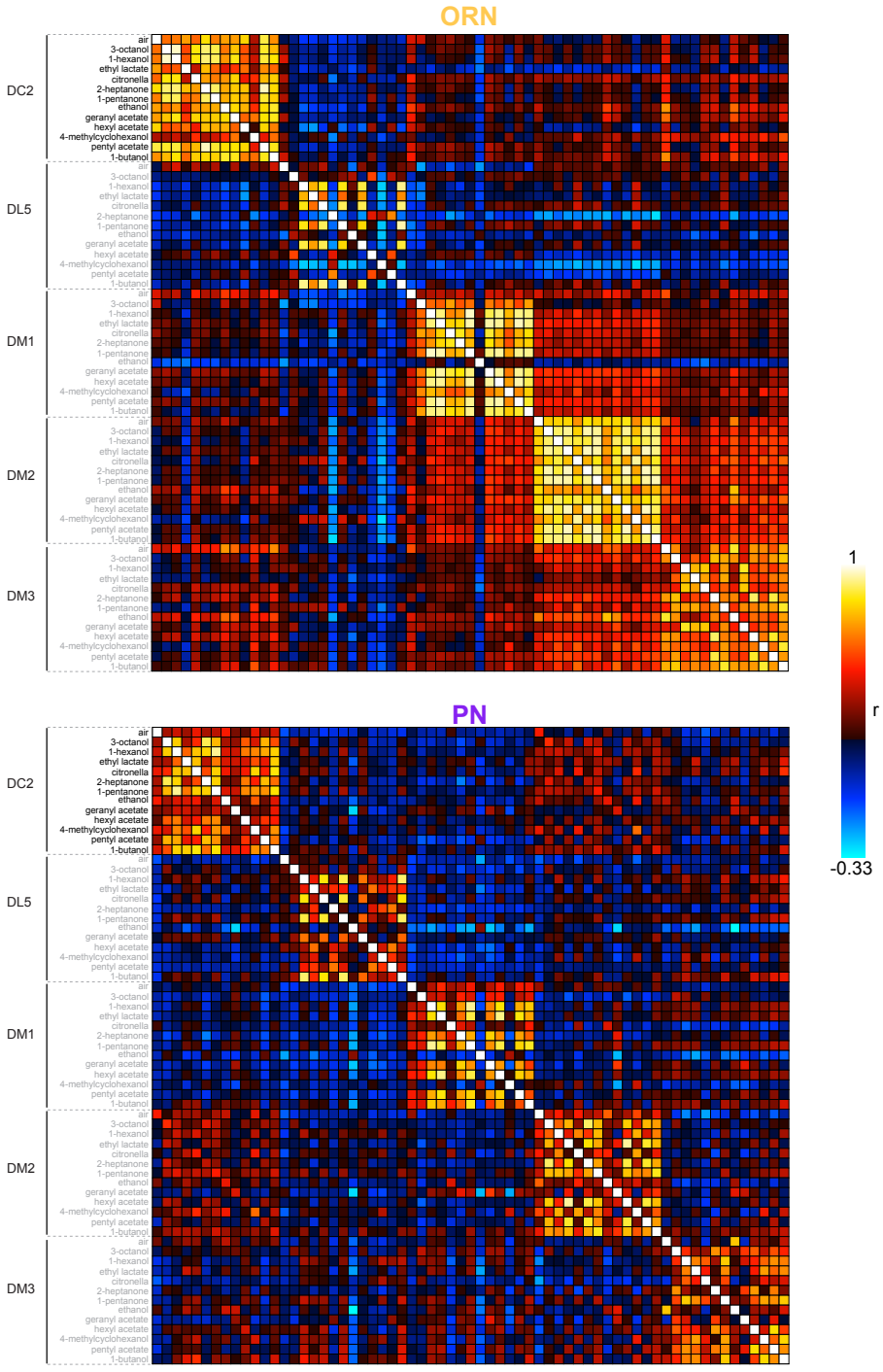

a
ORN
PN
DC2
DL5
DM1
DM2
DM3
air
3-octanol
1-hexanol
ethyl lactate
citronella
2-heptanone
1-pentanone
ethanol
geranyl acetate
hexyl acetate
4-methylcyclohexanol
pentyl acetate
1-butanol
1
65
individuals
1
122
individuals
-0.53
4.3
Δf/f


b
ORN left lobe
ORN right lobe
PN left lobe
PN right lobe
trial 1
trial 2
PC 2 Score (18.0%)
PC 2 Score (13.9%)
PC 1 Score (50.4%)
PC 1 Score (30.5%)

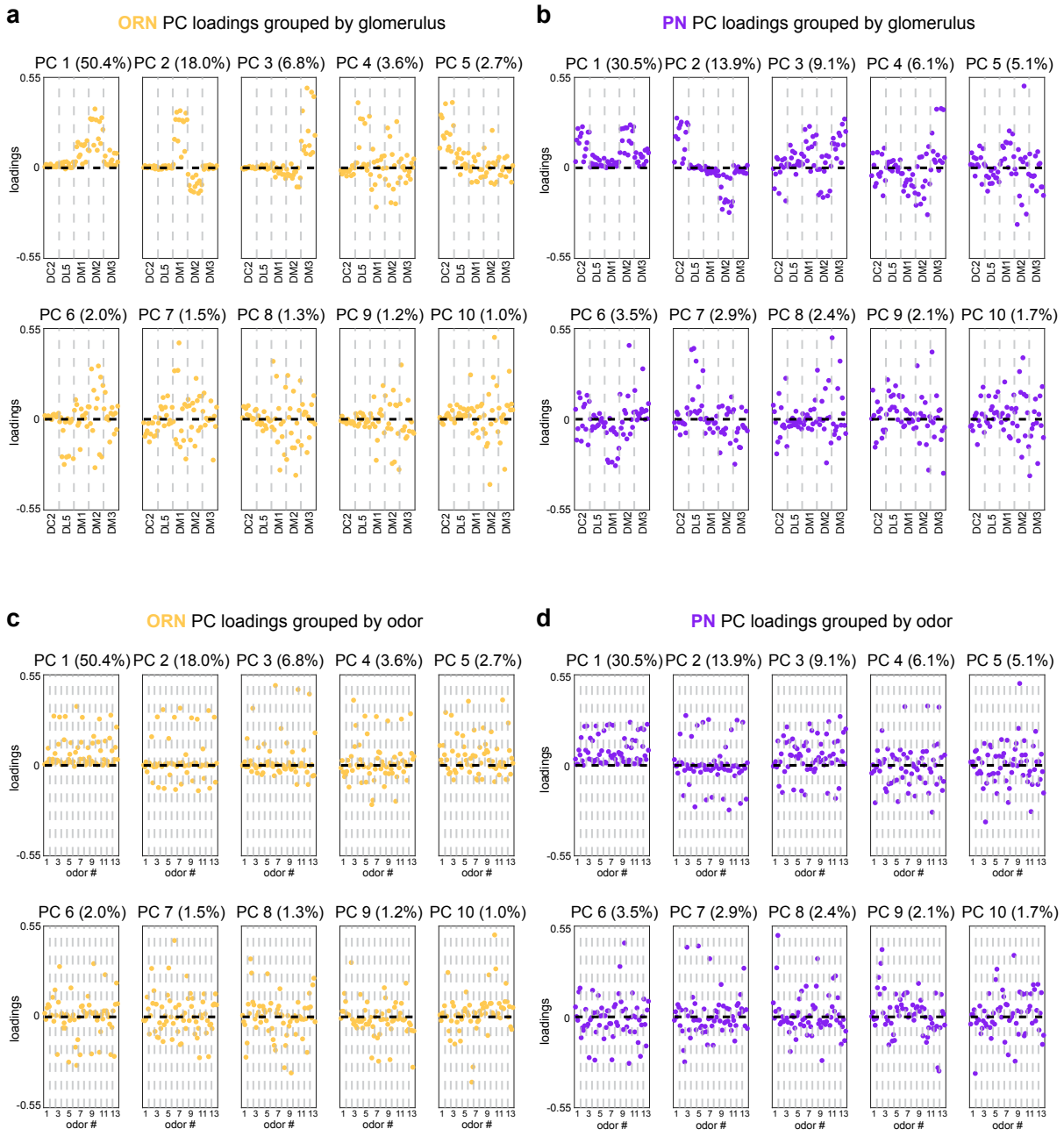

c
Euclidean distance in full coding space distance
0
7
within lobe (ORN)
across lobe (ORN)
across fly (ORN)
within lobe (PN)
across lobe (PN)
across fly (PN)


d
ORN
ORN (identity shuffled)
PN
PN (identity shuffled)
individual identity decoding accuracy
1
0.5
0
20
40
60
80
% variance retained

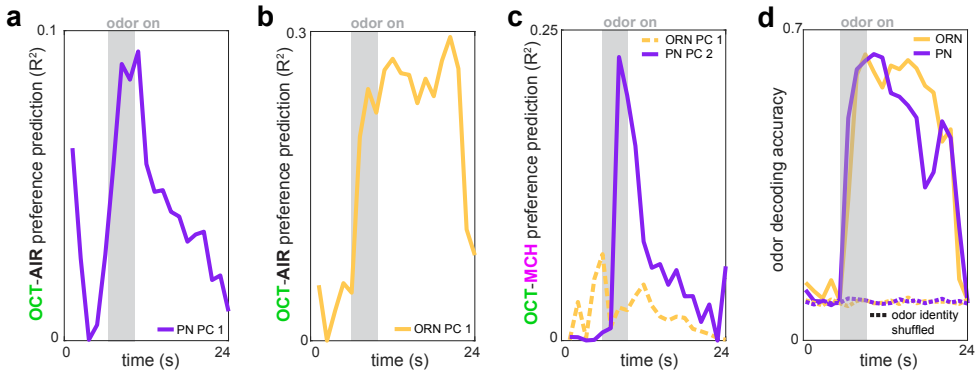
Extended Figure 4: Idiosyncratic odor coding. A) Idiosyncratic odor coding measured in ORNs (left, n=65 flies) and PNs (right, n=122 flies). Each column represents the response of a single fly averaged over up to 4 odor deliveries. Each row represents a glomerulus-odor response pair. Missing glomeruli are indicated in gray. **B)** Individual trial-to-trial responses embedded in PC 1-2 space. Responses for the same flies as Figure 1k-l are shown. Each color represents one fly. Trial 1 and trial 2 responses are shown for ORN left lobe (upper left), ORN right lobe (upper right), PN left lobe (lower left), and PN right lobe (lower right). **C)** Full coding space euclidean distance for within lobe (trial-to-trial), across lobe (within fly), and across flies for ORNs and PNs. **D)** Logistic regression classifier accuracy of decoding individual identity from individual odor panel peak responses. PCA was performed on population responses and the specified fraction of variance (x-axis) was retained. Individual identity can be better decoded from PN responses than ORN responses in all cases.



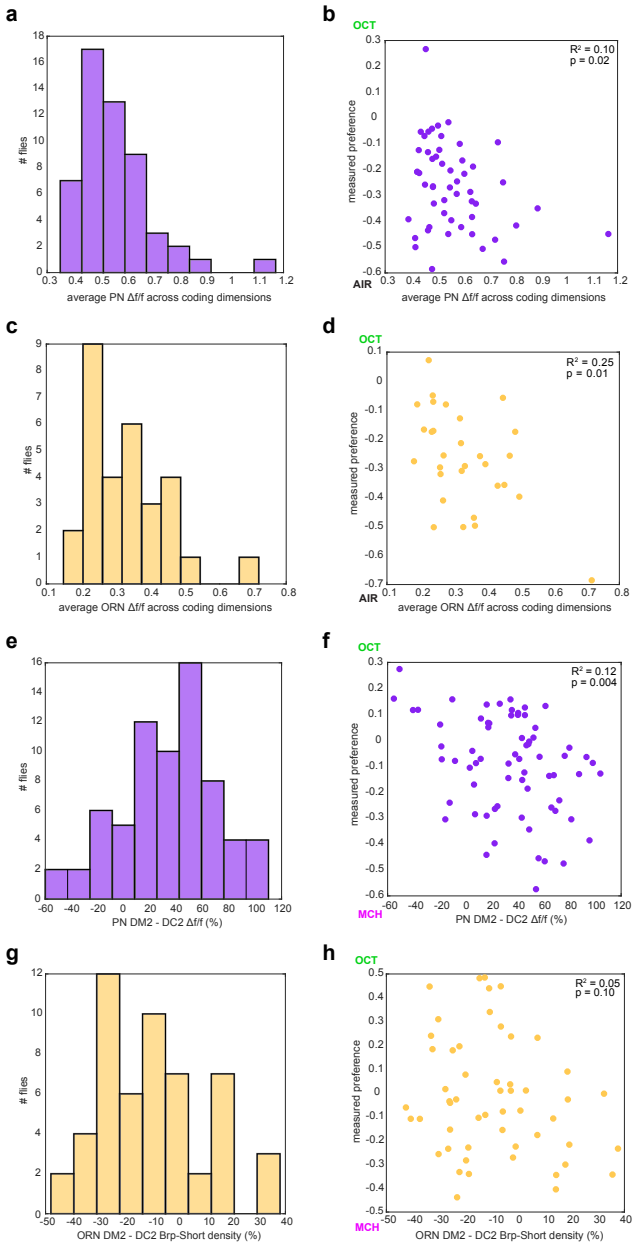
Extended Figure 5: Neural coding correlation matrices. Correlation between neural coding dimensions across flies measured in ORNs (top) and PNs (bottom). Inter-glomerulus correlations are more prominent in ORNs than PNs, consistent with known AL transformations which result in decorrelated PN responses[22,43].



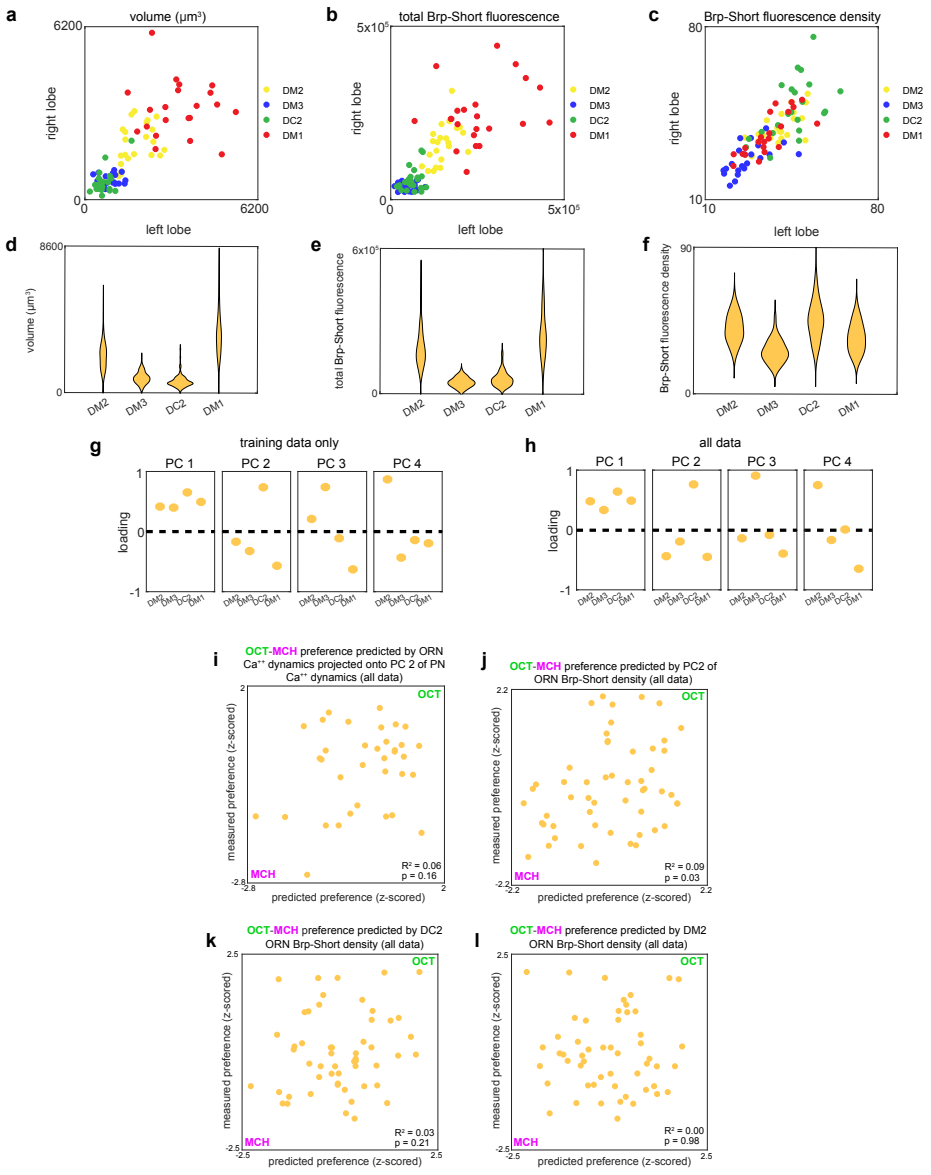
Extended Figure 6: Calcium imaging principal component loadings. A,B) First 10 principal component loadings measured from calcium responses in ORNs (a, n=65 flies) and PNs (b, n=122 flies). Loadings are grouped by glomerulus, with each loading within a glomerulus representing the response of that glomerulus to one odor in the odor panel. Odors are the same as those listed in Figure 1j. **C,D)** The same 10 principal component loadings as those shown in panels (A,B) grouped by odor rather than glomerulus.



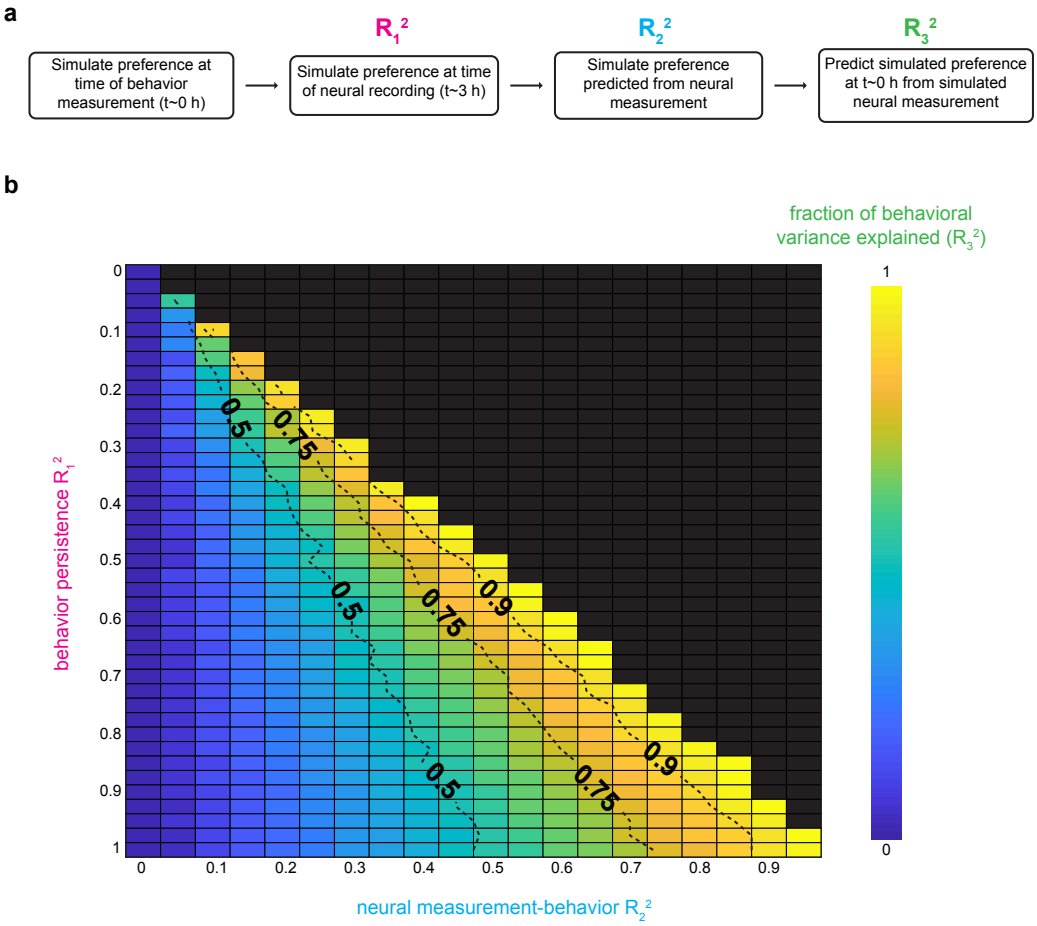
Extended Figure 7: Time-dependent preference and odor decoding. A) R^2 of OCT-AIR preference predicted by PC 1 of PN activity as a function of time (n=53 flies). **B)** R^2 of OCT-AIR preference predicted by PC 1 of ORN activity as a function of time (n=30 flies). **C)** R^2 of OCT-MCH preference predicted by PC 2 of PN activity (solid plum, n=69 flies) or PC 1 of ORN activity (dashed peach, n=35 flies) as a function of time. **D)** Logistic regression classifier accuracy of decoding odor identity from 5 glomerular responses as a function of time. Dashed curves indicate chance performance.



Extended Figure 8: Calcium and Brp-Short predictor variation. A) Histogram of average PN Δf/f across all coding dimensions in flies in which OCT-AIR preference was measured. **B)** Measured OCT-AIR preference versus average PN Δf/f (n=53 flies). **C)** Histogram of average ORN Δf/f across all coding dimensions in flies in which OCT-AIR preference was measured. **D)** Measured OCT-AIR preference versus average ORN Δf/f (n=30 flies). **E)** Histogram of % Δf/f difference between DM2 and DC2 PN responses in flies in which OCT-MCH preference was measured. **F)** Measured OCT-MCH preference versus % Δf/f difference between DM2 and DC2 PN responses df/f (n=69 flies). **G)** Histogram of % Brp-Short density difference between DM2 and DC2 ORNs in flies in which OCT-MCH preference was measured. **H)** Measured OCT-MCH preference versus % Brp-Short density difference between DM2 and DC2 ORNs (n=53 flies).



Extended Figure 9: Confocal imaging data characterization and additional model predictions. A-C) Right versus left glomerulus properties measured from z-stacks of stained Orco>Brp-Short samples. **A)** Volume, **B)** total Brp-Short fluorescence, **C)** Brp-Short fluorescence density. **D-F)** Same data as panels **A-C)** represented in violin plots (kernel density estimated). **G)** Principal component loadings of Brp-Short density calculated using only training data (n=22 flies). **H)** Principal component loadings of Brp-Short density calculated using all data (n=53 flies). **I)** Measured OCT-MCH preference versus preference predicted by ORN calcium dynamics projected onto PC 2 of PN dynamics calculated using all data (n=35 flies). **J)** Measured OCT-MCH preference versus preference predicted by PC 2 of Brp-Short density calculated using all data (n=53 flies). **K)** Measured OCT-MCH preference versus preference predicted by DC2 Brp-Short density calculated using all data (n=53 flies). **L)** Measured OCT-MCH preference versus preference predicted by DM2 Brp-Short density calculated using all data (n=53 flies).



Extended Figure 10: Computational simulation of behavioral variation explained from neural measurements. A simulation relates how the fraction of behavioral variance explained is a function of trial-to-trial behavioral variation and the measured explanation of behavior from neural measurements. **A)** Simulation outline. **B)** Fraction of behavioral variance explained (R_3^2, green) by neural measurements (colormap) as a function of the behavioral persistence (R_1^2, y-axis, pink) and neural-behavior variance explained (R_2^2, x-axis, blue).

Extended Table 1: Predictive calcium models

Behavior measured	Neural Predictor	Figure Panel	n	β_0	β_1	R^2	p-value
OCT vs. AIR	PN PC 1 (Fig. 2a)	1l	18	-0.258	-0.079	0.161	0.099
OCT vs. AIR	PN Average all dimensions	2c	53	-0.051	-0.379	0.098	0.022
OCT vs. AIR	ORN PC 1 (Fig. 2d)	1n	30	-0.286	-0.053	0.230	0.007
OCT vs. AIR	ORN Average all dimensions	2f	30	-0.032	-0.709	0.246	0.005
OCT vs. MCH	PN PC 2 (Fig. 2g)	1p	47	-0.058	-0.081	0.154	0.006
OCT vs. MCH	PN DM2 - DC2 (% difference)	2i	69	-0.032	-0.004	0.120	0.004
OCT vs. MCH	ORN PC 1	1r	35	-0.138	-0.027	-0.031	0.315

Extended Table 2: Predictive Brp-Short models

Behavior measured	Neural Predictor	Figure Panel	n	β_0	β_1	R^2	p-value
OCT vs. MCH	ORN PC 2 (train data only) (Fig. 3e)	3f	22	-0.087	0.017	0.218	0.028
OCT vs. MCH	ORN PC 2 (all data) (Extended Figure 9h)	Extended Figure 9j	53	-0.019	0.012	0.088	0.031
OCT vs. MCH	ORN DM2 - DC2	3h	53	-0.051	-0.007	0.053	0.096
OCT vs. MCH	ORN DC2	Extended Figure 9k	53	-0.202	0.004	0.030	0.213
OCT vs. MCH	ORN DM2	Extended Figure 9l	53	-0.014	0	0	0.978

Page was intentionally left blank

Appendix III – Chapter III Supplemental Material

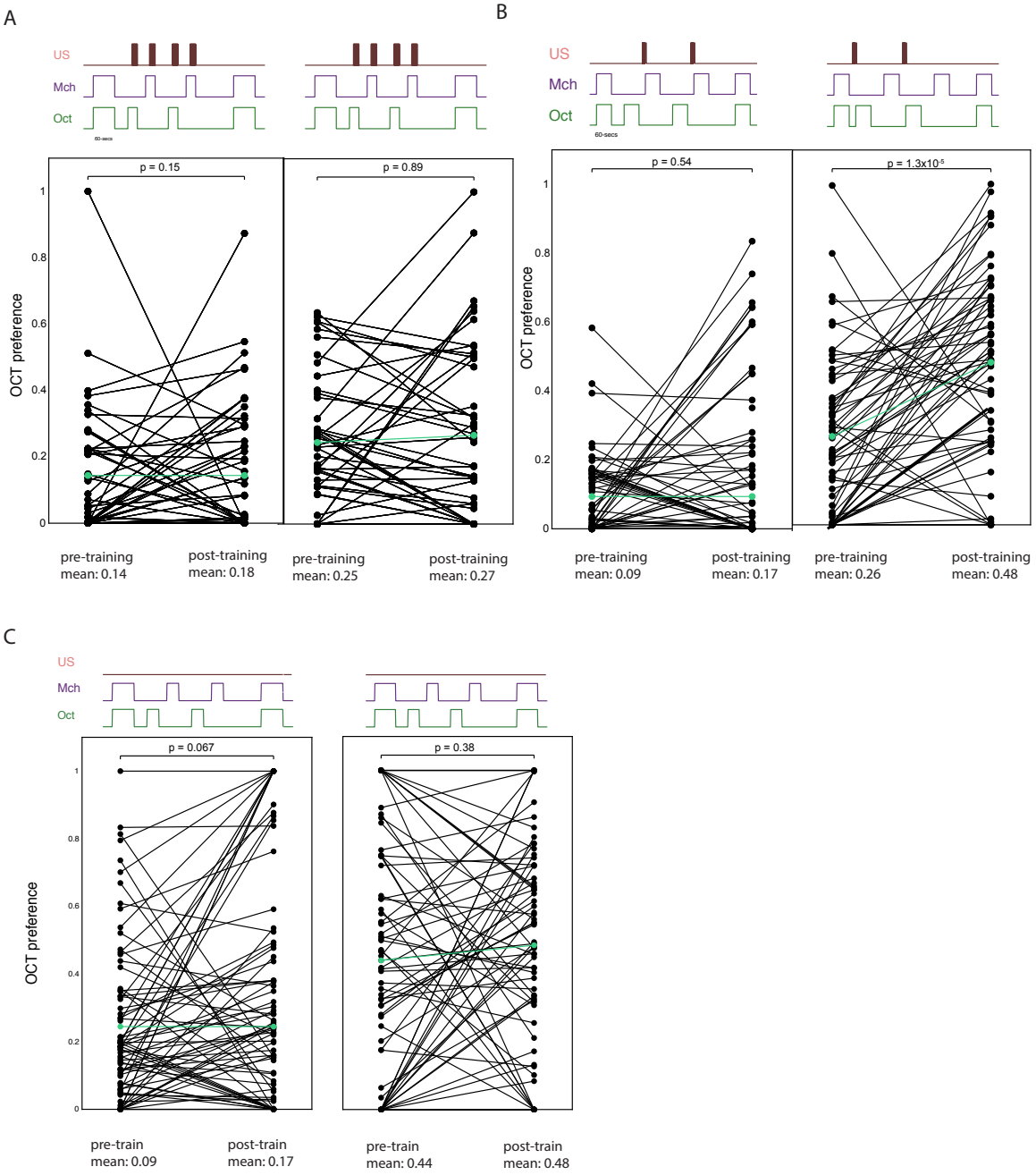


Figure S1 — Associative conditioning control experiments — OCT preference of individual flies across pre- and post-contioning periods (left and right dots in each panel, respectively) with two conditioning blocks corresponding to forward- and reverse-conditioning experiments. Dots are individual flies. Thick black line represents mean pre- and post-training. (A) US paired with both OCT and MCH. (B) US presented before the CS. (C) No US presentation. Schematics in style of Figure 1C.

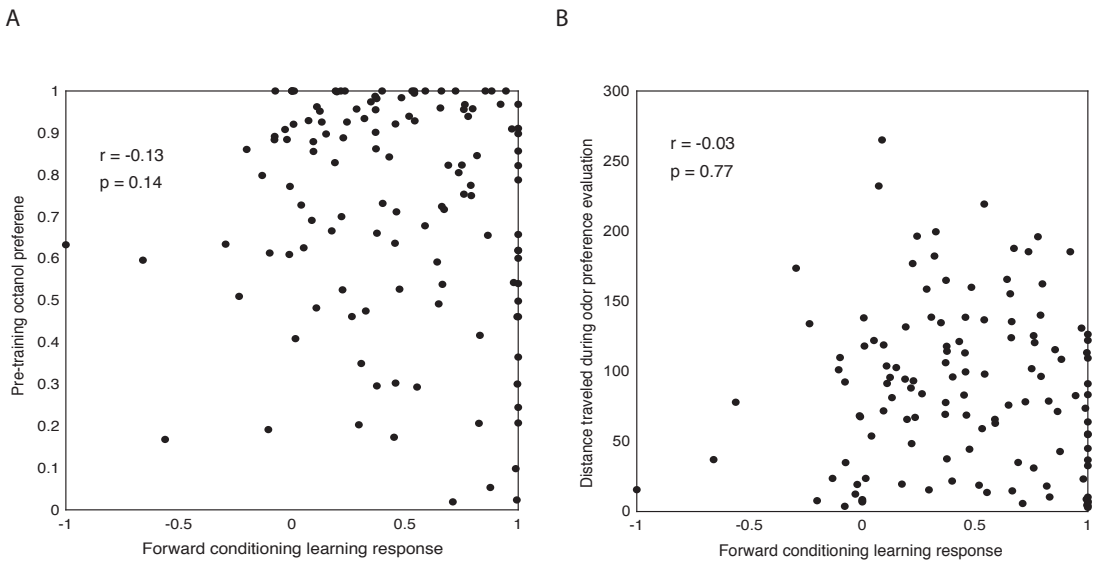


Figure S2 — (A) Scatter plot of individual forward-conditioning learning scores vs their OCT preference in the pre-conditioning block (r = -0.13; p = 0.14). (B) Scatter plot of individual forward-conditioning learning score vs distance traveled during the pre-conditioning block (r = -0.03; p = 0.77).

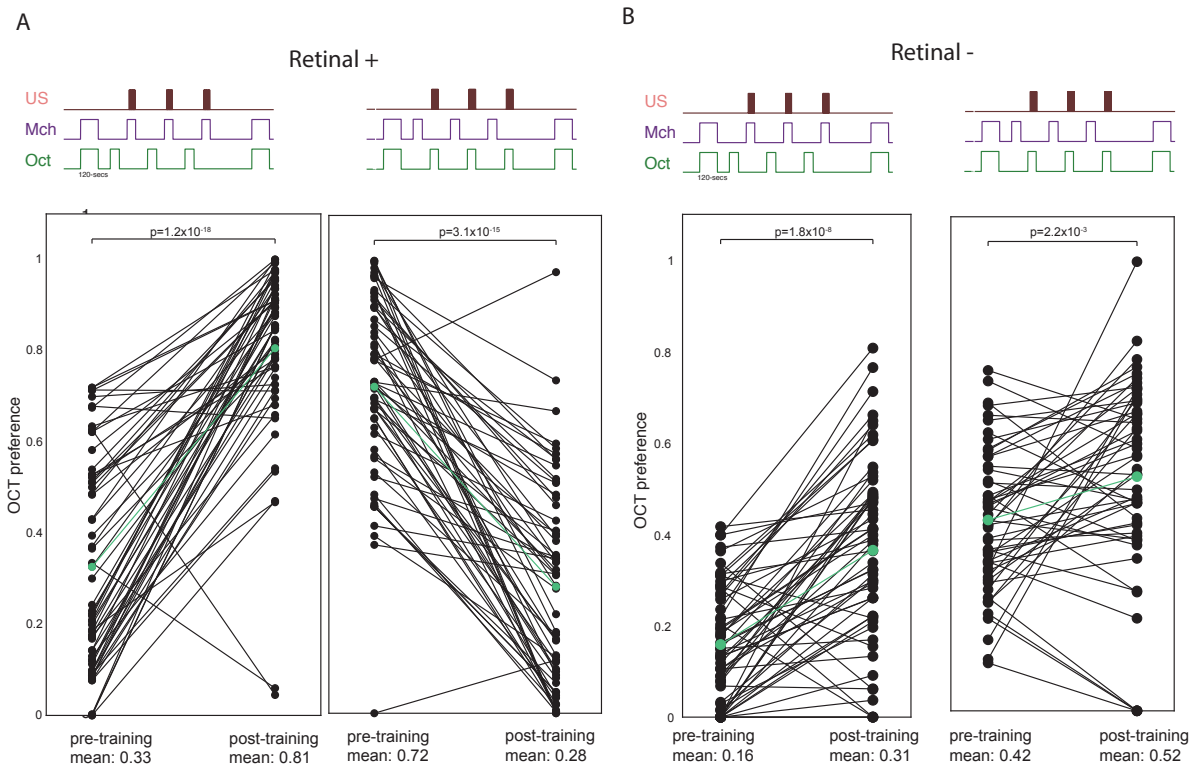


Figure S3 — (A) OCT preference of *Gr66a-LexA>LexAop-CsChrimson* flies fed all-trans-retinal undergoing forward- and reverse-conditioning. Dots are individual flies. Thick black line represents mean pre- and post-training. (B) OCT preference of *Gr66a-LexA> LexAop-CsChrimson* flies not fed all-trans-retinal.

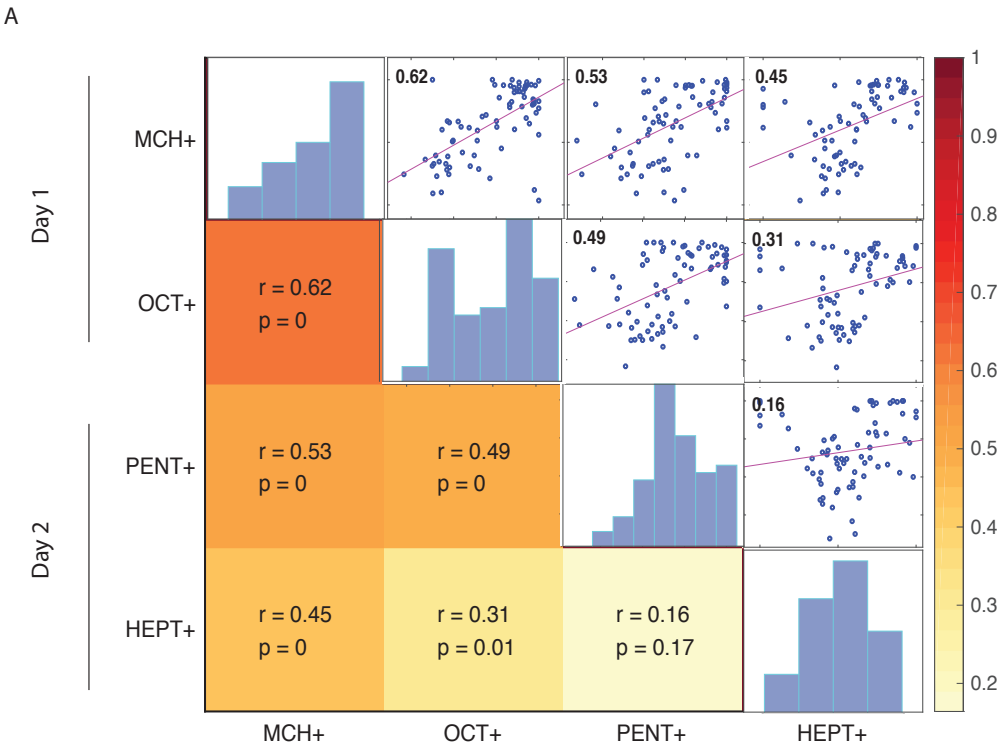


Figure 4S — (A) Schematic of the two day conditioning protocol with two different odor pairs and optogenetic US, and Correlation matrix for individual fly learning responses for all pairs of the four different conditioning blocks.